AD-A146 638 A COMPARISON OF STORM TRACKING AND EXTRAPOLATION ALGORITHMS(U) MASSACHUSETTS INST OF TECH LEXINGTON LINCOLN LAB J C BRASUNAS 31 JUL 84 ATC-124 1/2

UNCLASSIFIED DOT/FAA/PM-84-1 DTFA01-80-Y-10546 F/G 4/2 NL

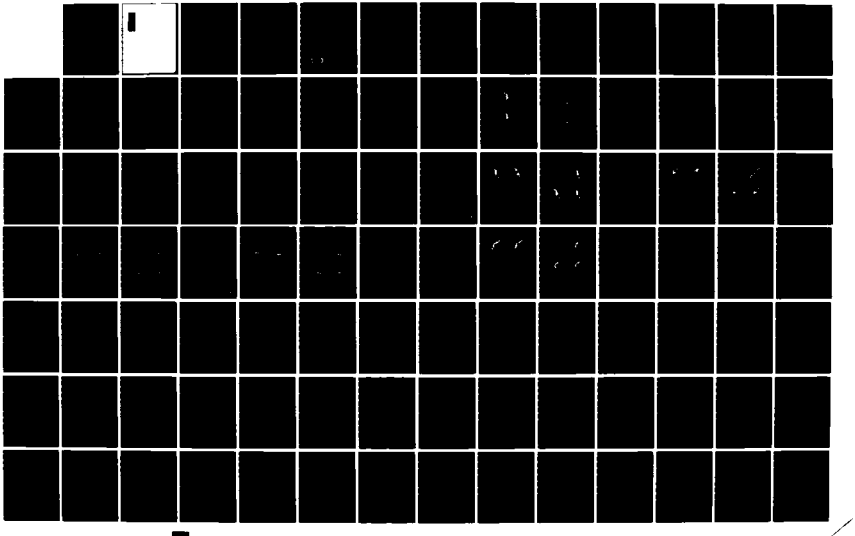

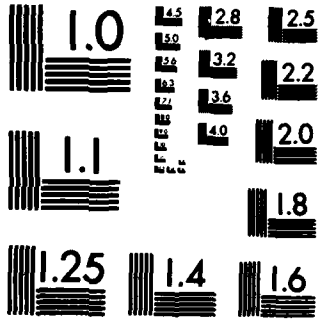

OPY RESOLUTION TEST CHART

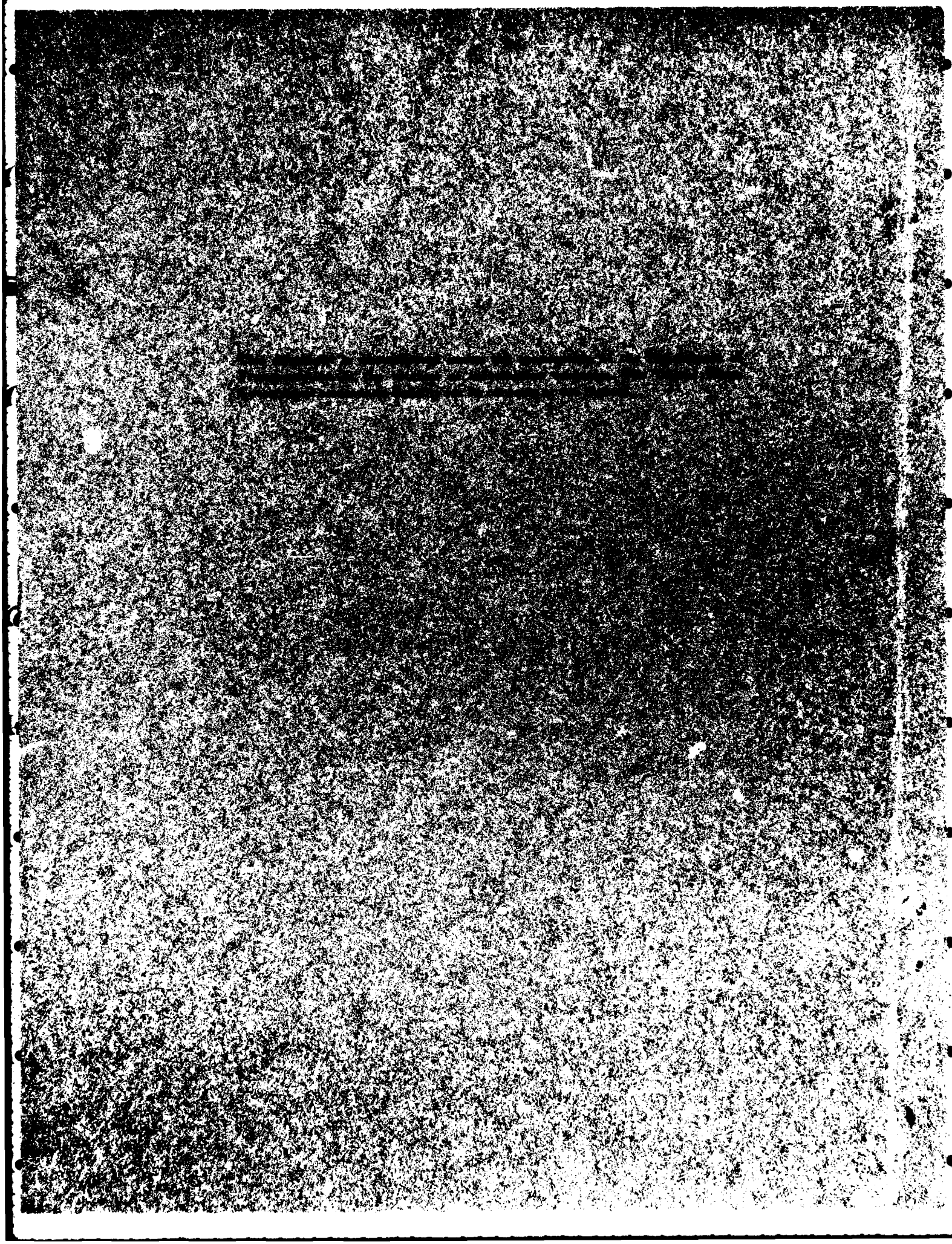

Technical Report Documentation Page

1. Report No.	2. Government Accession No.	3. Recipient's Catalog No.
DOT/FAA/PM 84-1	AD-A146 638	

4. Title and Subtitle	5. Report Date
A Comparison of Storm Tracking and Extrapolation Algorithms	31 July 1984
	6. Performing Organization Code

7. Author(s)	8. Performing Organization Report No.
John C. Brasunas	ATC-124

9. Performing Organization Name and Address	10. Work Unit No.
Massachusetts Institute of Technology Lincoln Laboratory, M.I.T. P.O. Box 73 Lexington, MA 02173-0073	11. Contract or Grant No. DT-FA01-80-Y-10546
	13. Type of Report and Period Covered Project Report
12. Sponsoring Agency Name and Address Department of Transportation Federal Aviation Administration Systems Research and Development Service Washington, DC 20591	14. Sponsoring Agency Code

15. Supplementary Notes

The work reported in this document was performed at Lincoln Laboratory, a center for research operated by Massachusetts Institute of Technology, under Air Force Contract F19628-80-C-0002.

16. Abstract

The FAA requires short-term forecasts of the development and motion of high reflectivity regions to plan for weather avoidance in the en route and terminal areas. Specific needs include choice of air routes and anticipating when to open or close approach/departure gates, descent corridors, and runways. This report compares storm-tracking algorithms for making short-term (0-30 minute) forecasts of high reflectivity areas, to serve these air traffic control needs. The area forecasts are made by moving the key features of the current reflectivity map according to the velocities derived from the storm trackers. The NEXRAD centroid, correlation, and Crane peak-cell trackers are compared against themselves, persistence, and a best-fit extrapolation. Two performance measures are used:

(a) overlap of predicted versus actual areas

(b) accuracy in flight-path choice.

The second method is a new way of scoring the predictor performance and is particularly suited to aviation needs.

Five storms are considered, three in Massachusetts and two in Oklahoma. The correlation and peak-cell trackers generally performed well in the Massachusetts storms, close to a best correlation fit extrapolator. The centroid tracker behaves erratically, due to contour merging and splitting. The centroid tracker performed well on compact, Oklahoma storms where the correlation and peak-cell trackers were misled by storm propagation, an effect to be expected when there is high vertical shear of the horizontal wind.

It is recommended that either the correlation or centroid tracker be used, depending on the type of storm expected. The centroid tracker would be used on compact storms; the correation tracker would be used on storms without substantial propagation. The forecasts appear to be skillful in predicting high-reflectivity areas; however, they are less skillful in anticipating flight-paths which do not intersect these areas. Inclusion of forecasts of storm growth and decay will probably be required to improve the performance; anticipating growth and decay will also be important for forecasts of greater than 30 minutes.

17. Key Words		18. Distribution Statement
NEXRAD Doppler weather radar tracking	prediction aviation weather hazards flight paths	Document is available to the public through the National Technical Information Service, Springfield, Virginia 22161

19. Security Classif. (of this report)	20. Security Classif. (of this page)	21. No. of Pages	22. Price
Unclassified	Unclassified	128	

Form DOT F 1700.7 (8-72) Reproduction of completed page authorized

ABSTRACT

The FAA requires short-term forecasts of the development and motion of high reflectivity regions to plan for weather avoidance in the en route and terminal areas. Specific needs include choice of air routes and anticipating when to open or close approach/departure gates, descent corridors, and runways. This report compares storm-tracking algorithms for making short-term (0-30 minute) forecasts of high reflectivity areas, to serve these air traffic control needs. The area forecasts are made by moving the key features of the current reflectivity map according to the velocities derived from the storm trackers. The NEXRAD centroid, correlation, and Crane peak-cell trackers are compared against themselves, persistence, and a best-fit extrapolation. Two performance measures are used:

(a) overlap of predicted versus actual areas

(b) accuracy in flight-path choice.

The second method is a new way of scoring the predictor performance and is particularly suited to aviation needs.

Five storms are considered, three in Massachusetts and two in Oklahoma. The correlation and peak-cell trackers generally performed well in the Massachusetts storms, close to a best correlation fit extrapolator. The centroid tracker behaves erratically, due to contour merging and splitting, but the centroid tracker performed well on compact, Oklahoma storms where the correlation and peak-cell trackers were misled by storm propagation, an effect to be expected when there is high vertical shear of the horizontal wind.

It is recommended that either the correlation or centroid tracker be used, depending on the type of storm expected. The centroid tracker would be used on compact storms; the correlation tracker would be used on storms without substantial propagation. The forecasts appear to be skillful in predicting high-reflectivity areas; however, they are less skillful in anticipating flight-paths which do not intersect these areas. Inclusion of forecasts of storm growth and decay will probably be required to improve the performance; anticipating growth and decay will also be important for forecasts of greater than 30 minutes.

CONTENTS

LIST OF ILLUSTRATIONS

LIST OF TABLES

I. INTRODUCTION

A. Air Traffic Needs

There is a need within the air traffic community for accurate, real-time predictions of hazardous weather areas in the short look-ahead time frame (0-4 hours). Accurate predictions lead both to the efficient utilization of airspace and to an improved safety factor. Such predictions would be of use both to the pilot himself and to the air traffic controller. For the controller, accurate predictions allow him to anticipate pilot deviation requests and to give avoidance advisories.

This report concentrates on zero to 30-minute forecasts. Since storm speeds typically do not exceed 1 to 2 km/min, the relevant spatial scales are 30 to 60 km. A half-hour forecast is not suited to strategic planning in the en route environment. Rather, this report addresses itself to tactical decisions which must be made in the terminal control area, the en route-terminal control area transition region, and in en route airspace. Specific points of concern are storm cell avoidance; route planning within and near the terminal area; use of approach and departure gates, descent corridors, and runways; and the general impact of a storm system on an airport.

This report concerns itself with forecasting actual storm extents rather than just centroids. The actual forecasts generated are quantitatively scored in terms of the areas forecasted to be hazardous, and the impact of these forecasted areas on air route usage.

There are various kinds of hazards which need to be anticipated. This report addresses itself to short-term forecasts of high reflectivity (dBz) areas. FAA rules call for a buffer zone of avoidance around 40 dBz contours; however, these rules are not always observed in practice. Reflectivity is a radar measurable quantity, and there are standard relationships between dBz and rainfall rate; these are shown in Fig. I-1. Typically, something close to the upper curve is used by the NWS for a thunderstorm situation (see Zittel, 1978). The Marshall-Palmer curve is considered suitable for stratiform rain.

Forecasts of high reflectivity are useful for several reasons. Heavy rain can cause an engine to flame out. Heavy rain can also lead to a degradation in airfoil performance and to a weight penalty on the aircraft. High reflectivity can also indicate the presence of hail, and is often associated with storms which generate significant turbulence.

B. NEXRAD

NEXRAD (Next Generation Weather Radar) is a joint undertaking of the Departments of Commerce, Transportation, and Defense. It will provide the

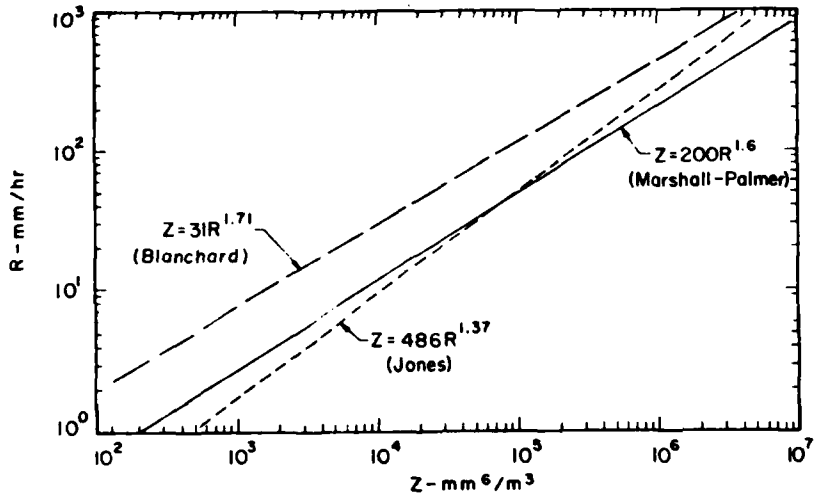

Figure I-1. Plots of various Z-R relationships. (Battan)

nation with a network of solid-state, S-band pulsed-Doppler radars. NEXRAD will provide volume coverage with a pencil-beam (~1 degree) unlike present NWS radars which generally scan at one elevation angle only and which also lack a Doppler capability. The pencil-beam is preferable for accurate reflectivity measurements to the fan-beams of current and planned airport surveillance radars.

There will be over 100 NEXRAD radars, and they will provide nearly continuous coverage in the continental United States. Each radar will provide estimates of reflectivity to a range of 460 km, and estimates of mean Doppler velocity and the spread of Doppler velocities to a range of 230 km.

C. Purpose of this Report

The spatial and time scales of this report focus on the region known as the "mesoscale" in the meteorological community. Research in mesoscale phenomena is less mature than research in the larger scale often referred to as "synoptic". Whereas numerical forcasts based more or less on basic physical principles have been made with varying degrees of success for over thirty years, mesoscale forecasts are in a much cruder state (see, for instance, Browning, 1982b). In the mesoscale, forecasts (or predictions) are generally restricted to: simple, linear extrapolation; statistical extrapolation, involving the use of a typical life cycle for the phenomenon being forecasted; and simple physical models based on particular mechanisms; for instance, topographic forcing of storms in certain areas.

This report concerns itself only with linear extrapolation, and this extrapolation is applied only to storm positions. The storm size and intensity are not changed, and this is what keeps the focus of this study on a very short time scale. Thus to refer to the algorithms in this report as "forecasts" or "predictions", while accurate, may be somewhat misleading. This report concerns itself with storm tracking, and with the extrapolation of these tracks into the near future.

This report examines forecasts of reflectivity areas based on data from NEXRAD-like radars, to assess the suitability of the proposed NEXRAD storm tracker for air traffic needs. This suitability is determined by comparing the proposed NEXRAD tracker with various other contemporary trackers which have been extensively described in the literature. The goal of this study has been to determine which of the already available trackers is best suited to the air traffic needs described previously.

Once the choice of trackers has been made, the question naturally arises of to what to apply the track velocities in order to make forecasts of future storm areas. Two candidates are pixels of some canonical size (say 1 km by 1 km) and contours defined by fixed reflectivity levels.

Since the NEXRAD tracker works on fixed-level contours, and since there is a natural association between the contours and the NEXRAD track vectors, it was decided to apply the velocities derived from other tracking algorithms to these very same fixed-level contours. As the centroid tracker generally works well at 30 dBz, 30 dBz contours were used in the predictions unless there was too little or too much storm coverage at that level.

Thus this report compares the forecasts made by running a set of tracking algorithms, attaching the derived velocities to fixed-level contours, and moving the various contours with the various velocities for the desired extrapolation time interval. Preliminary results were reported in Brasunas and Merritt (1983). Performance differences are due principally to the trackers, as their velocities are all attached to a common set of cells. The forecasts so made are quantitatively scored in terms of false safe and false alarm statistics. These statistics are defined both in terms of an area-intersection approach, and a flight-path approach.

D. Previous Research

1. Trackers

The trackers we have considered have all been discussed in the literature:

Centroid tracking. The NEXRAD tracker is a centroid tracker that follows the dBz-weighted centroids of fixed-dBz-level contours. A description may be found in Bjerkaas and Forsyth (1980b). Much work has been done in England predicting rainfall up to 6 hours in advance by linearly tracking echo centroids (Browning et al. 1982a).

Correlation tracking. This tracker has been described in various guises in Rinehart and Garvey (1978) (interstorm tracking) and Smythe and Zrnic' (1983) (clear-air tracking). Extensive use has been made of a correlation-based tracker at McGill University for making rainfall forecasts (Austin and Bellon, 1974; Bellon and Austin, 1978).

Peak-cell tracking. This tracker follows local maxima in the reflectivity field, and has been described in Crane (1979).

2. Performance Assessment

Previous work on comparing radar trackers has been done by Elvander (1976). Elvander compared a centroid tracker, a correlation tracker producing one velocity for the entire field, and a pattern-recognition type algorithm developed at SRI (Stanford Research Institute) which isolates and tracks areas within the radar coverage. Elvander applied these algorithms to the same data sets, and used a uniform set of criteria for verification, something not available in the literature prior to the Elvander report.

Elvander used the vectors from the three trackers to translate echoes and thereby produce maps of predicted reflectivity. Elvander divided his coverage area into regions, and kept records on a region-by-region basis of hits (anticipating reflectivity will exceed a threshold), misses (not anticipating), and false alarms (incorrectly forecasting reflectivity will exceed a threshold). Hits, misses, and false alarms were combined into a single number, the "critical success indicator."

Elvander found the cross-correlation algorithm generally superior for use with zero tilt data (single elevation scan at 0.0 degrees), and the centroid tracker superior for use for volume coverage data. A significant result was that the more sophisticated SRI tracker did not provide any improvement. This report reaches a similar conclusion insofar as the Crane algorithm, another sophisticated tracker, does not provide marked improvement over centroid or correlation tracking. One thing to keep in mind, however, is that Elvander used a verification region of 4x4 or 8x8 nm (nautical mile), whereas the verification region in this report is 1 km by 1 km. Hence the Elvander report only gives a sense of the goodness of the gross features of the forecasts, and does not indicate whether the forecasts support planning for detailed, tactical cell avoidance.

A more recent report (Wieler et al., 1982) has compared the centroid and Crane trackers and has found general agreement between the two in terms of the estimated velocities, although the fine-structure velocity information in the Crane tracker was found to be suspect at greater ranges. They did not actually construct maps of predicted reflectivity.

Forecast of reflectivity areas for air traffic control purposes was done by Alaka et al. (1979). Using a grid box of 3x5 nm, the predicted reflectivity is a linear function of zero tilt reflectivity, echo top, and vertically integrated liquid-water content. The predicted reflectivity is also a linear function of extrapolated maps of the above three quantities, with the extrapolation based on a correlation-like algorithm (binary match). The predicted reflectivity is also a linear function of the reflectivity trend and the time of day. The actual coefficients of the linear functions are determined by multiple linear regression. A lower-limit criterion of 1 percent reduction of variance was used in the selection of predictors. Follow up work was done by Saffle and Elvander (1981) on a larger data set. For 12-minute forecasts of reflectivity, position extrapolation plus the inclusion of dBz trends was found superior to persistence in terms of reduction of variance between forecasted and actual reflectivity. For 36-minute forecasts, position extrapolation alone appeared to provide the best forecast. When volume scan data were available, extrapolated echo tops were also found to be a useful predictor of reflectivity level. Given the set of reflectivity predictors determined by multiple linear regression, Saffle and Elvander determined the resulting hits, misses, and the corresponding critical success index.

Neither Alaka et al. nor Saffle and Elvander discussed at length the implications of their reflectivity forecasts for air traffic control. Their performance assessment is in terms of area only, and hence does not address flight-path choice. Also, their verification region is fairly large (3x5 nm) and thus does not indicate whether detailed, tactical cell avoidance is supported by the forecasts. This report will introduce an additional performance criterion to assess flight-path choice, and will use a finer resolution grid to determine whether reflectivity forecasts provide useful, fine-scale reflectivity information.

II. THE TRACKING AND EXTRAPOLATION OPERATION

A. General Overview

1. Preprocessing

Any radar data set generally requires some pre-processing before it is suited to meteorological interpretation. The storm cases in this report have all been gathered at the MIT 10-cm radar (see Table II-1) or at the NSSL (National Severe Storm Laboratory) 10-cm Norman and Cimarron radars. Clutter suppression is done at MIT using a block mean level canceller (Anderson, 1981) and is not done at NSSL. To handle range ambiguities, the MIT radars use a random phase technique (Laird, 1981) while the NSSL radars have an expanded integrator mode.

The NSSL data required special pre-processing because of the presence of range-rings in expanded integrator data. In expanded integrator mode, three out of every four reflectivity mode pulses are suppressed, but during the suppression the klystron acts as a large noise source: hence rings appear. (See Appendix C for a description of how the rings are removed.) Also, the data sets obtained were not collected with automated tracking in mind: There is less than 360° coverage, the azimuthal limits change, and sometimes the number of elevation angles changes. Also, occasional glitches have been found in the indicated azimuth.

The data are run through a series of programs to produce fairly consistent volume scans: collections of fixed elevation scans in azimuth, with elevation varying from near zero to 10.0 degrees or so. The MIT data are collected with full 360° coverage. In both the MIT and NSSL data, the volume scan update time is approximately 5.0 minutes, as it will be in NEXRAD.

The MIT site is in the vicinity of many skyscapers; often "cells" will appear that in reality are only reflections from storms in other areas. The reflections occur in the azimuth sector 90° to 180° (north being 0°). For the cases observed, however, there was not a substantial amount of reflection at the dBz levels under investigation. If there were, echoes would be introduced with a velocity opposite to that of the true echoes.

For either radar, reflectivity estimates are not accepted unless the signal-to-noise ratio S/N exceeds 0 dB. For the MIT radar, a 0 dBz target at a range of 25 km produces a 0 dB S/N return. All returns within 30 km and below 1.5° elevation are censored from both data sets to minimize close in clutter.*

*This ability to ignore the clutter-contaminated bottom elevation tilt data at close range was an important advantage of volume scan data.

TABLE II-1

M.I.T. TESTBED RADAR CHARACTERISTICS

Antenna	
Aperture	18 feet
Gain	42 dB
Sidelobe Levels	-26 dB minimum
Beamwidth	1.45° one-way
Polarization	horizontal
Maximum rotation rate	6 r.p.m. (both axes)
Height	312 ft. above m.s.l.
Transmitter	
Source	VA87 klystron
Frequency	2705 MHz
Peak Power	1 MW
Pulse Width	1 microsecond
P.R.F.	Variable (1200 Hz max.)
Receiver	
Pre-selector	tunable cavity
RF amplifier	solid state
Noise figure	4 dB
STALO	crystal controlled
COHO	30 MHz crystal
Bandwidth	1.1 MHz
STC	PIN diode at RF
STC curve	Programmable
M.D.S.	-103 dBm
Digital Signal Processor	
A/D Converters	10 bits I; 10 bits Q
Range sample spacing	1/16, 1/8, 1/4, 1/2 n.m.
Number of range gates procesed	288
Algorithm	pulse-pair processing
Processor output	0th, 1st, 2nd moments

P.R.F. - pulse repetition frequency
STALO - stable local oscillator
COHO - coherent oscillator
STC - sensitivity time control
M.D.S. - minimum detectable signal

For the purpose of computing the altitude of a radar cell and in the interests of simplicity, a flat-earth is assumed with straight-line propagation.

2. Tracking and Forecast Map Generation

The three trackers are then run on the pre-processed data. Figure II-1 shows how the track associations are performed. As a byproduct, the centroid tracker produces volume cells, sets of fixed-level contours on conical surfaces at the various elevation angles. In the actual generation of forecasted reflectivity maps, it has been decided initially to ignore storm growth and decay. What remains is to utilize the displacement vectors from the various trackers to make forecasted maps. Section I briefly discussed the rationale for attaching the tracking vectors to fixed-dBz-level contours in order to make reflectivity predictions. The alternative would be to translate the radar cells themselves or the cells resampled onto a Cartesian grid. The problem with this is that differential motion will cause the cells to move apart, producing a confusing-looking reflectivity map. Methods to put the cells back together into storm segments would necessarily be heuristic. An attractive alternative and our chosen approach is to translate the fixed-dBz-level contours. Contours represent a useful compaction of the information content of the raw pixel positions. As the prediction time is increased and fine-scale information becomes less useful, the information content of the contours can be reduced still further by keeping only the lower-order coefficients of a Fourier expansion of the contours (Duda and Blackmer, 1972): this provides a natural way of smoothing the contours.

One difficulty with using reflectivity contours is that, due to the technical details of contour generation, small storm patches may be excluded. This is of concern for very short forecast times, where the reflectivity pixels themselves (truth map) may provide a better forecast (so-called persistance forecast) than translated contours. To address this problem, the contour algorithm has been adjusted to incorporate small storm areas. Figure II-2 is a typical truth map for a Massachusetts storm; Fig. II-3 shows the corresponding contours, without translation. Figures II-4 and II-5 are a comparison pair from an Oklahoma storm. The contours are quite faithful to the reflectivity actually present.

The next step is to attach track velocities to the various volume cells. In the case of the centroid tracker, the association between track velocity and volume cell is already defined. For the correlation and Crane trackers, volume cells are assigned averages of the track velocities in the immediate neighborhood of the dBz-weighted cell centroid.

The forecast is made by assuming constant track speed, thus curved tracks would not be handled correctly. The volume cells are translated in

INITIAL APPROACH: STRAIGHT-LINE EXTRAPOLATION OF CURRENT WEATHER PATTERN BASED ON LOCAL OR GLOBAL TRACKS

THE TRACKERS:

(1) FIXED-LEVEL REFLECTIVITY CELLS TRACKED BY CENTROID

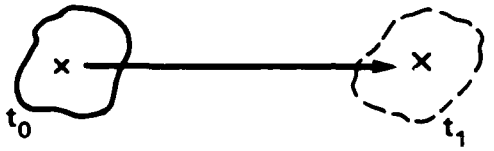

(2) TRACK LOCAL MAXIMA IN REFLECTIVITY FIELD

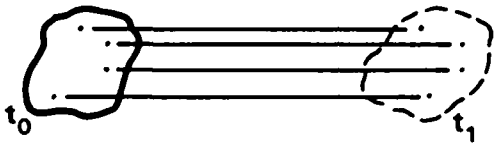

(3) CROSS-CORRELATE REFLECTIVITY FIELDS AT DIFFERENT TIMES

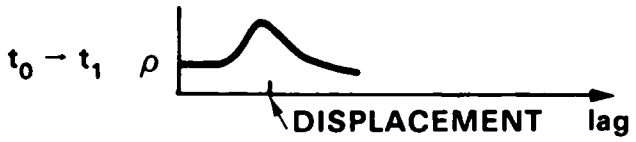

Figure II-1. Tracking/prediction methods we have evaluated.

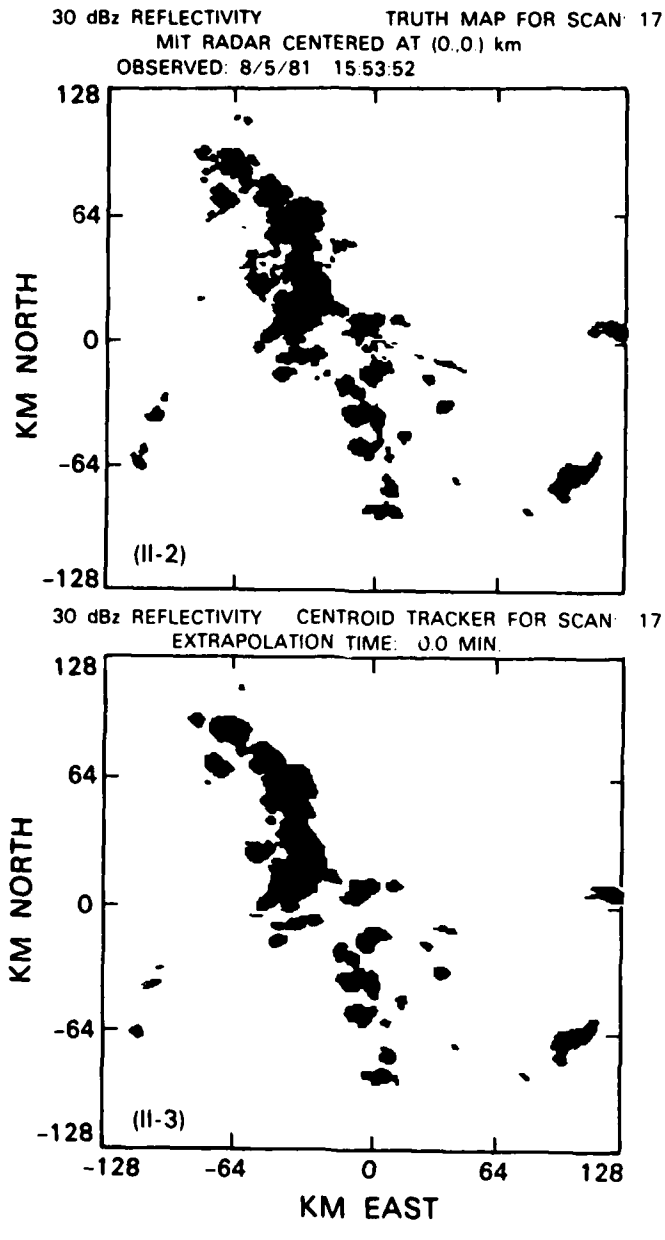

Figure II-2., II-3. Truth map and filled contours for a Massachusetts storm.

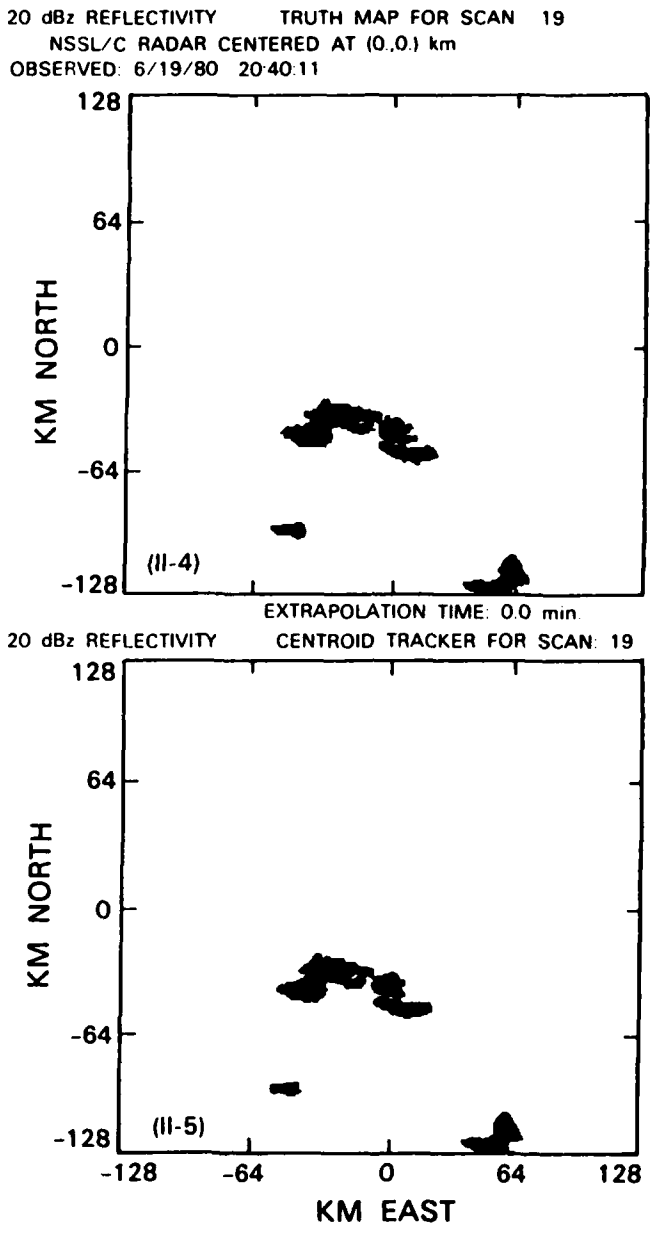

Figure II-4., II-5. Truth map and filled contours for an Oklahoma storm.

a straight-line horizontal motion with no provision for growth or decay. There is no limitation on which reflectivity level could be forecast, but typically 30 dBz has been chosen in this report because that appears to be a favorable level for the centroid tracker. In one case the data have required the choice of a 20 dBz level, and 40 dBz was suitable for another case. There is no reason why something closer to the full dBz information originally found within the volume cell could not be kept during the forecast, and in fact such a procedure is suggested in Appendix A, which describes a forecasted reflectivity product designed for NEXRAD implementation.

After the contours are translated, they are clipped between two specified altitude limits. The limits in this report were chosen to be 0 and 4 km (~12,000 feet) to be analogous to a NEXRAD, low-altitude reflectivity layer. These clipped contours are then projected downwards onto a Cartesian grid, with a pixel size of 1 km by 1 km.

B. Details of the Storm Slices

The details of construction of the storm slices generally follow Bjerkaas and Forsyth (1980a). A radial is searched for a segment of minimum length 2.3 km which exceeds the chosen threshold, typically 30 dBz. Adjacent radial segments are combined to form a cell slice if the segments overlap by a minimum amount of 1.2 km. These cell slices define a set of contours on conical surfaces. Bjerkaas and Forsyth combine cell slices at different elevations into a volume cell if their centroids are separated by no more than 2 km in the x or y coordinates (horizontal). We examined tracking of such volume cells previously (Brasunas and Merritt, 1981), and we decided to form volume cells instead by looking for an area overlap of cell slices. Typically, we require a 10 percent overlap. Figure II-6 shows centroid track results with the original volume cell definition for an MIT August 5, 1981 storm. Figure II-7 shows the same storm tracks with the revised definition of a volume cell. (The square is for the initial scan). Note the improvement in track error.

C. Details of the Centroid Tracker

Our implementation of the (dBz-weighted) centroid tracker follows the description in Bjerkaas and Forsyth (1980a). Starting with the largest volume cell in the current volume scan, associate with it the largest volume cell in the previous scan whose centroid lies in a box of length $2V_{max}\,\Delta t$ km, where Δt is the volume scan time difference in minutes and V_{max} is the storm speed limit (2.0 km/min for the work described here.) The box is centered on the current volume cell position. The association list is kept for up to 12 time steps, and the current track velocity is determined by passing a best-fit line through the associated centroid positions.

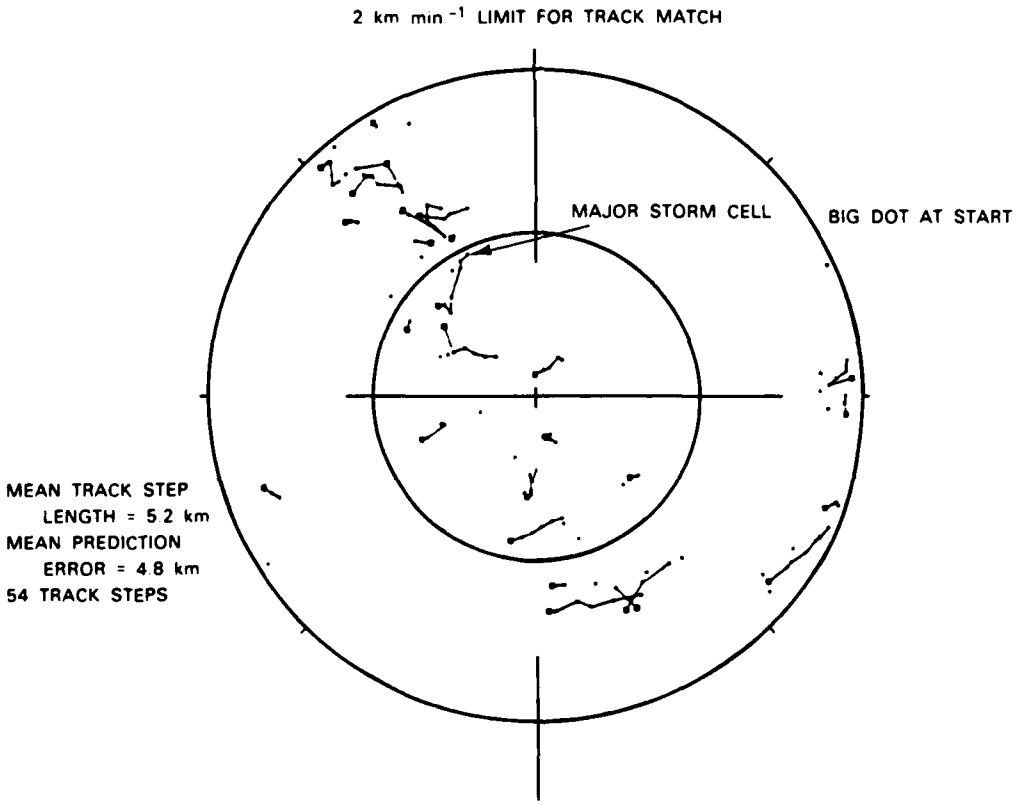

Figure II-6. Tracks of original volume cells.

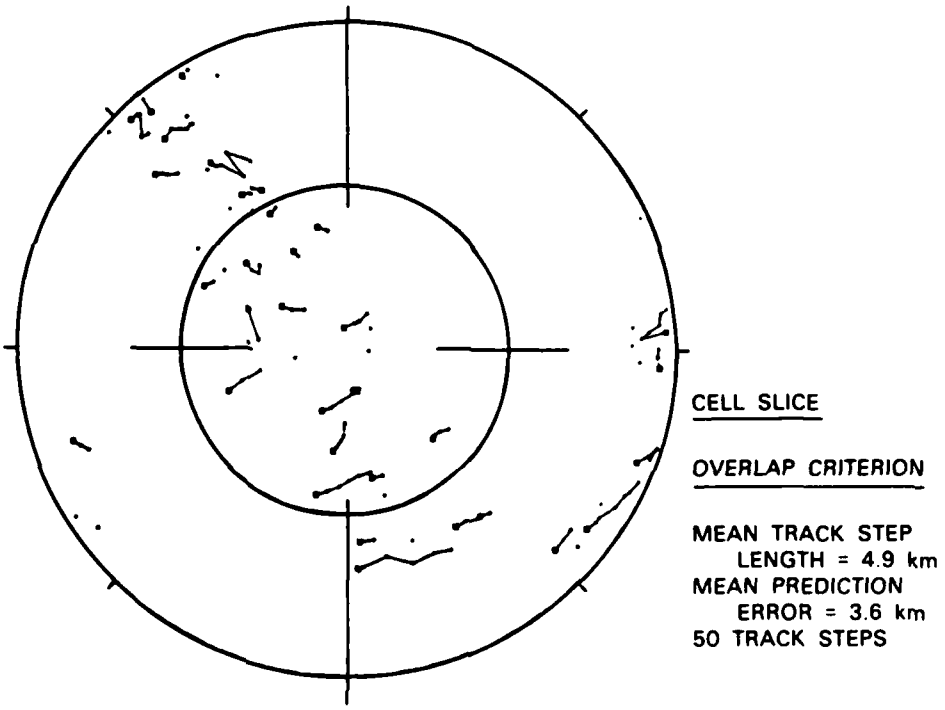

Figure II-7. Tracks of revised volume cells.

D. Details of the Correlation Tracker

The correlation tracker is a simple, single-displacement tracker with no consideration of track history, because it does not track "objects". The current observation field is divided into a square-box array, with a typical box length of 28 km. Each square is translated to find the best correlation match within the prior radar volume scan. The derived displacement determines the tracker velocity. Further details can be found in Appendix A.

E. Details of the Crane Tracker

The original work on the Crane algorithm was done at Lincoln Laboratory in the mid-70's under FAA sponsorship (Crane, 1979). The algorithm finds local maxima in reflectivity within a minimum-dBz-level contour, which we have variously chosen to be 20, 30, or 40 dBz. We have set this level to the same value we use for the centroid tracker. We keep all local maxima inside the contour, by resetting the parameter which determines the minimum peak kept. Peak cell characteristics such as area are determined from the contour 3 dB down from the local maxima. It is hoped that these peak cells correspond to convective cells. Peak cell match is determined over time by a weighted consideration of agreement in reflectivity level, area, height, and advection-corrected centroid position. The set of peak cells that match at any one time form a three-dimensional entity known as a volume cell, much smaller than the volume cells found by the centroid tracker. The current track velocity is determined recursively, by computing a weighted average of the most recent displacement and the previous-step track velocity. The weights used are 0.4 for old track velocity and 0.6 for current displacement. Unlike the other trackers, there is a non-zero initialization velocity; we have used 17 $m\text{-}s^{-1}$ from the direction of 250°. After the second displacement, the Crane tracker results generally appear to be close to their "steady-state" value. We have noted erratic tracker performance if the volume scan time difference approaches 15 minutes.

Although the Crane algorithm can process Doppler information in addition to reflectivity, this does slow down the algorithm and we did not find an improvement in tracker performance. Thus we have chosen to work on reflectivity alone.

F. Persistence/Status-Quo

A persistence forecast simply predicts that nothing at all changes. Our persistence forecasts are not generated from contours. All radar cells in the altitude range of 0-4 km are kept which exceed the reflectivity threshold (generally 30 dBz) of our centroid tracker volume cells. Point targets are removed by rejecting radial segments less than three bins long.

The remaining radar cells are projected downwards on a Cartesian grid of pixel size 1 km by 1 km. This pixel map serves both as "truth", against which the other forecasts are compared, and as the persistence forecast itself.

III. METHODS OF SCORING THE FORECASTS

A. Subjective Methods

Each tracker produces a vector field which is updated with each new volume scan. These fields can be checked for internal consistency, both spatially and temporally. These fields can be checked for agreement with wind data obtained from soundings, and with the actual storm motion that occurs.

The trackers in combination with the storm contours produce pixel-based prediction maps. These maps can be qualitatively compared with the true reflectivity maps.

B. Objective Methods

The forecast map and the truth map are both pixel-based. Our objective scores are in terms of false alarms and false safes; the first scoring method, the "area" method, tallies false alarms and false safes on a pixel-by-pixel basis. A false alarm occurs when a pixel is predicted to be above threshold, but is not. A false safe occurs when a pixel is predicted to be below threshold, but is not. The probability of false alarm (PFA) is defined as the ratio of false alarms to alarms. The probability of false safe (PFS) is defined as the ratio of false safes to "hazards" (pixels above threshold). Hence the probability of false safe satisfies the equation

$$PFS = 1 - POD \ ,$$

where POD is the probability of detection. Figure III-1 shows, by means of cross-hatching, how false alarms and false safes are related to the extent to which forecasted areas and "true" areas do not overlap.

Due to the finite range of the radar, accurate predictions cannot be made near the periphery. Hence false alarms and false safes are determined only out to the maximum range minus a distance equal to the product of storm speed and prediction time interval. Furthermore, errors of one pixel are not counted in the false alarm and false safe statistics. That is, when a contour is being translated, a tiny error may determine whether or not it crosses a particular pixel boundary. To free the statistics of this pixel "quantization" effect, a false alarm is not recorded unless, for a predicted pixel, neither that pixel nor any of its eight nearest neighbors is above the threshold. A similar approach is taken to tallying false safes. This approach will of course make the false safe and false alarm statistics look better, but it is felt that a one pixel error is not meaningful, especially in light of the technical differences in the construction of the truth maps and forecast maps.

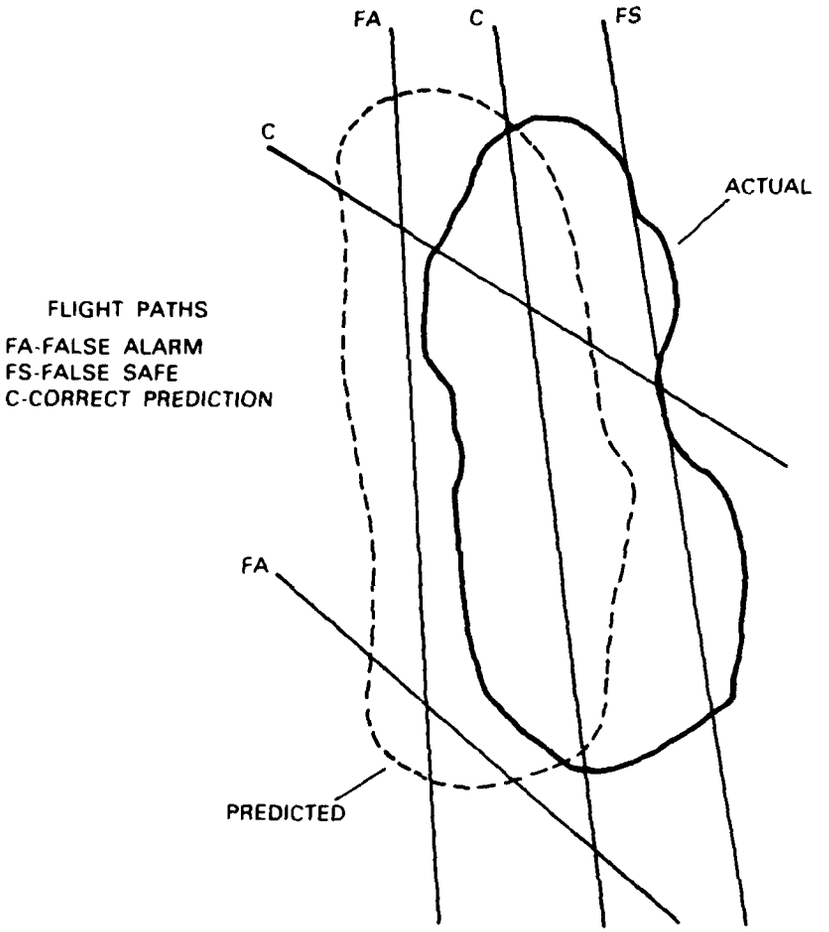

Figure III-1. Objective evaluation of forecasts.

The area approach to false safes and false alarms reflects our success in putting the storm cells in the right places. It is of obvious use in watershed management. It is of use to air traffic control because if the storm cells are extrapolated to correct positions, we will know when departure gates, descent corridors, and so on will certainly be affected by a storm.

Our second approach to tallying statistics, the so-called "flight-paths" approach, is not done on a pixel-by-pixel basis. Rather, flight-paths are drawn through the radar data. If a given flight path intersects at least one pixel predicted to be above threshold, but not a single pixel actually above the threshold, this is one false alarm. Similarly if a given flight path intersects at least one above-threshold pixel, but not a single pixel predicted to be above threshold, this is one false safe. (See Fig. III-1.) The flight-path approach takes into consideration quantization effects and the edge of field effect, as does the area method.

Rather than use actual air-routes, we have chosen so far to use many air routes, such that almost every location has flight-paths going through it in all directions. We use a Monte-Carlo technique to generate 2000 straight paths; this appears sufficient to give us a uniform density of paths. Also, in the highly specialized case where the predicted and truth contours are circles of the same diameter, it is possible to derive an analytic answer for false safes and false alarms for both the area and flight-paths methods. This has been done, verifying our area statistics to be correct, and our flight-path statistics to be correct to within a few percent. Figure III-2 shows the results of the analytic calculations, although it must be warned that the curves are somewhat loosely drawn. Note that POD and PFA sum to one in this specialized case.

Figure III-2 indicates that the flight-path statistics will generally look better than the area statistics. This is a real effect, since even when a storm contour is extrapolated to a slightly wrong position, it may still prevent some flights from entering the hazardous region.

The flight-path statistics obviously depend on the lengths of the paths used to generate the statistics. On the one hand, the area statistics are mathematically equivalent to employing very short paths. On the other hand, our flight paths are randomly placed in a circle of radius 135 km, and so have a maximum length of 270 km. These issues are discussed at greater length in section VI-B.

Tallying false alarms and false safes allows us to objectively compare the various trackers. However, it must be stated at the outset that the meaning of the statistics of the trackers in an absolute sense, as opposed to their relative ranking, is not well understood. The cost structure is not known for false alarms and false safes. It is probably correct

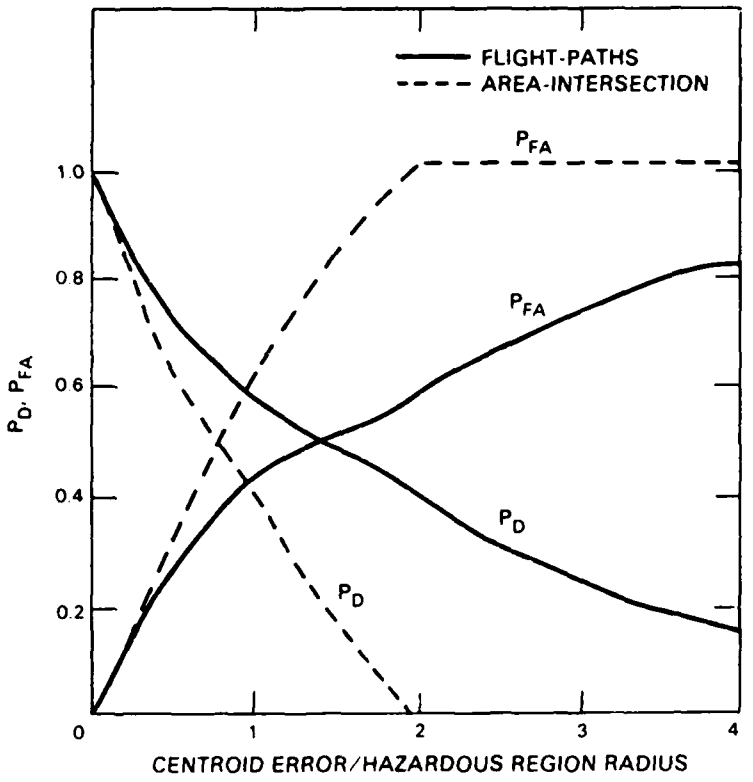

Figure III-2. Detection and false-alarm probabilities for circular hazardous regions.

to say that airway efficiency dictates the choice of a tracker whose false alarms do not exceed a certain rate, while safety demands that the sum total of false safes be minimized. Additionally, the credibility of the trackers will suffer if the false alarm rate is too high.

IV. FIVE STORM CASES

Five storm cases are examined in detail, three observed at MIT and two at NSSL. Data are considered out to a range of 130 km. We have full 360° coverage from M.I.T, and azimuthal sectors from NSSL. The volume scan update time is generally six minutes.

Other sources of data can be considered in the future, if these sources provide volume coverage with a pencil-beam radar, with an update time of roughly six minutes. All data, regardless of source, are put into a common format before further processing.

A. General Characteristics and Subjective Evaluation

1. August 5, 1981 at M.I.T.

On August 5, 1981, a cold front was approaching New England from the west. A very warm and humid air-mass lay ahead of the front, and active thunderstorms developed throughout New England. At the time of the radar observations, the front was in the vicinity of the New York-Massachusetts border. Table IV-1 gives various details of the storm and the various trackers. On this day the clutter filter was not implemented; therefore radar returns with mean speed less than 0.3 m s^{-1} have been rejected in software.

Figures IV-1 and IV-2 show two truth maps roughly thirty minutes apart. Track velocities appropriate for the earlier time are shown in Figs. IV-3, 4, and 5. For the centroid tracker, numerous volume cells are not in track; they are assigned zero velocity. In Fig. IV-3, the short crossbars are the vector tails, and the canonical length in the lower left-corner represents 1.0 km/min. Many of the centroid velocities are towards the north-east, but there is considerable scatter. There is definitely a problem in maintaining track; this has been a problem for the centroid tracker in all the cases we have investigated when a storm is spatially extended. By comparison, the correlation and Crane vectors show temporal and spatial consistency. The direction of the Crane vectors is not much different from the initial direction, but the speed is only half of the initial value. Figures IV-6, 7, and 8 show the various prediction maps.

The various trackers agree with actual storm motion, except for the considerable scatter in the centroid velocities. There is general agreement in direction between the storm motion and the environmental winds, as might be expected since there was little vertical shear of the winds.

2. August 11, 1981 at M.I.T.

On August 11, 1981, a squall line formed in advance of a N-S cold front in New York state. Table IV-2 gives the various details for this

TABLE IV-1

Storm	August 5, 1981 at M.I.T.
General storm motion	0.5 km/min., towards 67°
dBz structure	59 dBz maximum; approximate north-south line extending 150 km; centroid tracker and Crane tracker run with 30 dBz threshold; contours cover 7-13% of total area, and intercept 45-75% of flight-paths
Echo tops	Some cells up to 34 kft, most do not exceed 28 kft
Centroid velocity	0.7 km/min. towards 60°, much scatter
Correlation velocity	0.5 km/min. towards 70°
Crane velocity	0.5 km/min. towards 70°
Sounding at Chatham, MA	
0-10 kft	0.9 km/min. towards 75°
10-20 kft	0.9 km/min. towards 80°

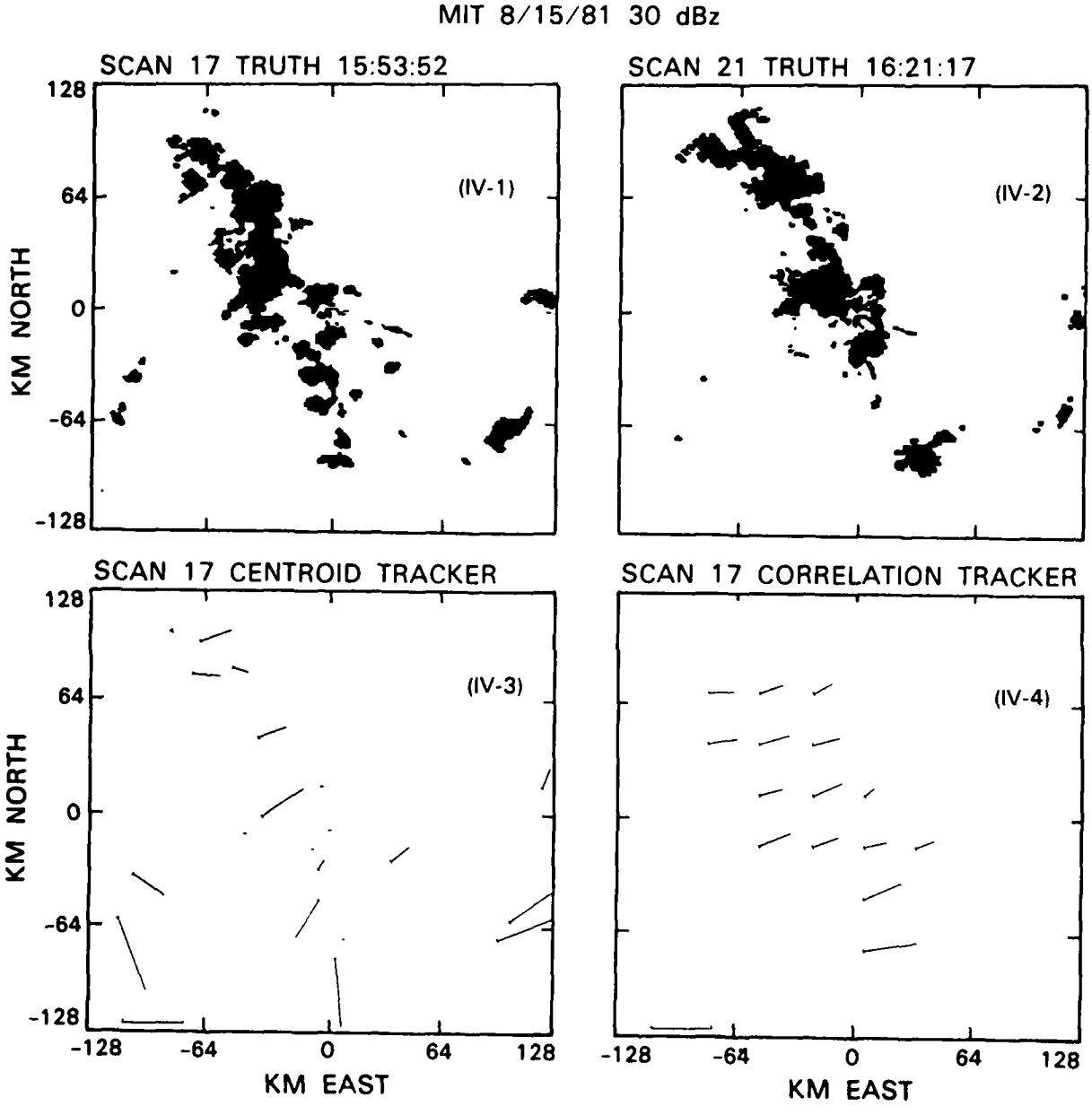

Figure IV-1. to IV-4. M.I.T. 8/5/81 30 dBz.

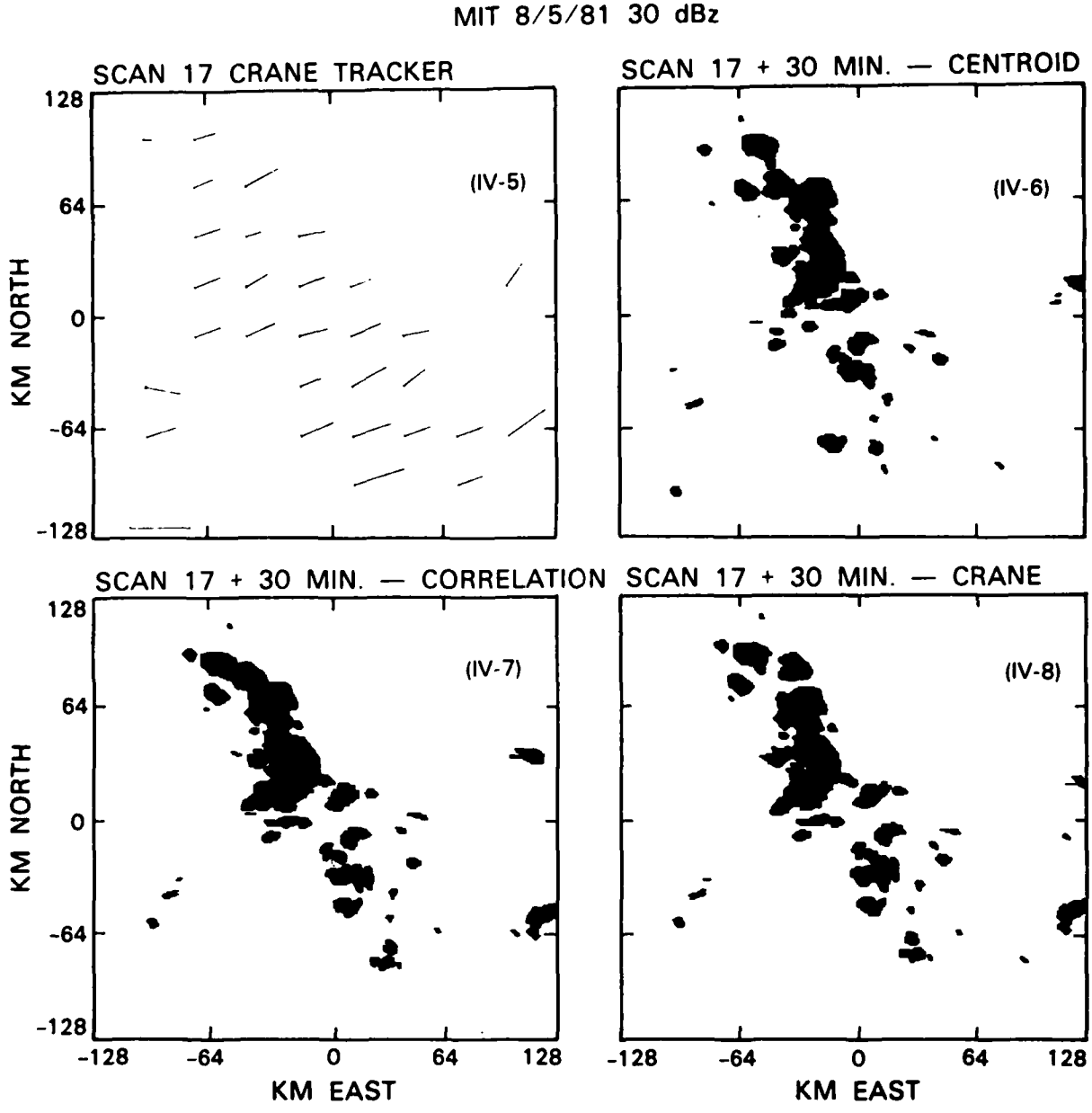

Figure IV-5. to IV-8. M.I.T. 8/5/81 30 dBz.

TABLE IV-2

Storm	August 11, 1981 at M.I.T.
General storm motion	0.6 km/min., towards 74°
dBz structure	54 dBz maximum; SW-NE line extending more than 200 km; centroid tracker and Crane tracker run with 30 dBz threshold; contours cover 5-10% of total area, and intercept 46-55% of flight-paths
Echo tops	Some cells up to 28 kft, more extensive area at 22 kft
Centroid velocity	0.8 km/min. towards 55°, much scatter
Correlation velocity	0.8 km/min. towards 60°
Crane velocity	0.8 km/min. towards 60°
Sounding at Chatham, MA	
0-10 kft	0.8 km/min. towards 45°
10-20 kft	0.8 km/min. towards 75°

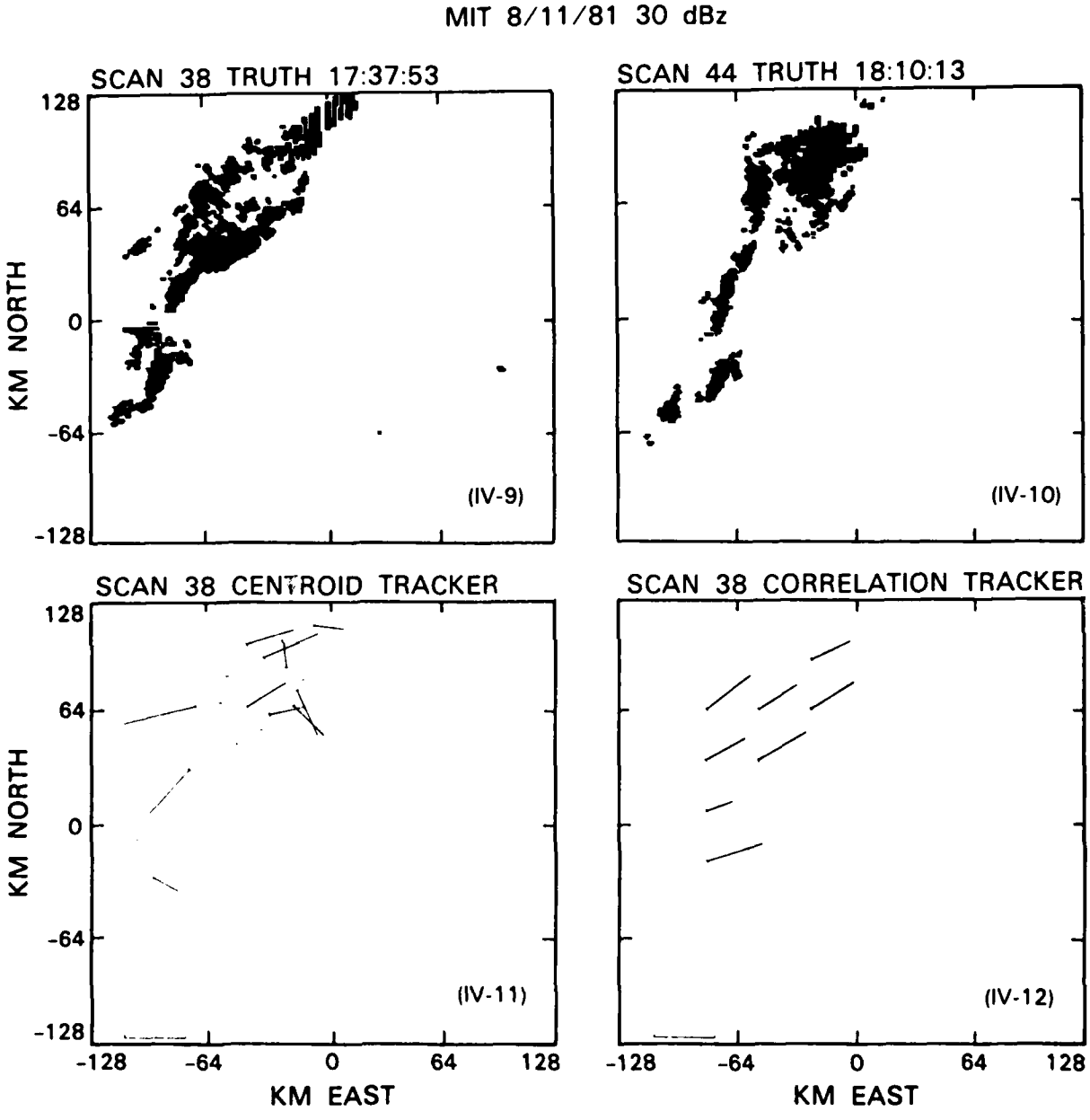

Figure IV-9. to IV-12. M.I.T. 8/11/81 30 dBz.

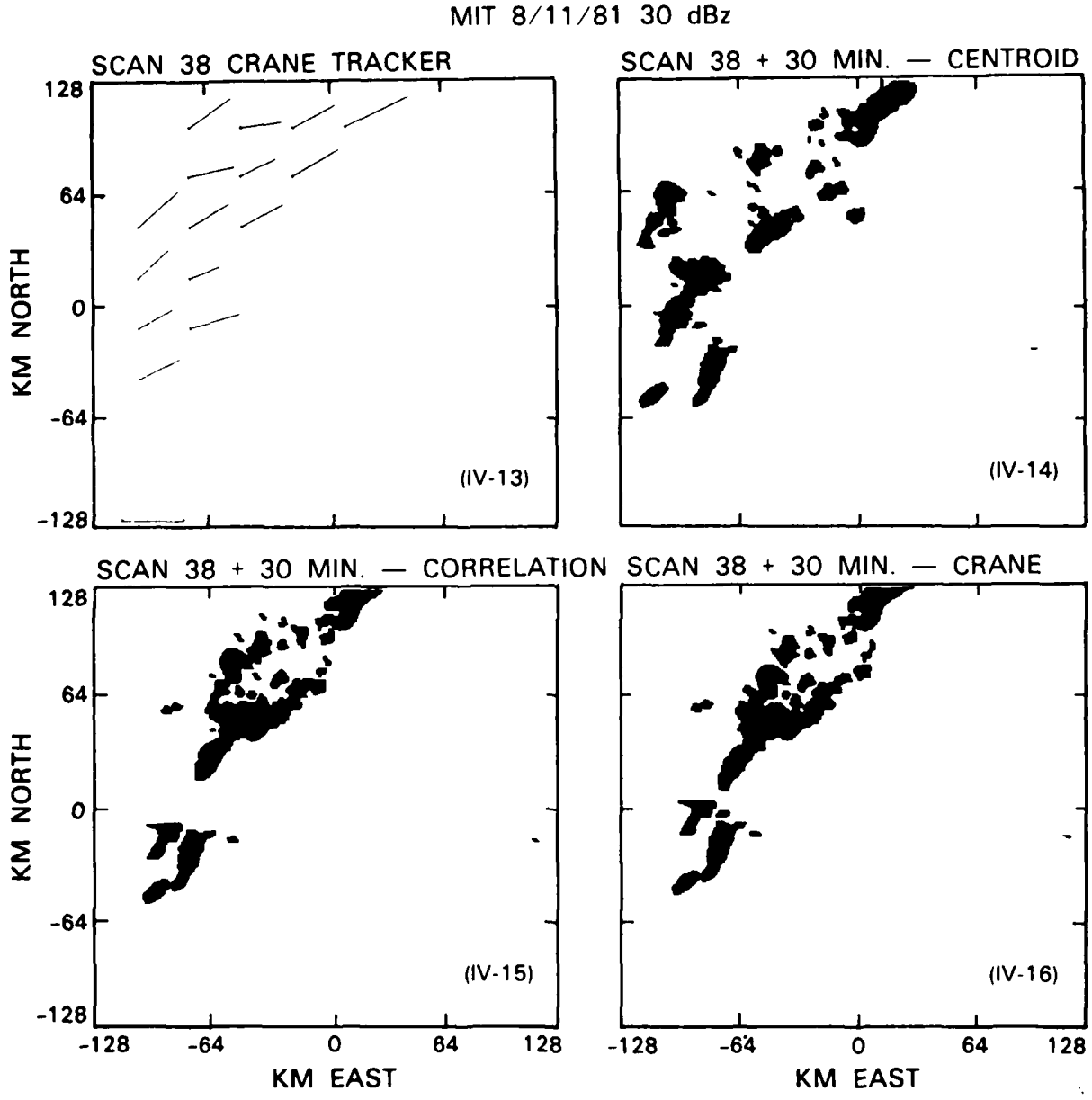

Figure IV-13. to IV-16. M.I.T. 8/11/81 30 dBz.

storm. Figures IV-9 and IV-10 are two truth maps spaced roughly thirty minutes apart.

Figures IV-11, 12, and 13 show the various track velocities for the earlier truth map. Figures IV-14, 15, and 16 show the corresponding prediction maps. The predominant motion is towards the northeast, but there is considerable scatter in the centroid velocities. This manifests itself in the scatter in the centroid-based prediction map.

The correlation and Crane track vectors agree fairly well with the actual storm motion, although they are about 15° counter-clockwise from the correct direction. Many of the centroid vectors do not agree with the storm motion, again reflecting difficulties in tracking extended storms. There is some vertical shear in the horizontal winds, and the higher-level winds agree fairly well with the actual storm motion.

3. August 12, 1981 at M.I.T.

On August 12, 1981, a storm system developed to the south of New England. Table IV-3 gives the details for this storm. Figures IV-17 and IV-18 are two truth maps spaced roughly thirty minutes apart.

Since this storm has compact elements, it would have been expected that the centroid tracker should perform well. Such, however, was not the case. The available storm fragments often did not qualify as volume cells; in this case we assign them a zero velocity. Figure IV-19 shows only one volume cell, which was assigned a fairly reasonable velocity. Figures IV-20 and 21 show that there were several correlation velocities, and many Crane velocities. Figures IV-22, 23, and 24 show the various prediction maps.

The correlation and Crane velocities agree fairly well with the actual storm motion. Agreement is less good with the centroid tracker, and many storm fragment do not qualify as volume cells. There is substantial speed shear but little direction shear in the horizontal winds; the upper level wind roughly agrees with the actual storm motion.

4. June 19, 1980 at NSSL

On June 19, 1980, severe thunderstorms formed in advance of a slow-moving warm front and an upper-level short wave. On this day, Cimarron reflectivities were about 10 dBz low, so 10 dBz have been added to the figures in Table IV-4. Figures IV-25 and 26 show two truth maps spaced 35 minutes apart. Figures IV-27, 28, and 29 give the track velocities, and Figs. IV-30, 31, and 32 show the corresponding prediction maps.

Unlike the M.I.T. cases, there is much better agreement between the actual storm motion and the centroid velocities than between the storm motion and the correlation or Crane velocities. One noticeable difference

TABLE IV-3

Storm	August 12, 1981 at M.I.T.
General storm motion	1.1 km/min., towards 45°
dBz structure	35 dBz maximum; very scattered 20 dBz cells; towards the end of the observation run, a 30 dBz cell appeared in the south; centroid tracker and Crane tracker run with 20 dBz threshold; contours cover 1.5 to 4.0% of total area, and intercept 26-50% of flight-paths
Echo tops	Some at 16 kft, but tops are generally near 10 kft
Centroid velocity	0.5 km/min. towards 65°, (cells often not in track)
Correlation velocity	1.0 km/min. towards 55°
Crane velocity	1.0 km/min. towards 45°
Sounding at Chatham, MA	
0-10 kft	0.6 km/min. towards 70°
10-20 kft	1.2 km/min. towards 75°

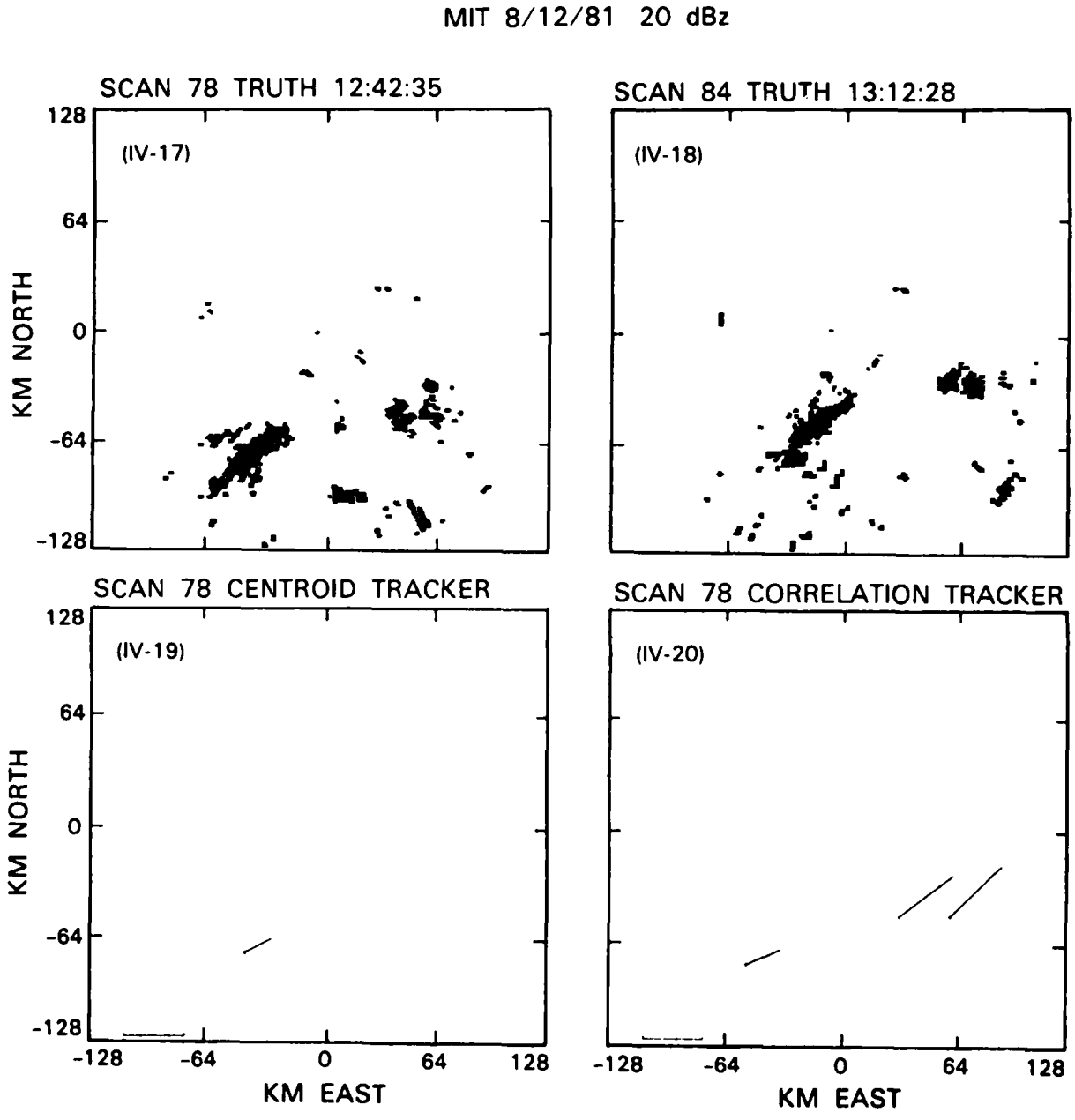

Figure IV-17. to IV-20. M.I.T. 8/12/81 20 dBz.

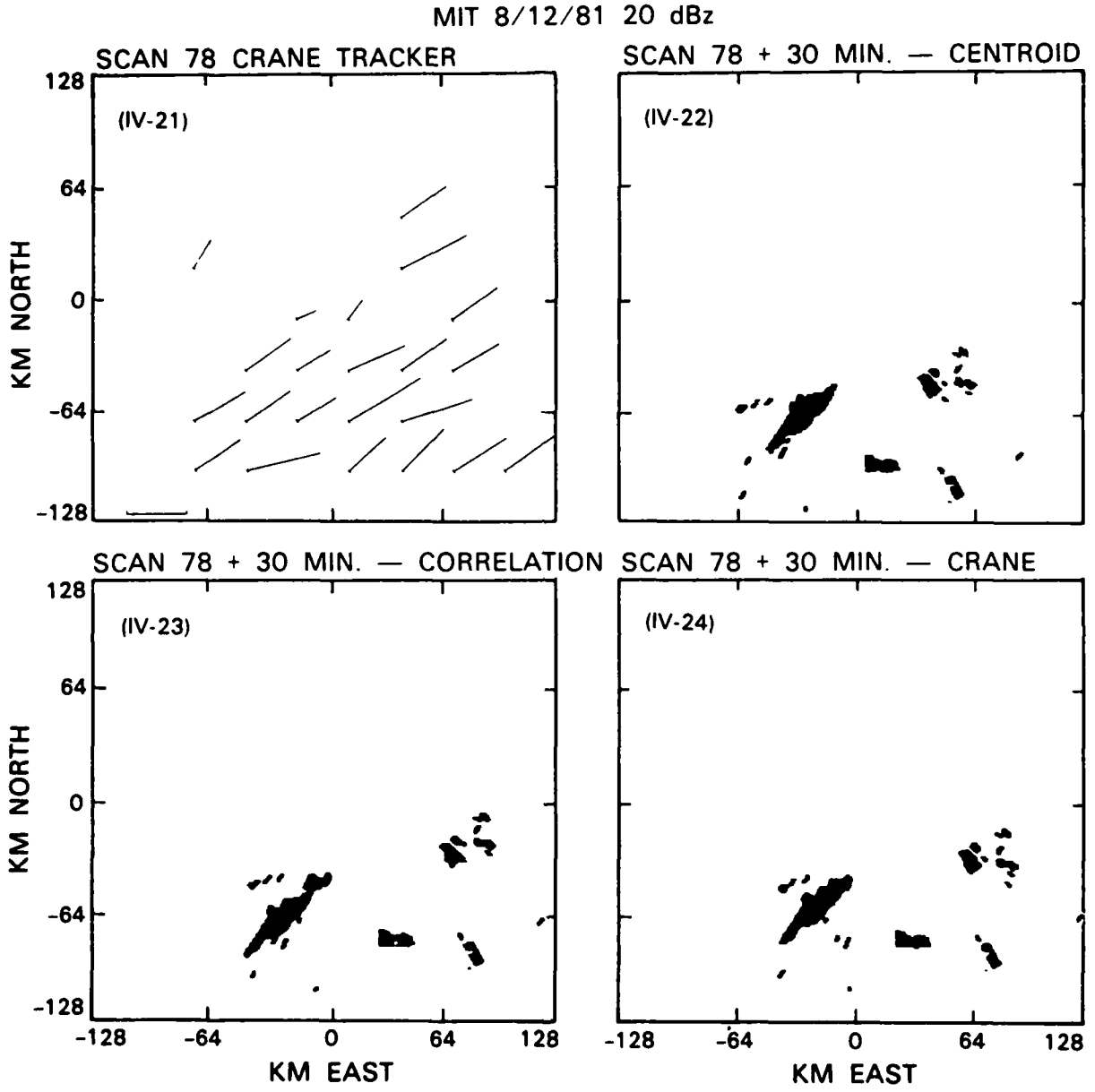

Figure IV-21 to IV-24. M.I.T. 8/12/81 20 dBz.

TABLE IV-4

Storm	June 19, 1980 at NSSL (Cimarron)
General storm motion	0.5 km/min., towards 125°
dBz structure†	57 dBz maximum; E-W "line" structure extending 60 km; centroid tracker and Crane tracker run with effective 30 dBz threshold; contours cover 2-3% of total area, and intercept 20% of flight-paths
Echo tops	Southern cell exceeds 40 kft; closer cell partly exceeds 40 kft
Centroid velocity	0.6 km/min. towards 140°, (scattered)
Correlation velocity	0.5 km/min. towards 90°
Crane velocity	0.7 km/min. towards 85°
Sounding at Oklahoma City	
0-10 kft	0.4 km/min. towards 0°
10-20 kft	0.7 km/min. towards 100°

† dBz's read low - 10 dBz have been added to the recorded data

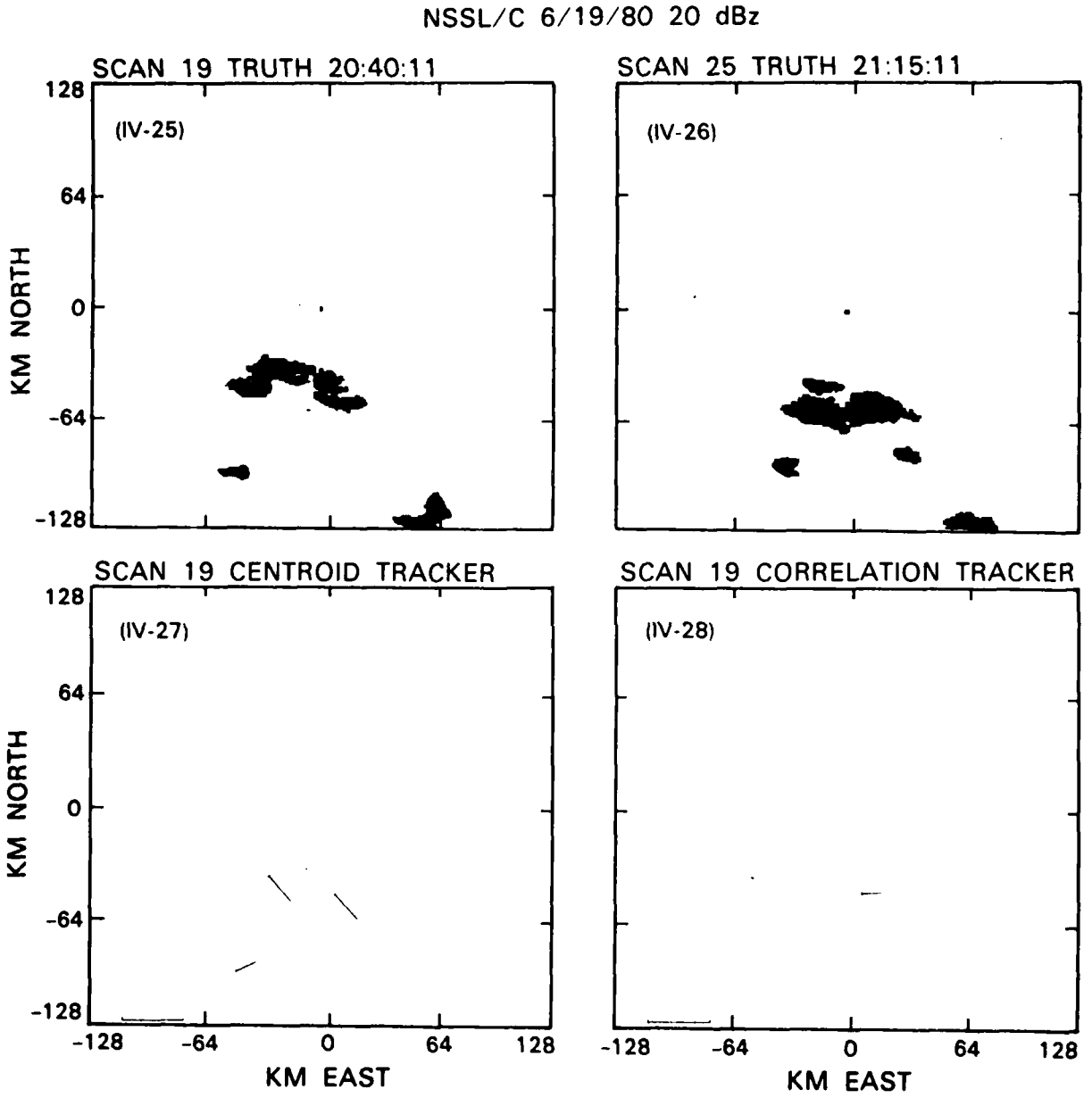

Figure IV-25. to IV-28. NSSL/C 6/19/80 20 dBz.

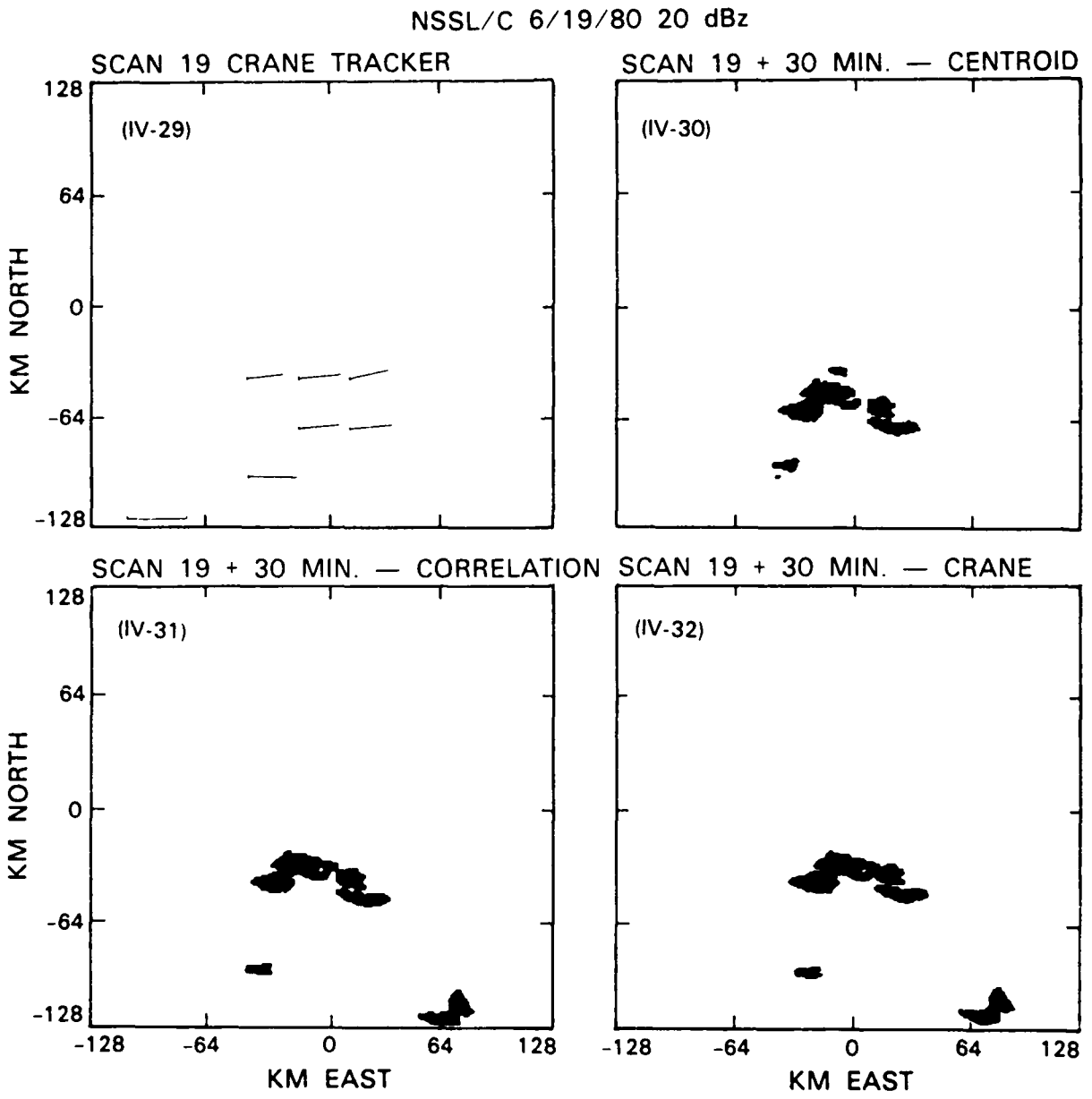

Figure IV-29. to IV-32. NSSL/C 6/19/80 20 dBz.

about this Oklahoma storm is that there is considerably more vertical shear of the horizontal wind, especially in direction. When substantial shear is present, there is greater likelihood of severe storms, and of the various storms moving in different directions.

On this particular day, our closer cell began with a motion to the east, and then intensified and turned to the southeast. A nearby storm also moved to the southeast, while another storm in the north moved due east. Eastern travel follows the higher-level winds, but travel to the southeast is not following the environmental winds. Previous research in storm tracking has divided storm motion into translation, which follows the environmental winds, and propagation, which results from steady-state growth/decay. When the environmental winds turn clockwise with height, a storm often travels to the right of the environmental winds.

The correlation and Crane trackers seem to be following the translation. This is not surprising in the case of the Crane algorithm, which was designed to follow the translation of individual cells. Various attempts were made to enable the correlation tracker to follow the net storm motion. Correlating dBz instead of liquid water content ($\sim Z^{1/2}$) had little effect. Correlating a higher altitude reflectivity layer, 4-8 km, had little effect. Changing the basic pixel size had little effect. Changing the size of the correlated region had little effect. What did matter was changing the time interval between correlated scans. Correlating scans fifteen minutes apart produced a velocity vector of 0.4 km/min. towards 120°, which is very close to the actual motion.

Over time the correlation and Crane algorithm consistently produce the wrong direction of storm motion. Hence the observed forecast errors are not the result of curved storm trajectories.

5. April 13, 1981 at NSSL

On April 13, 1981, severe thunderstorms developed along a cold front boundary. Storm details are given in Table IV-5. Figures IV-33 and IV-34 are two truth maps, roughly twenty minutes apart. Due to the vagaries of volume scan update times and azimuthal scan limits, we cannot verify a forecast longer than 20.0 minutes on this day. Figure IV-35 shows the centroid velocities, which are bothered by the extended nature of this storm. Figure IV-36 shows the correlation velocities. There is some scatter, but the same scatter is also observed in Hamidi et al. (1983), who also track this storm. The Crane velocities in IV-37 show considerably more uniformity. Figures IV-38, 39, and 40 show the corresponding prediction maps.

This NSSL storm also shows storm motion to the right of the correlation and Crane velocities, and substantial vertical shear of the horizontal wind. However, the centroid tracker is not noticeably better, as it is hindered by the extended nature of this storm.

TABLE IV-5

Storm	April 13, 1981 at NSSL (Norman)
General storm motion	1 km/min., towards 90°
dBz structure	68 dBz maximum; approximate SW-NE line extending beyond 200 km; centroid tracker and Crane tracker run with 40 dBz threshold; contours cover 5% of total area, and intercept 38% of all flight-paths
Echo tops	Exceeding 40 kft in some regions
Centroid velocity	1 km/min., erratic direction
Correlation velocity	0.8 km/min. towards 65°
Crane velocity	0.9 km/min. towards 65°
Sounding at Oklahoma City	
0-10 kft	0.6 km/min. towards 20°
10-20 kft	1.0 km/min. towards 70°

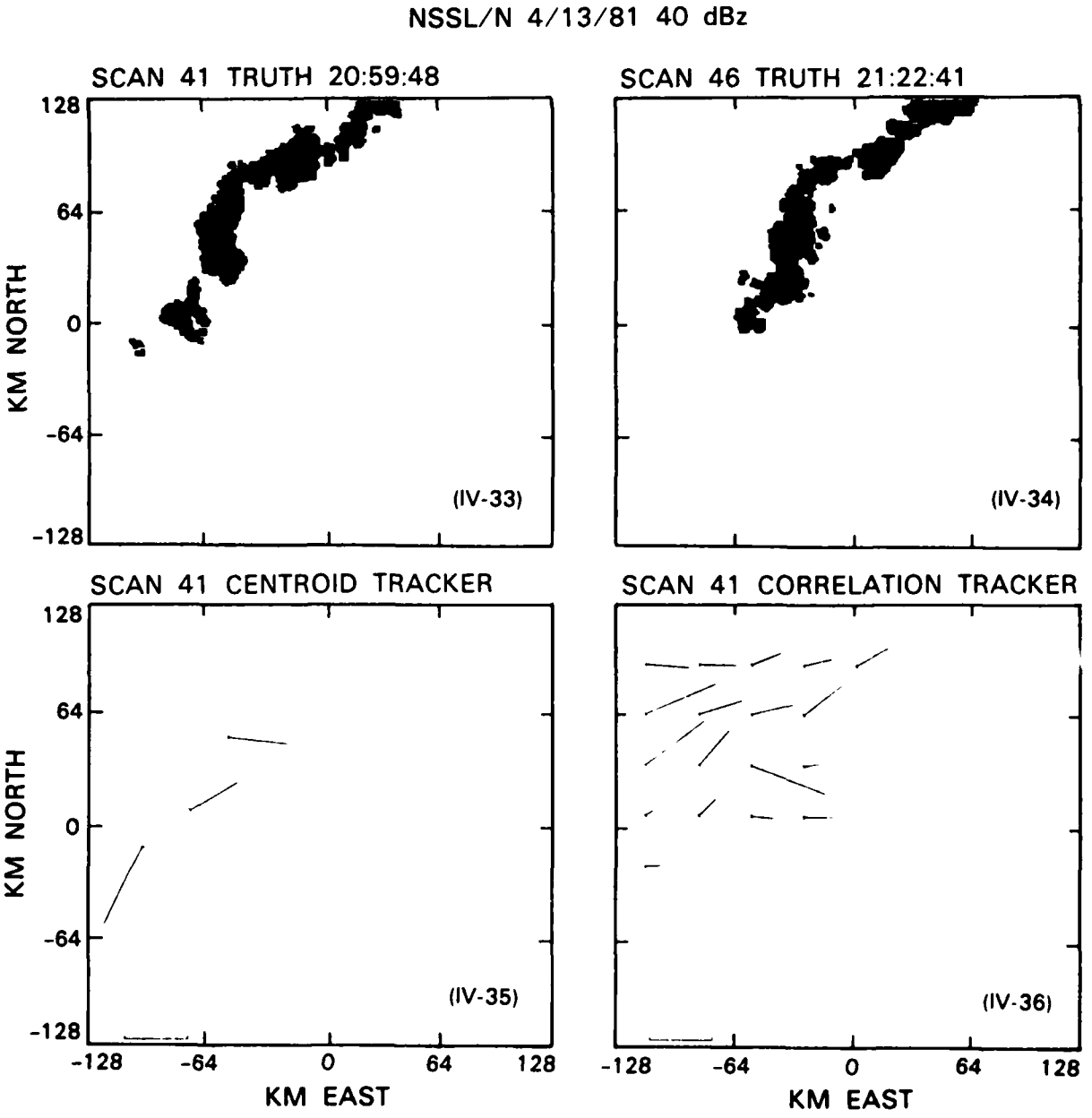

Figure IV-33. to IV-36. NSSL/N 4/13/81 40 dBz.

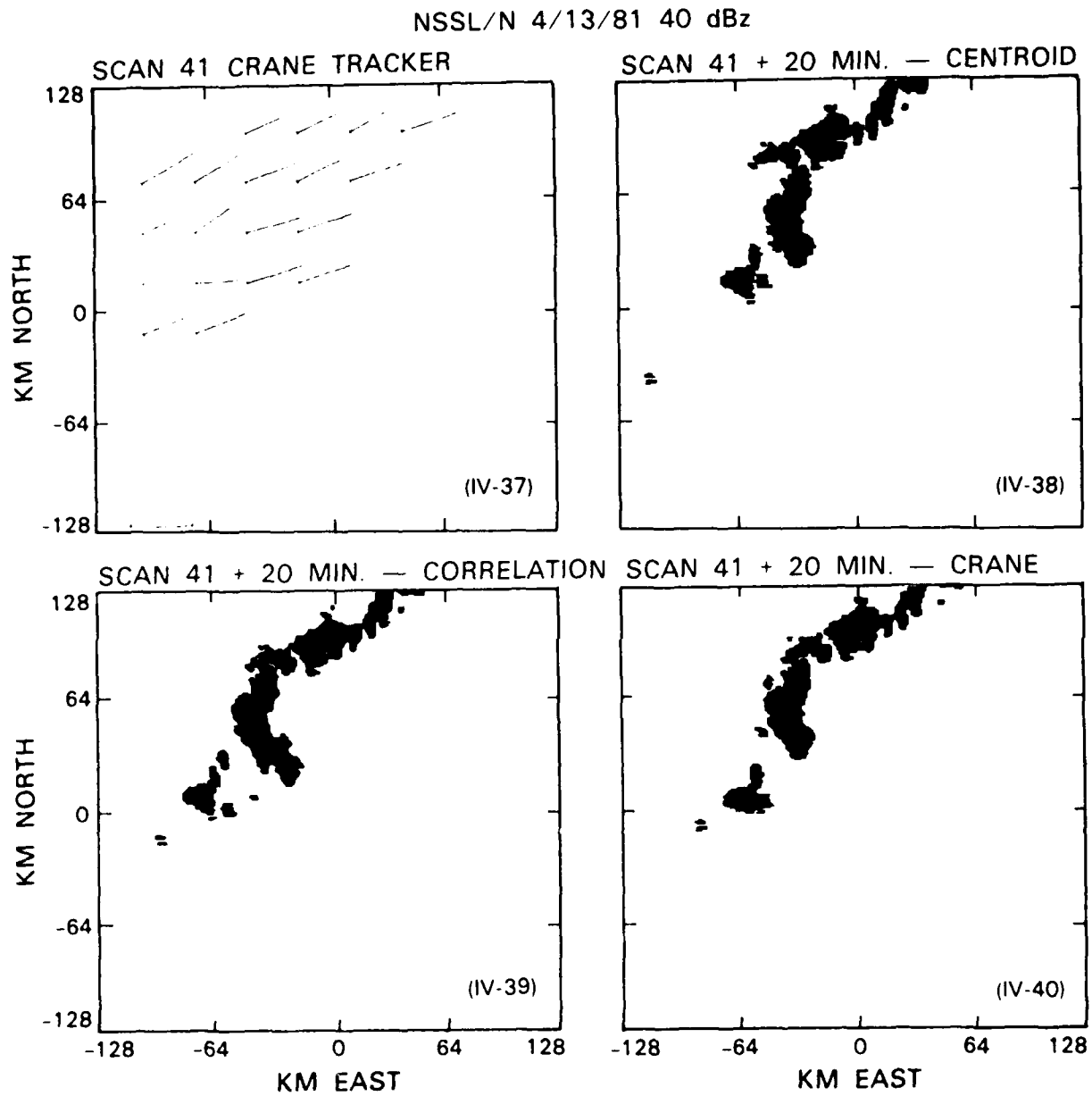

Figure IV-37. to IV-40. NSSL/N 4/13/81 40 dBz.

B. Objective Evaluation of the Forecasts

Figures IV-41 through IV-68 present the false safe and false alarm statistics for the five cases studied. Each storm, except for the fifth, has 10, 20, and 30 minute forecasts. These forecasts are evaluated by the area and flight-paths methods. The results will now be briefly summarized.

For August 5, 1981, area evaluation of the thirty-minute forecasts indicates that the correlation and Crane trackers both provided improvements over persistence in false alarms and false safes. The centroid tracker appears to have problems with extended storms. Similar improvement over persistence is seen in the twenty-minute forecasts, but not in the ten-minute forecasts. The ten-minute forecasts are more sensitive to the fact that the storm slices cover only 85-92 percent of the area covered by truth, and 90 percent of the flight paths covered by truth. Hence for short forecast times, the trackers have relatively high false safes. The relative ranking for ten-minute forecasts thus to some extent reflects this "missing area" effect rather than the goodness of the trackers.

The flight-paths performance results show no clear winner among the three trackers. There is also no clear preference for a tracker as opposed to persistence. It appears that growth and decay, and rearrangement of cells due to differential motion, made it difficult for a storm tracker to improve over persistence when it comes to identifying those flight-paths which cross a hazardous region versus those flight-paths which do not.

The results are much the same for August 11, when the storm also had a line structure. Here, however, the forecasts show skill† for correlation and Crane even at 10.0 minutes, by the area criterion. This case, furthermore, shows relative skill under the flight-paths criterion for the Crane and correlation trackers at 20 and 30 minutes.

August 12 was a day of fast-moving, compact storm fragments, and proved difficult for the Crane and correlation trackers. The centroid tracker might have been expected to perform well on compact storms, but there was a problem with storm fragments not qualifying as volume cells. Under the area criterion, Crane and correlation were superior to the centroid tracker, and showed occasional skill against persistence at 30 minutes. On this day of compact storms, no tracker proved skillful under the flight-path criterion.

†The skill of a tracker is determined relative to persistence. Since it is always possible to design a forecaster with either no false alarms or no false safes, a forecast is not considered skillful unless it has both fewer false alarms and fewer false safes than a persistence forecast.

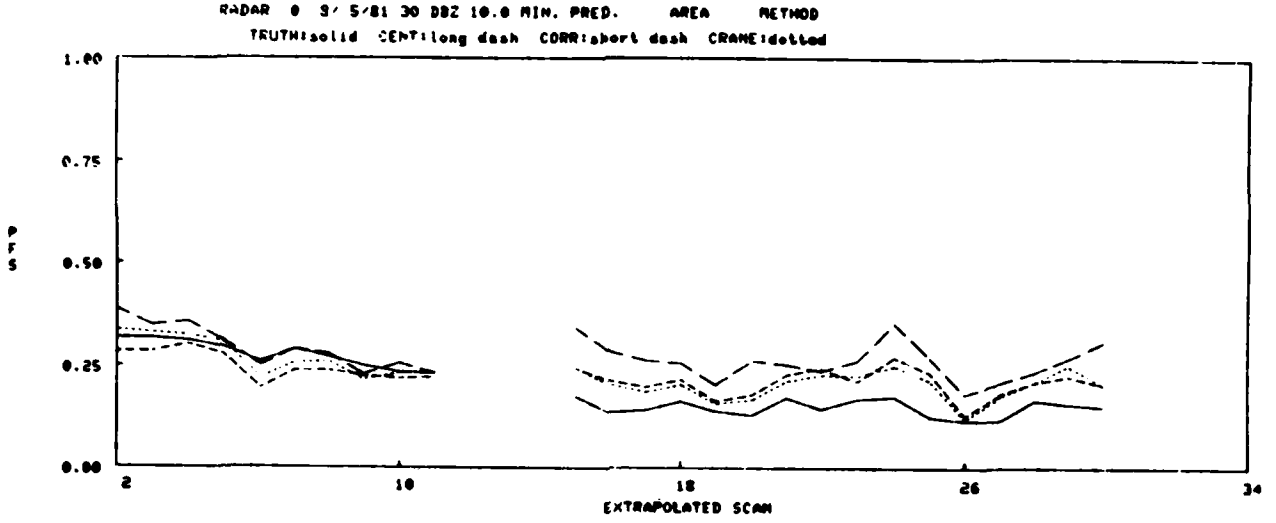

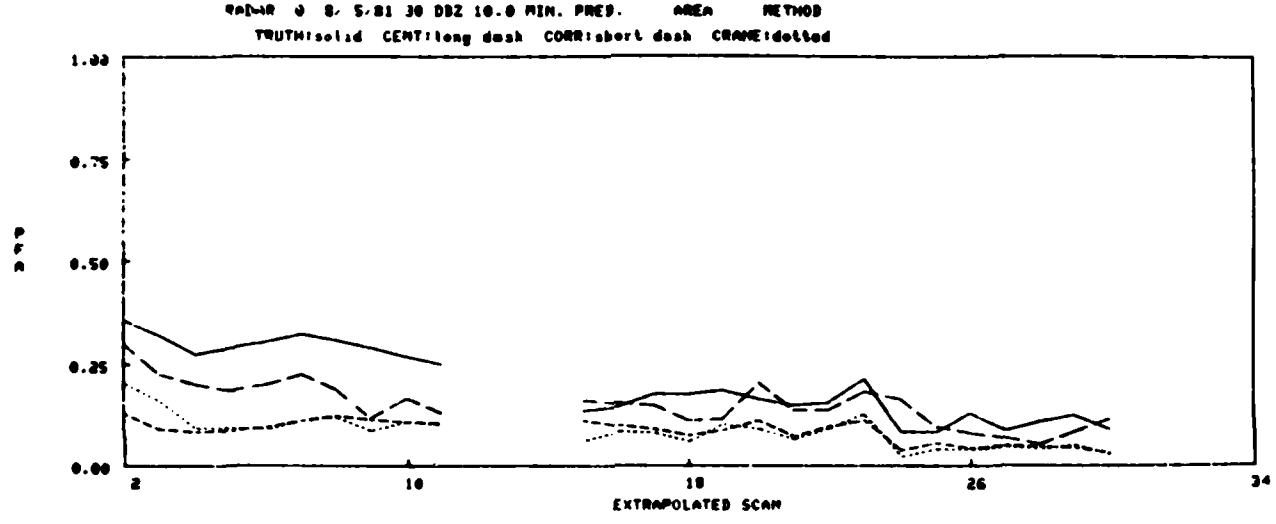

Figure IV-41. 8/5/81 10 min. pred., Area method.

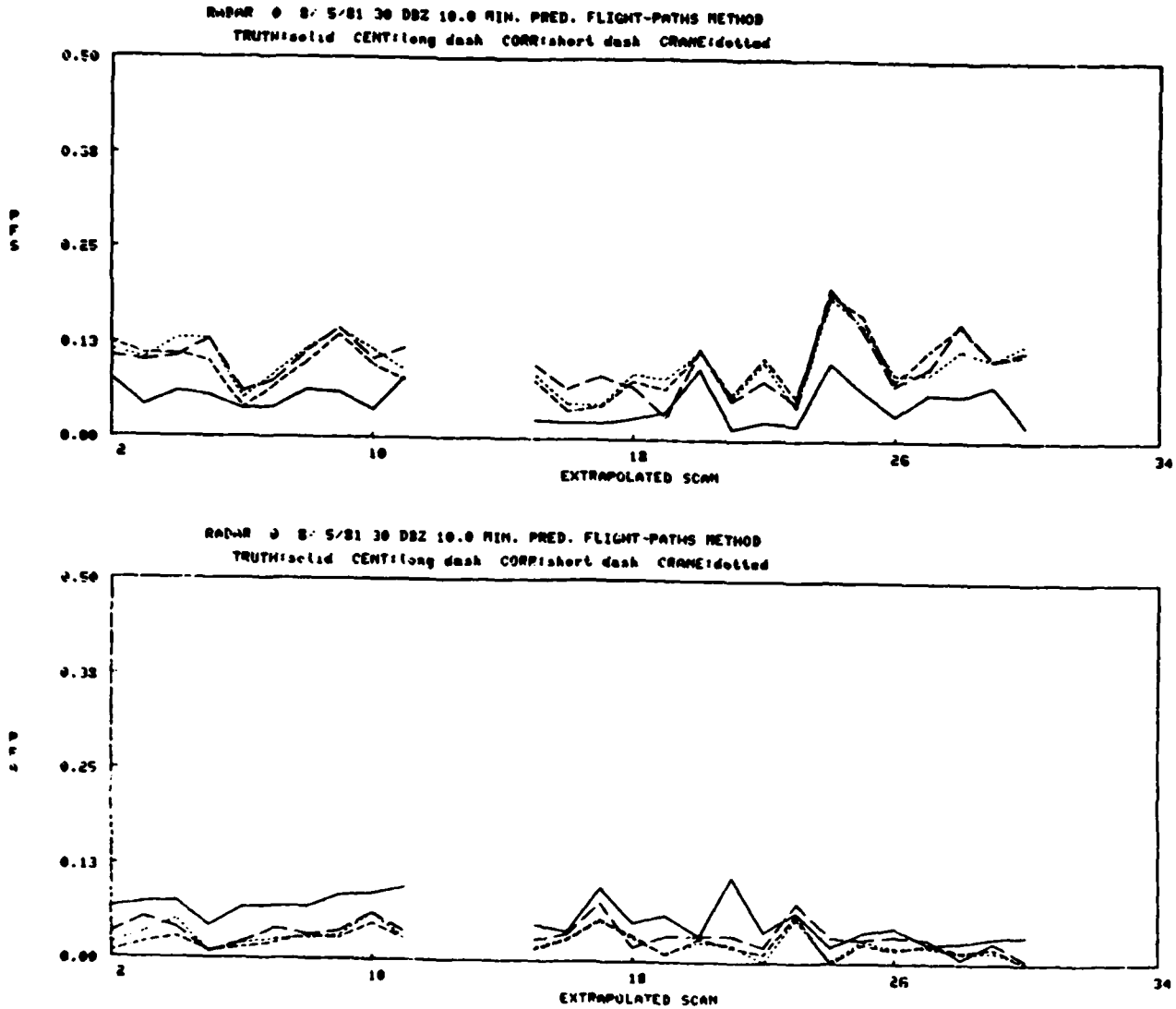

Figure IV-42. 8/5/81 10 min. pred., Flight-paths method.

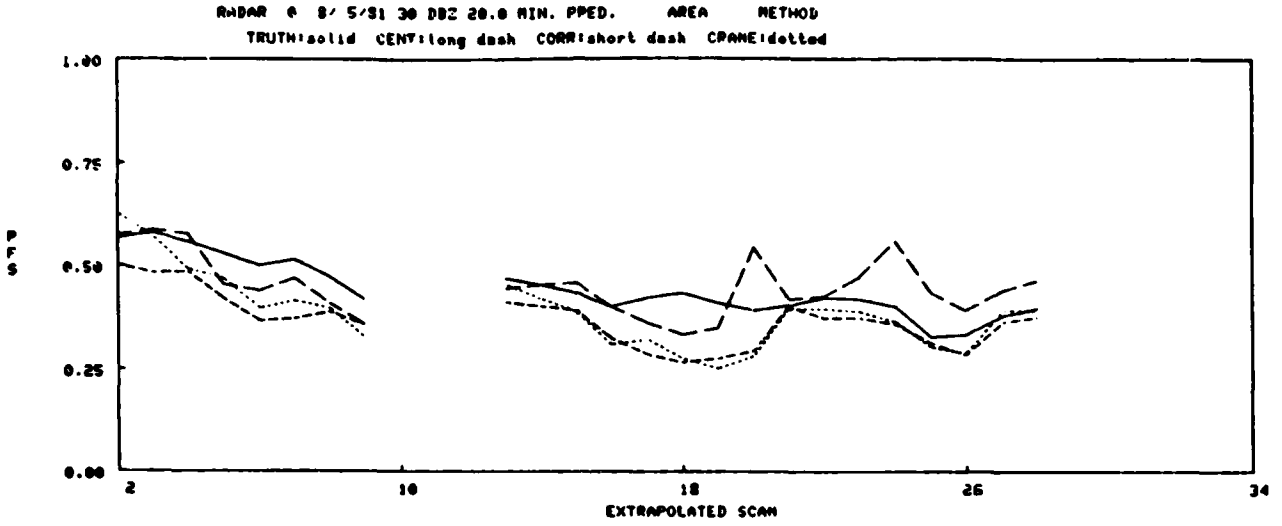

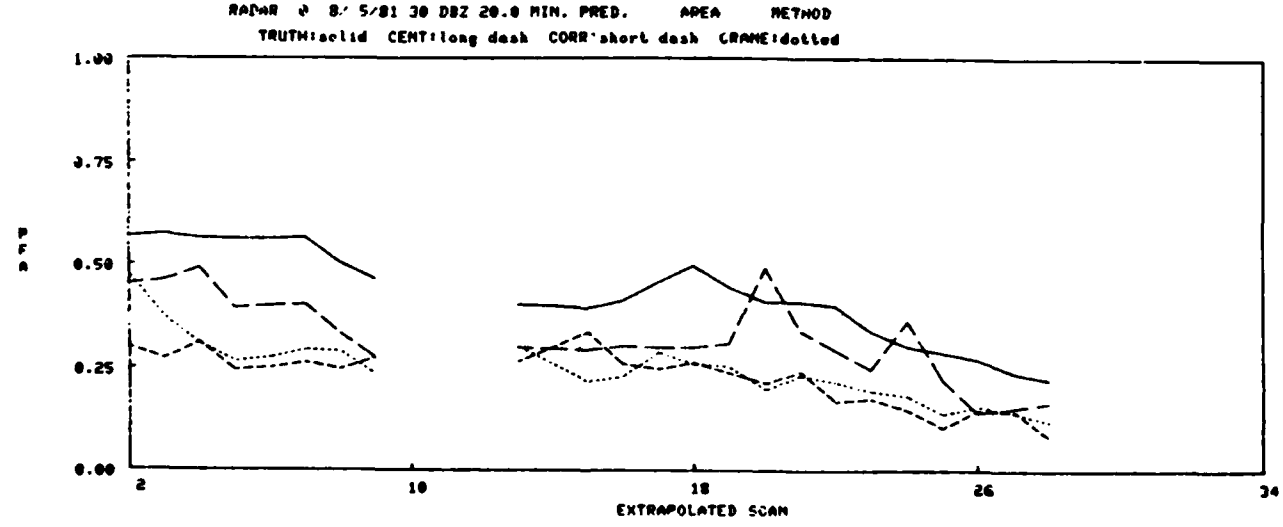

Figure IV-43. 8/5/81 20 min. pred., Area method.

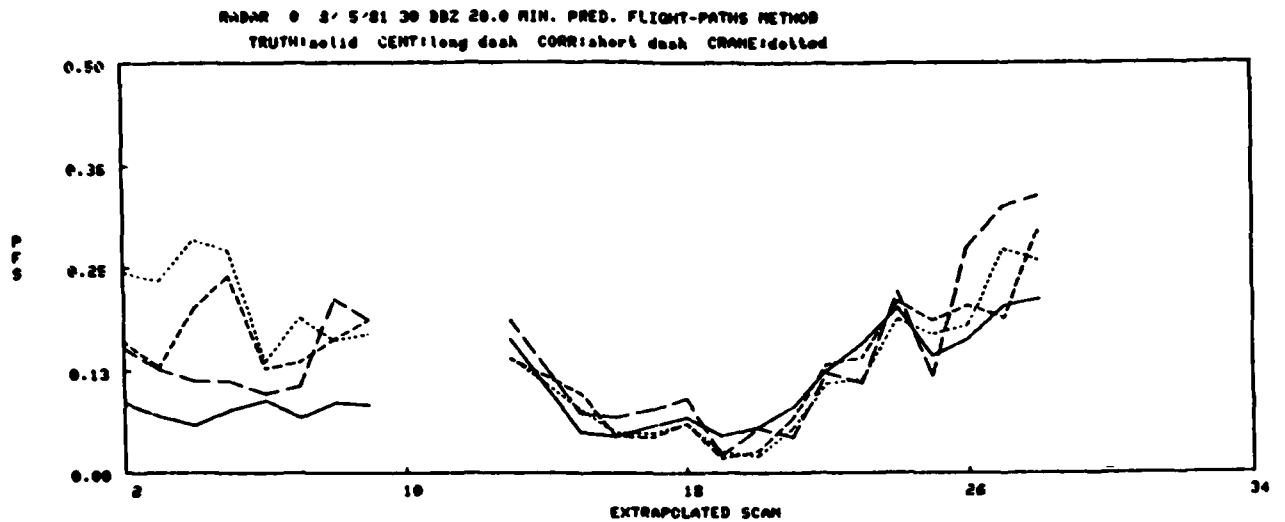

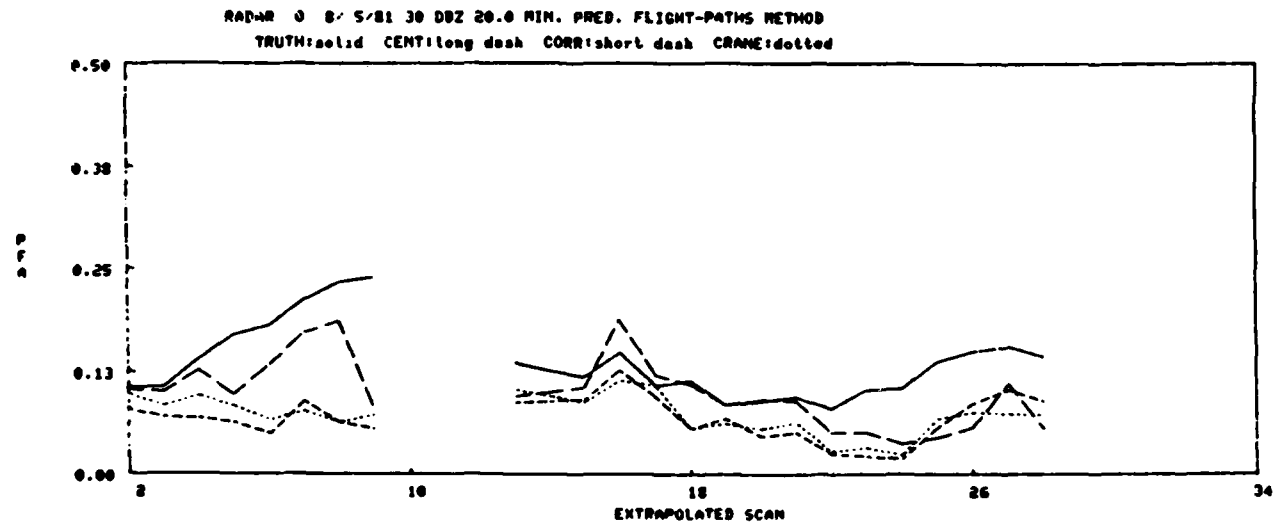

Figure IV-44. 8/5/81 20 min. pred., Flight-paths method.

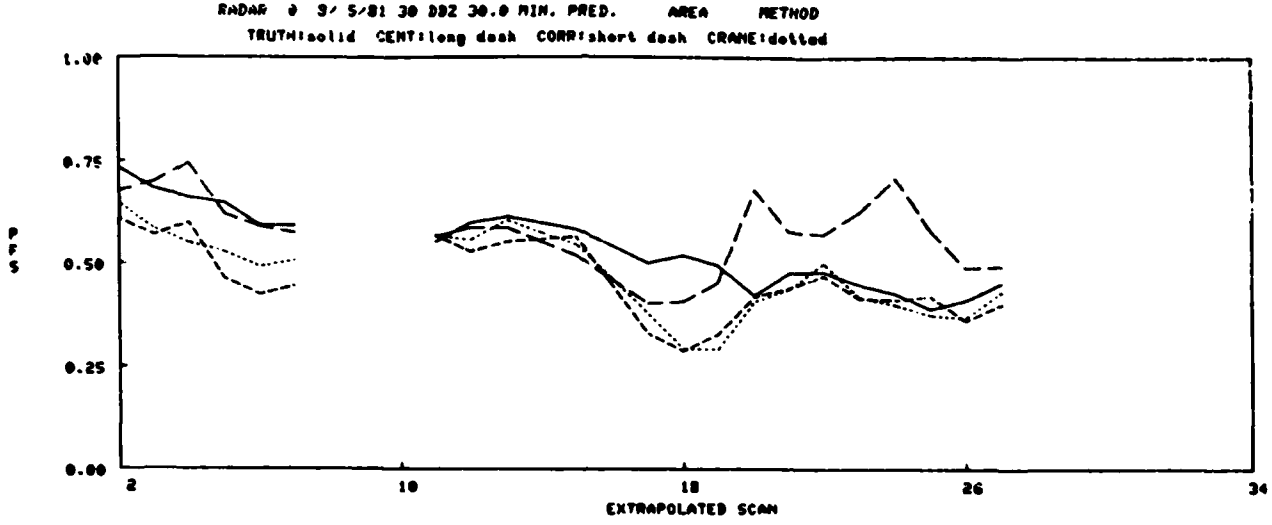

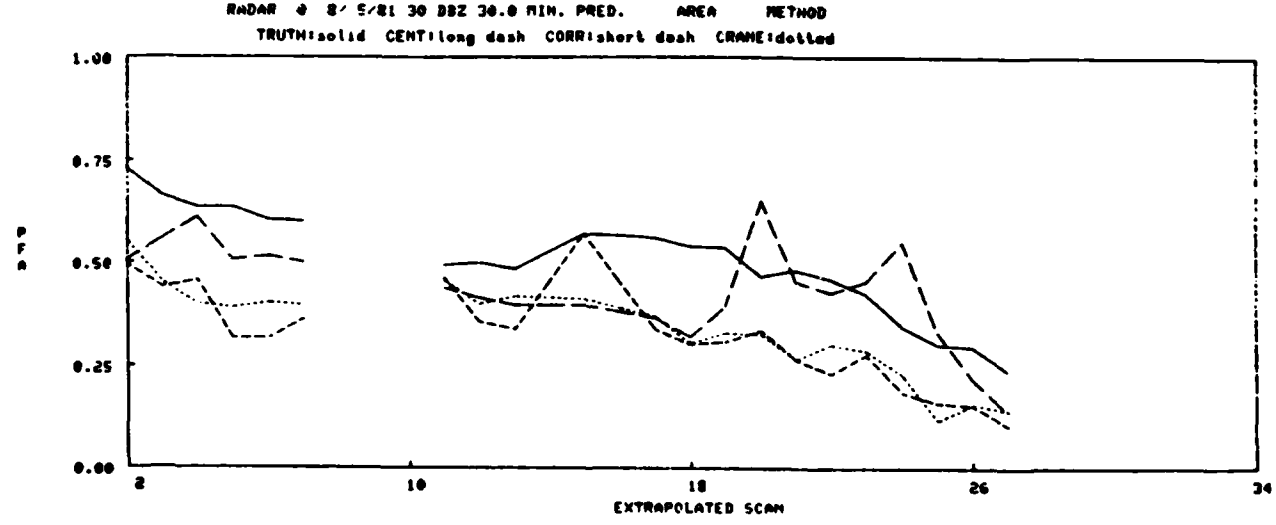

Figure IV-45. 8/5/81 30 min. pred., Area method.

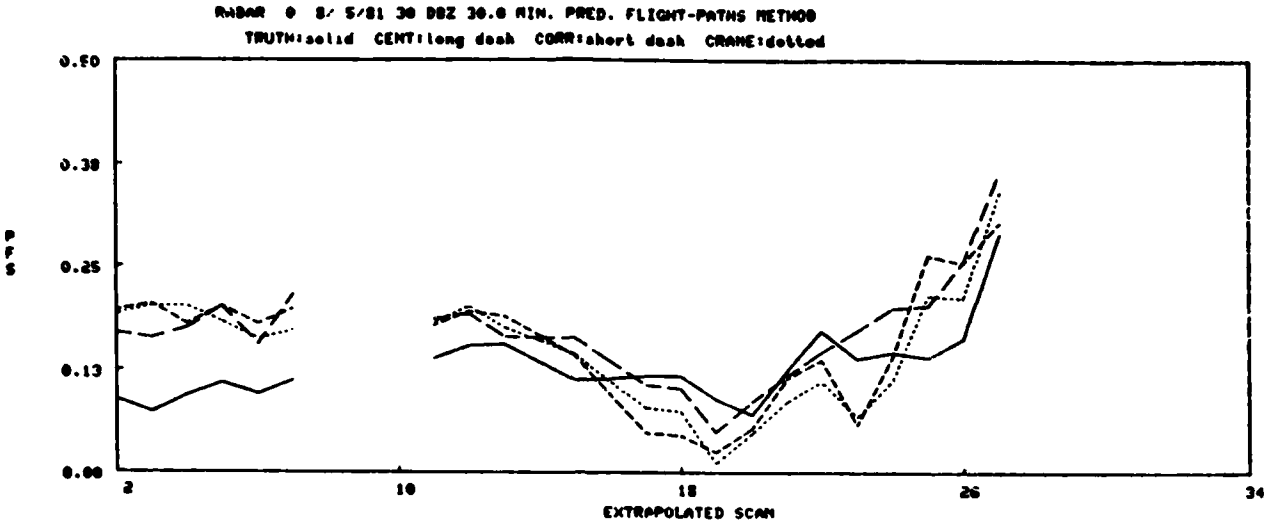

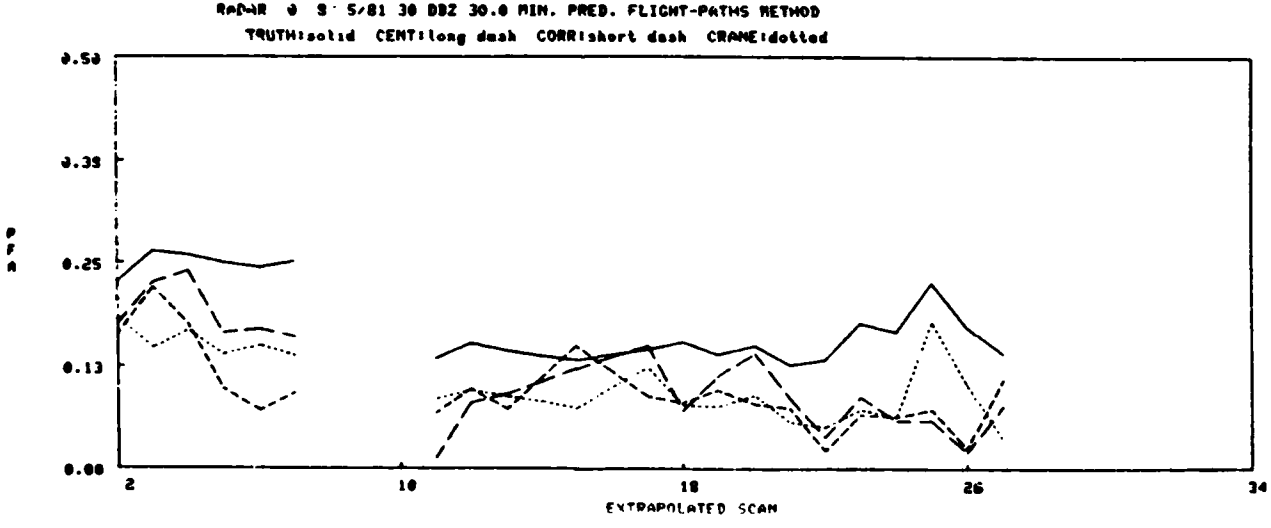

Figure IV-46. 8/5/81 30 min. pred., Flight-paths method.

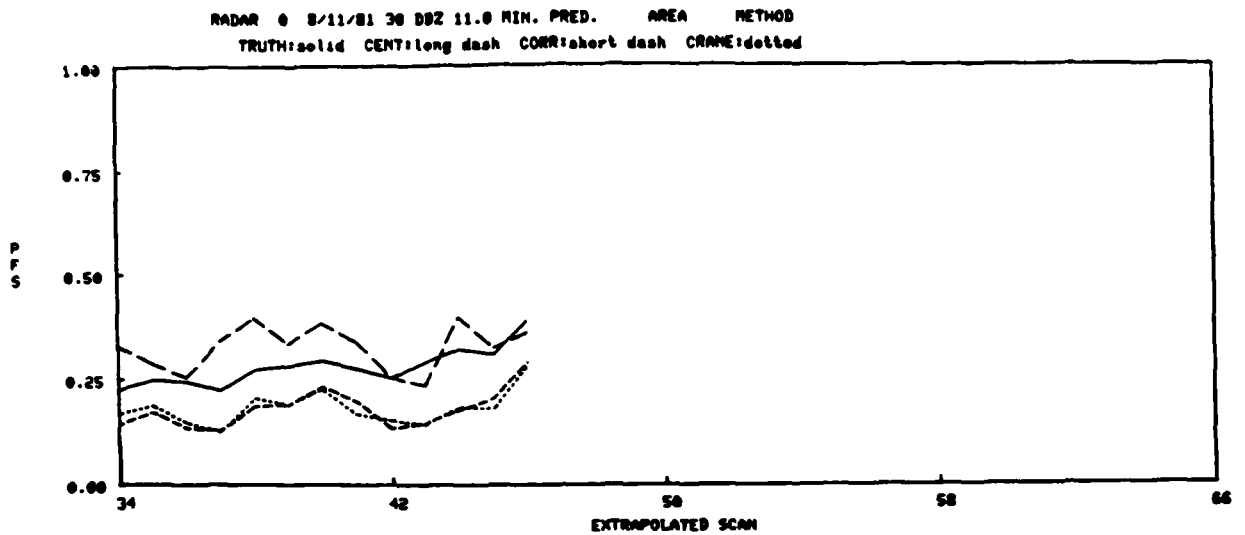

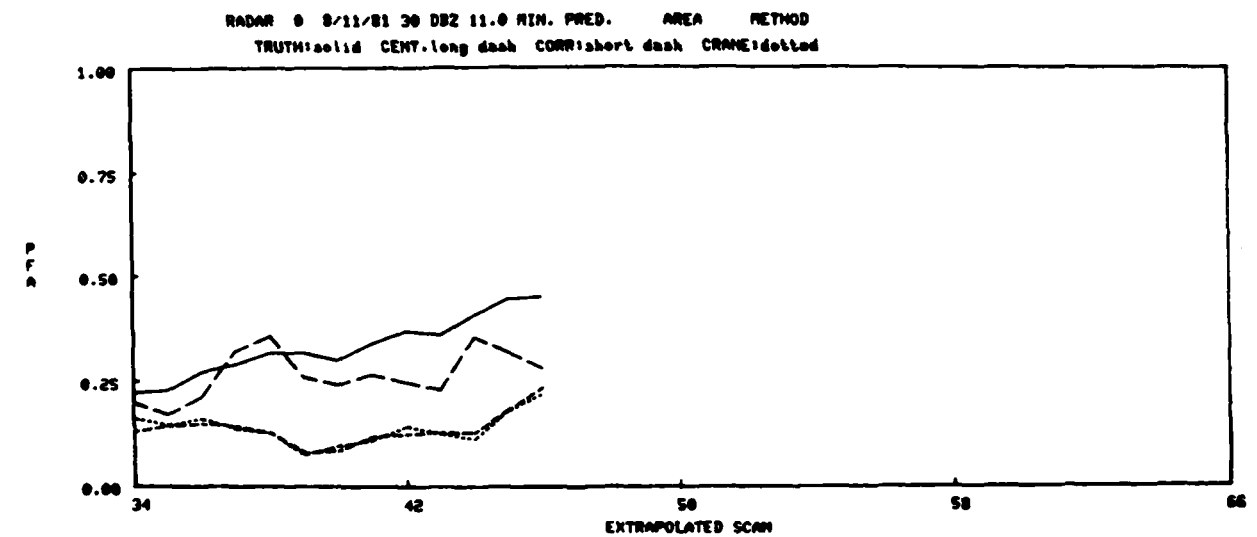

Figure IV-47. 8/11/81 11 min. pred., Area method.

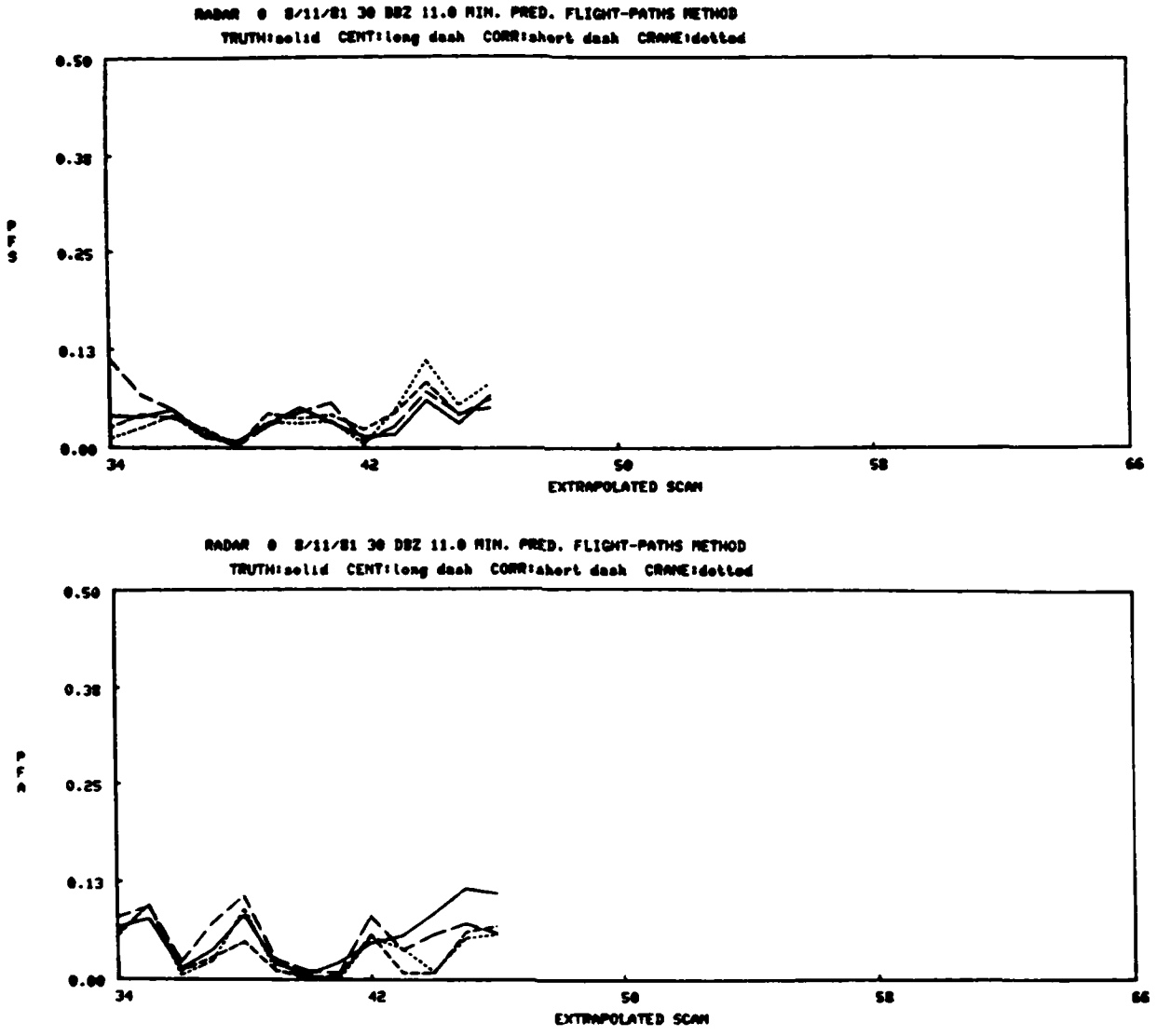

Figure IV-48. 8/11/81 11 min. pred., Flight-paths method.

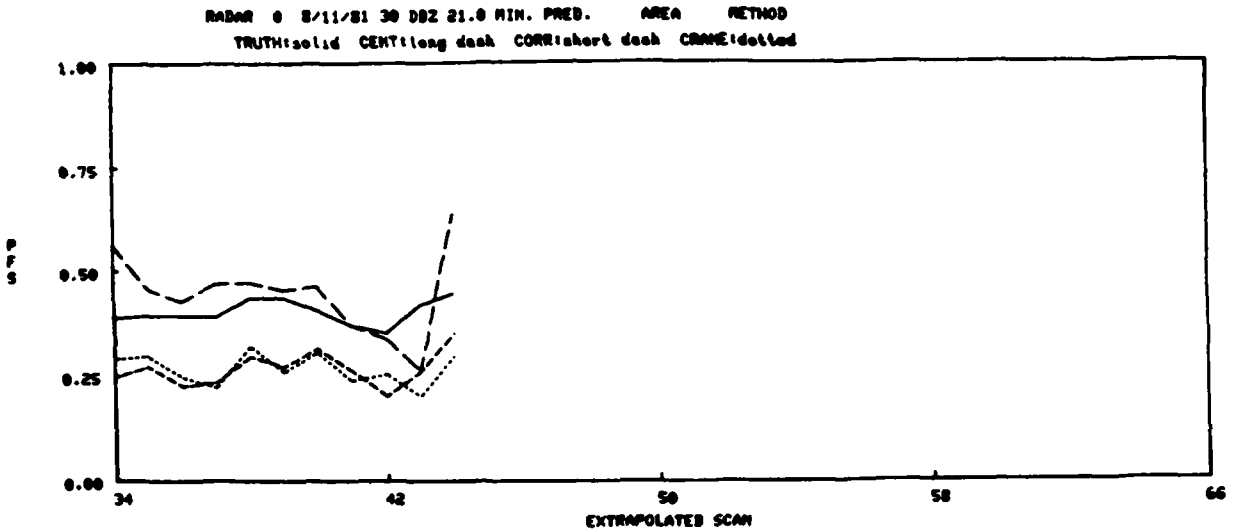

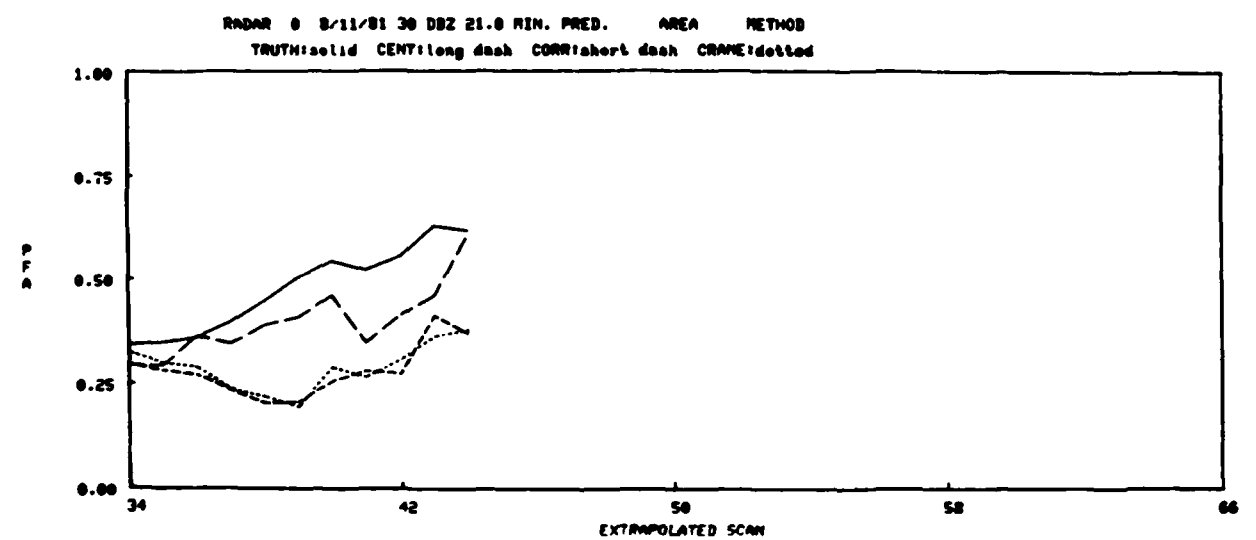

Figure IV-49. 8/11/81 21 min. pred., Area method.

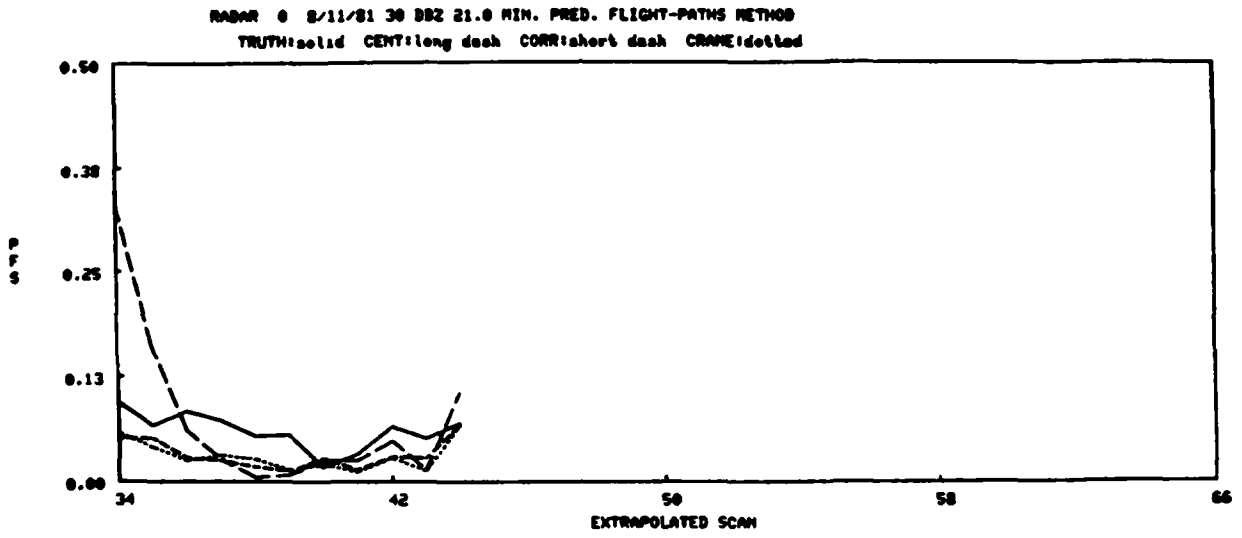

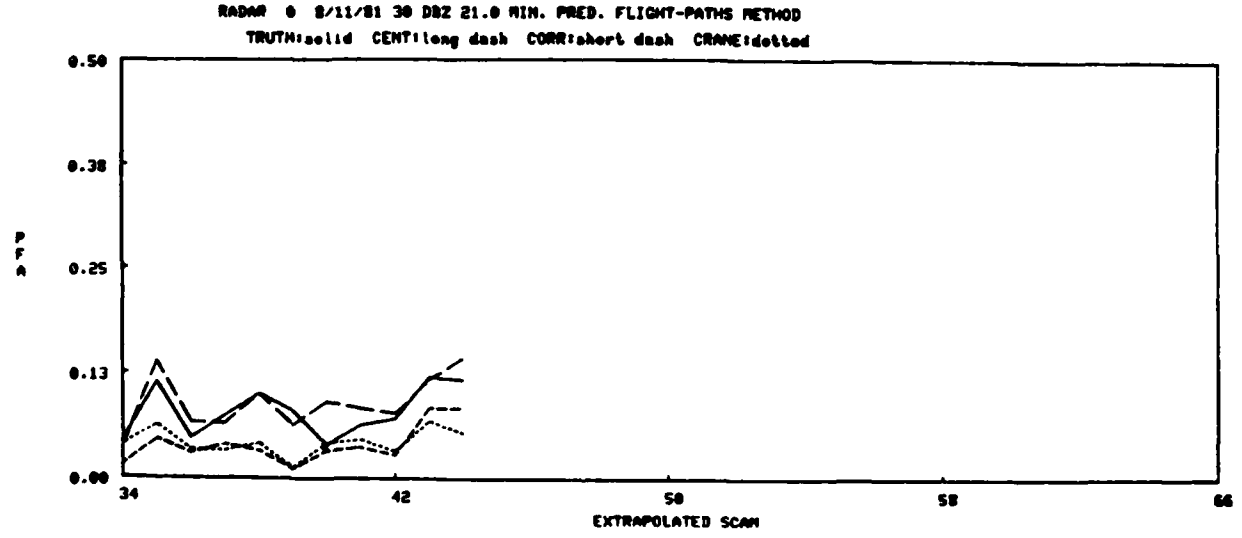

Figure IV.50. 8/11/81 21 min. pred., Flight-paths method.

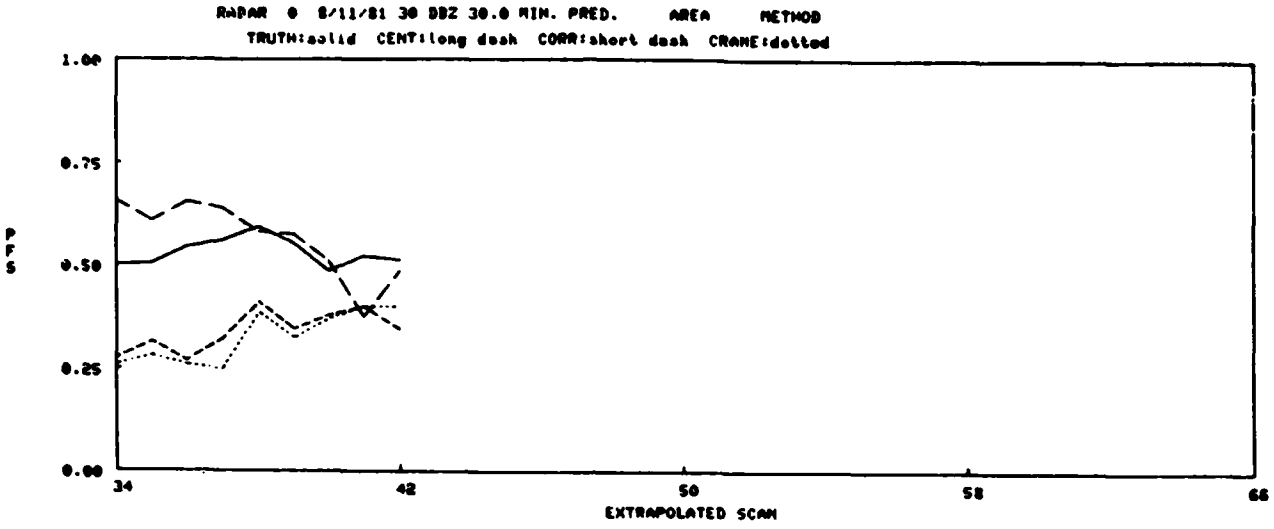

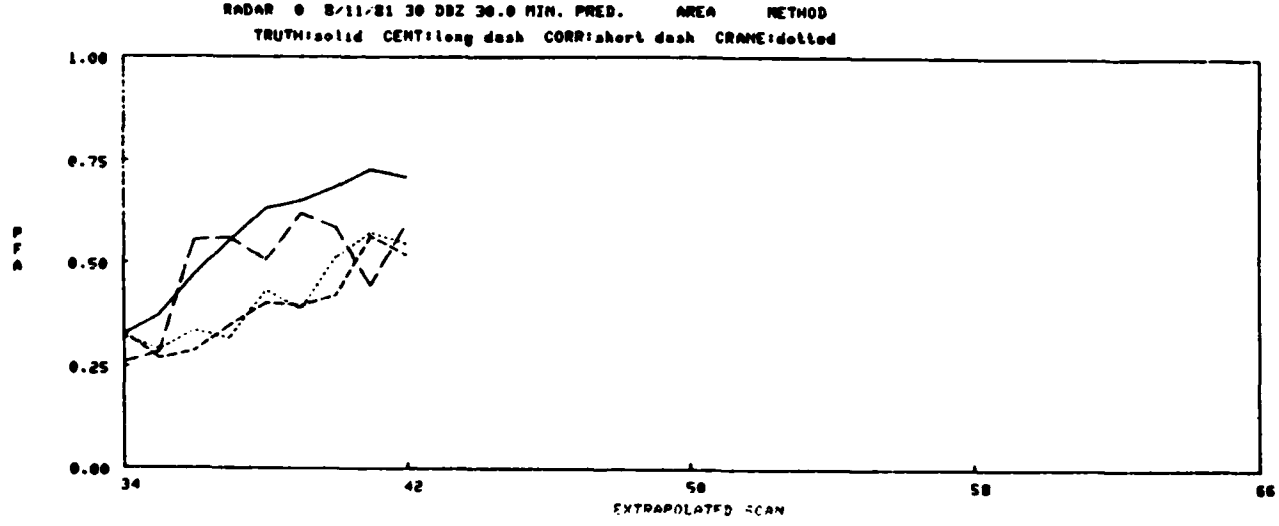

Figure IV-51. 8/11/81 30 min. pred., Area method.

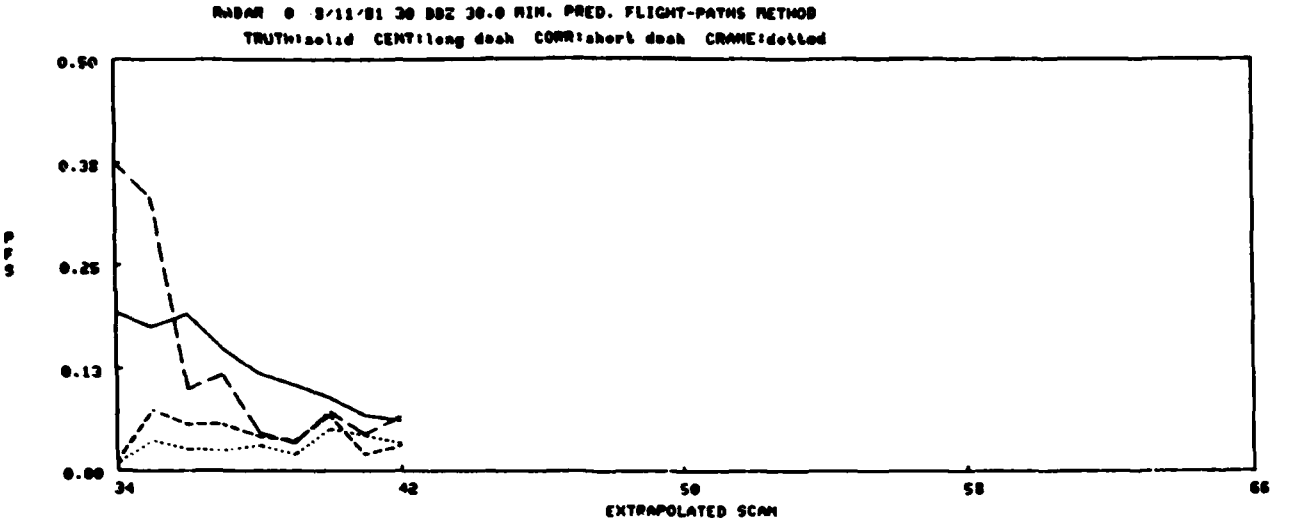

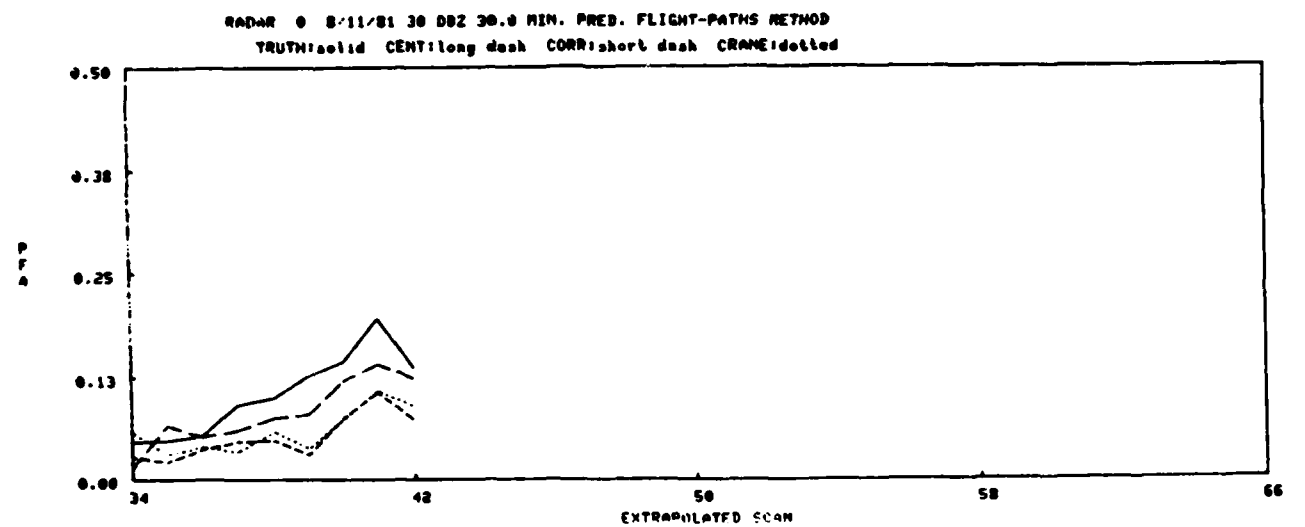

Figure IV-52. 8/11/81 30 min. pred., Flight-paths method.

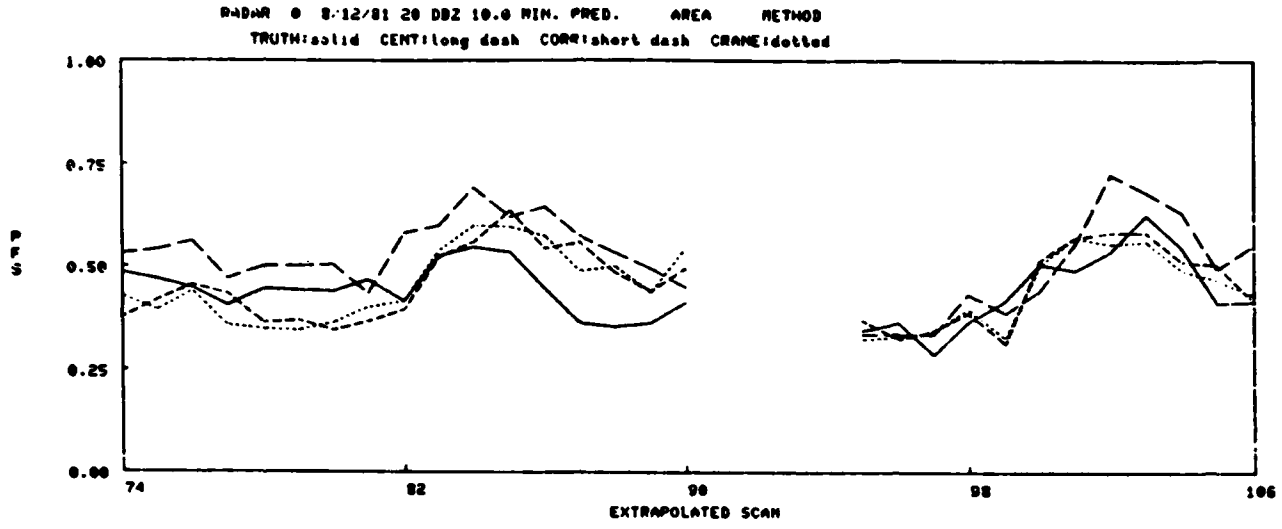

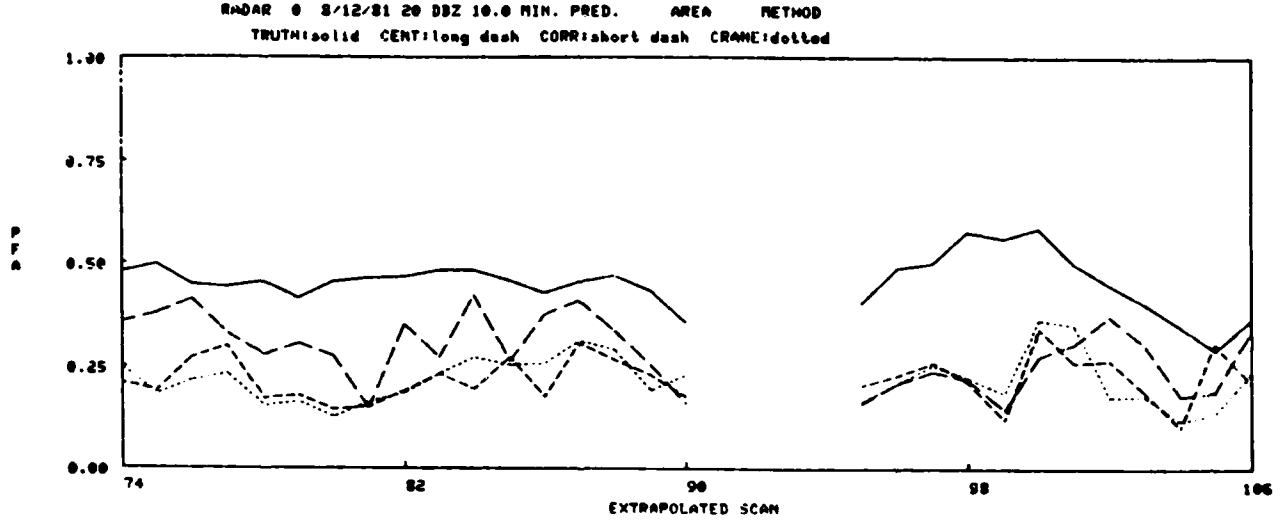

Figure IV-53. 8/12/81 10 min. pred., Area method.

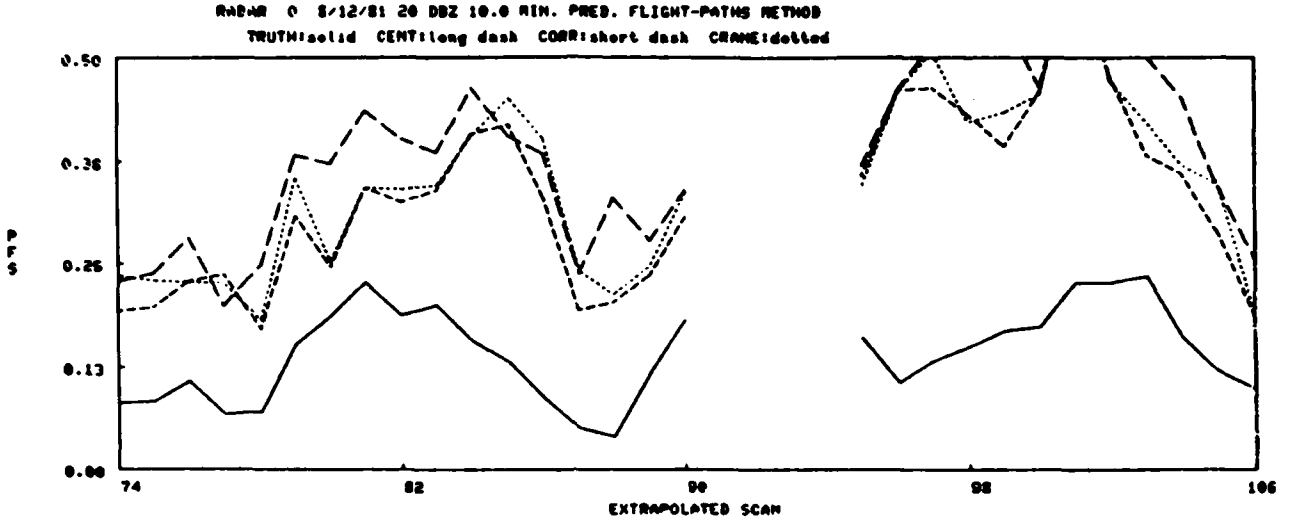

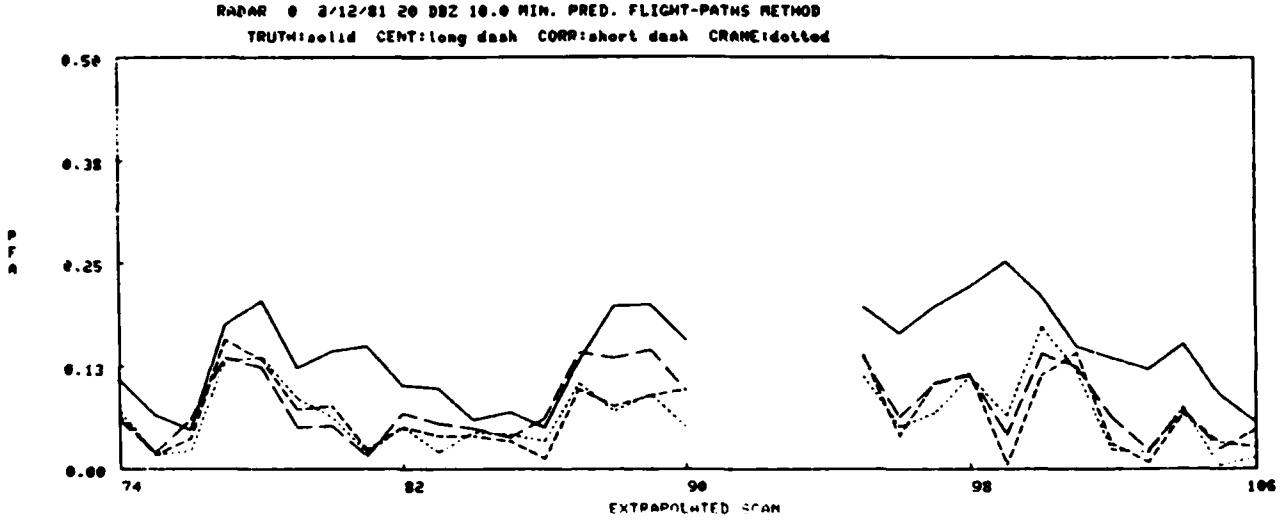

Figure IV-54. 8/12/81 10 min. pred., Flight-paths method.

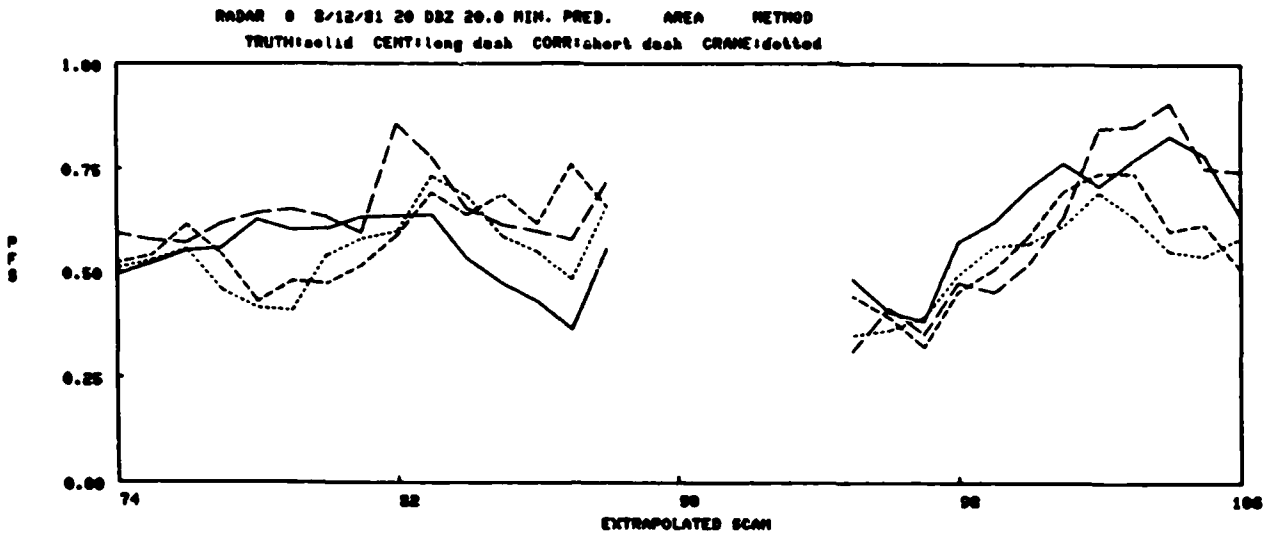

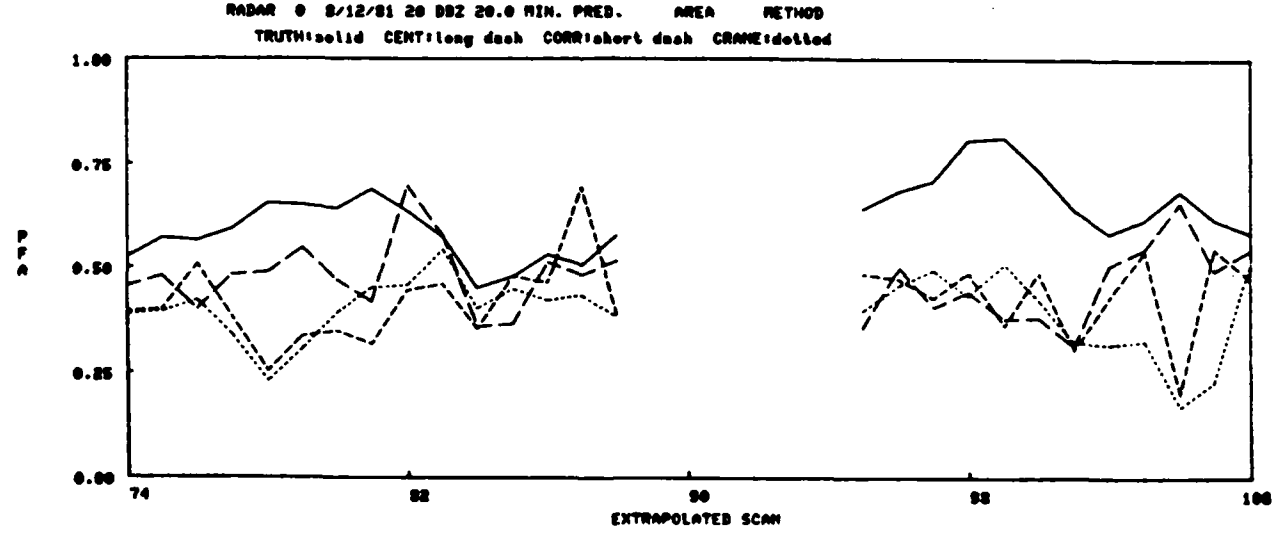

Figure IV-55. 8/12/81 20 min. pred., Area method.

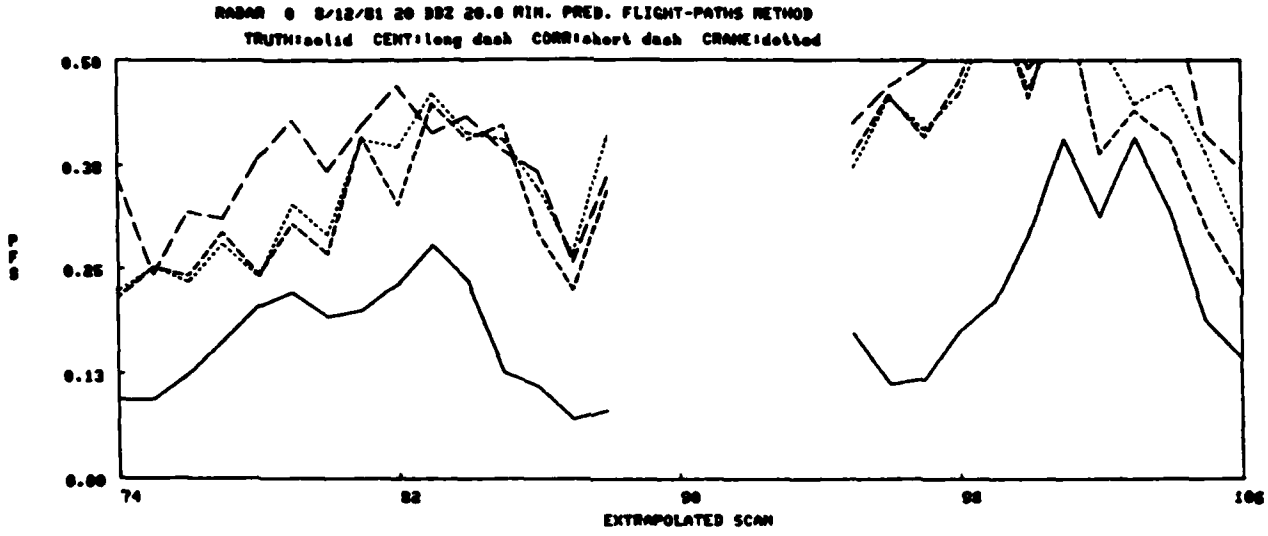

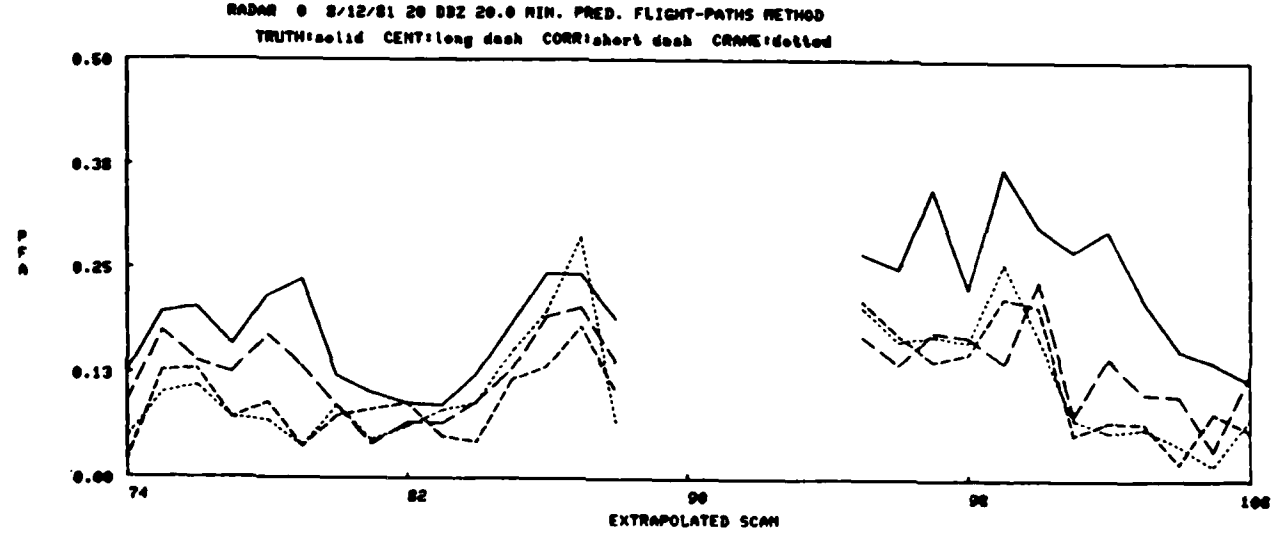

Figure IV-56. 8/12/81 20 min. pred., Flight-paths method.

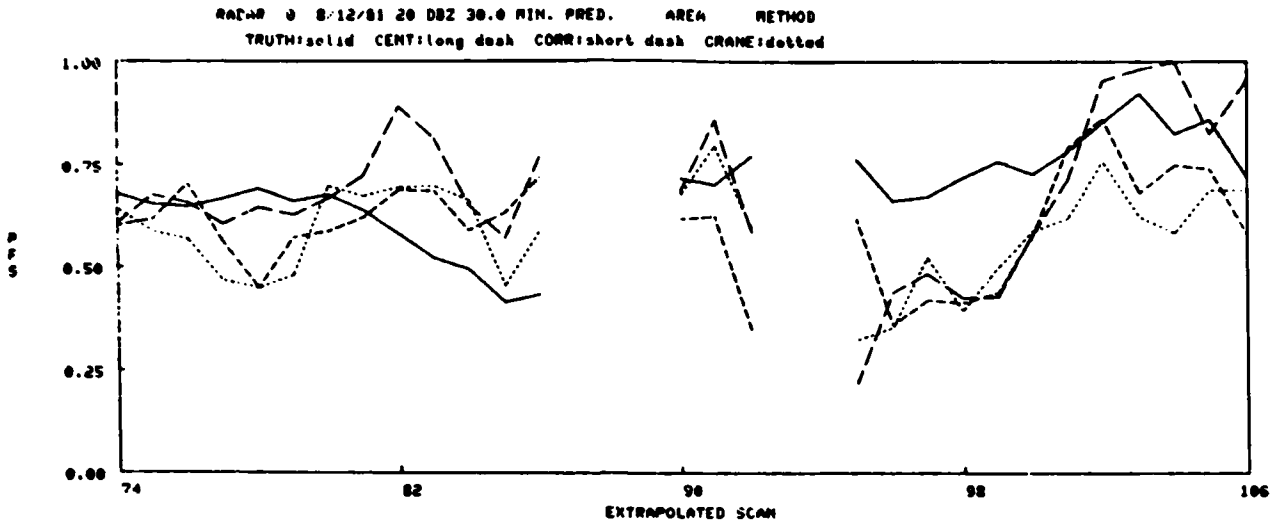

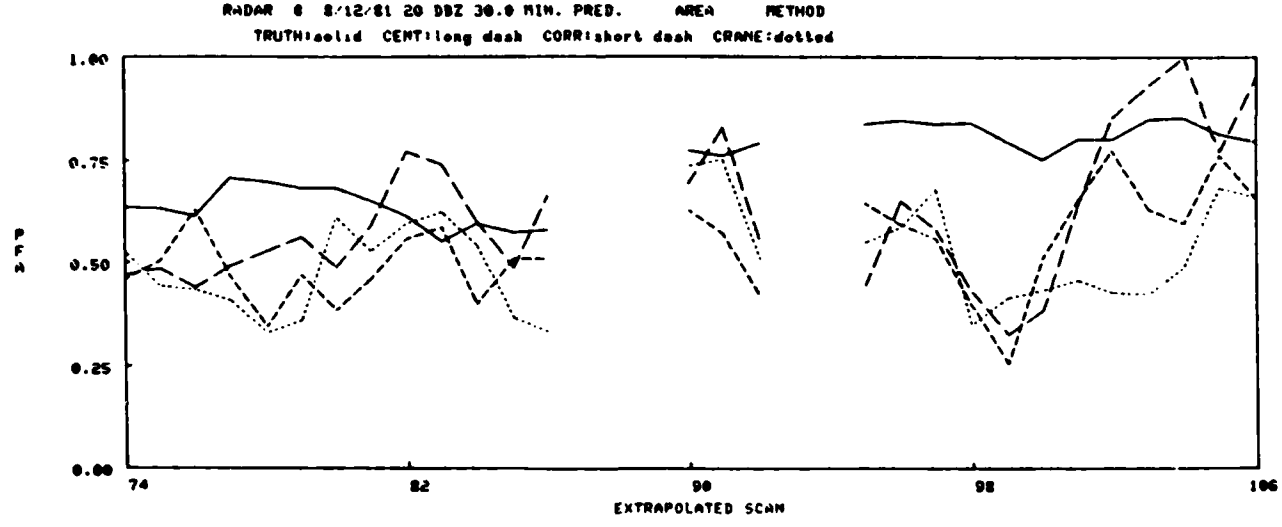

Figure IV-57. 8/12/81 30 min. pred., Area method.

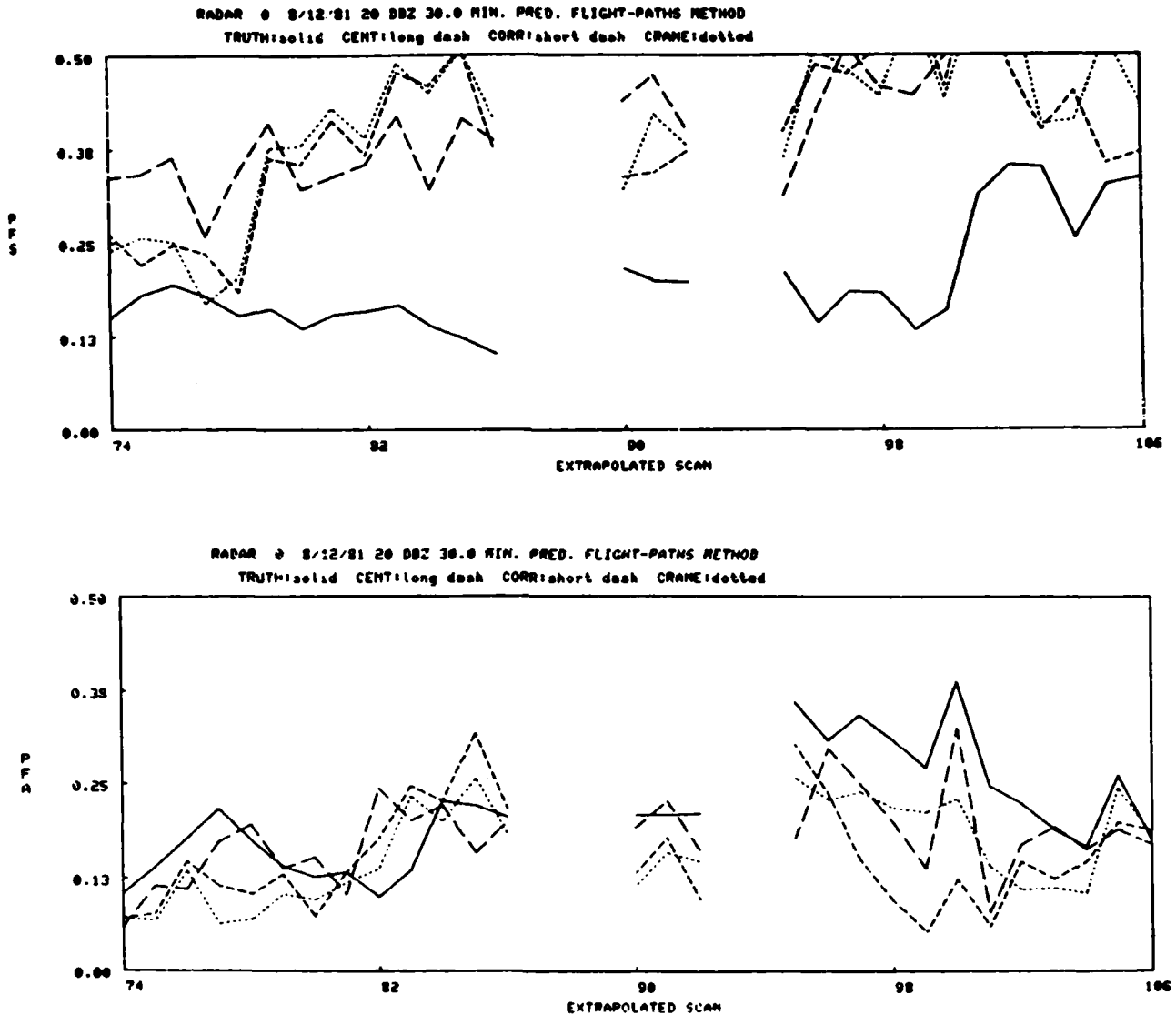

Figure IV-58. 8/12/81 30 min. pred., Flight-paths method.

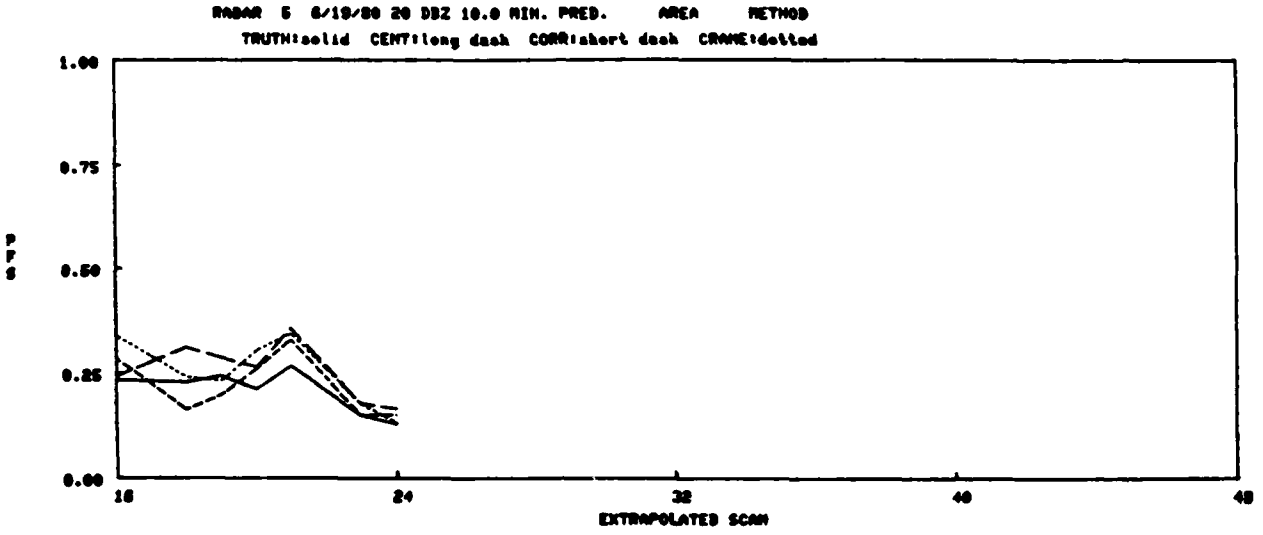

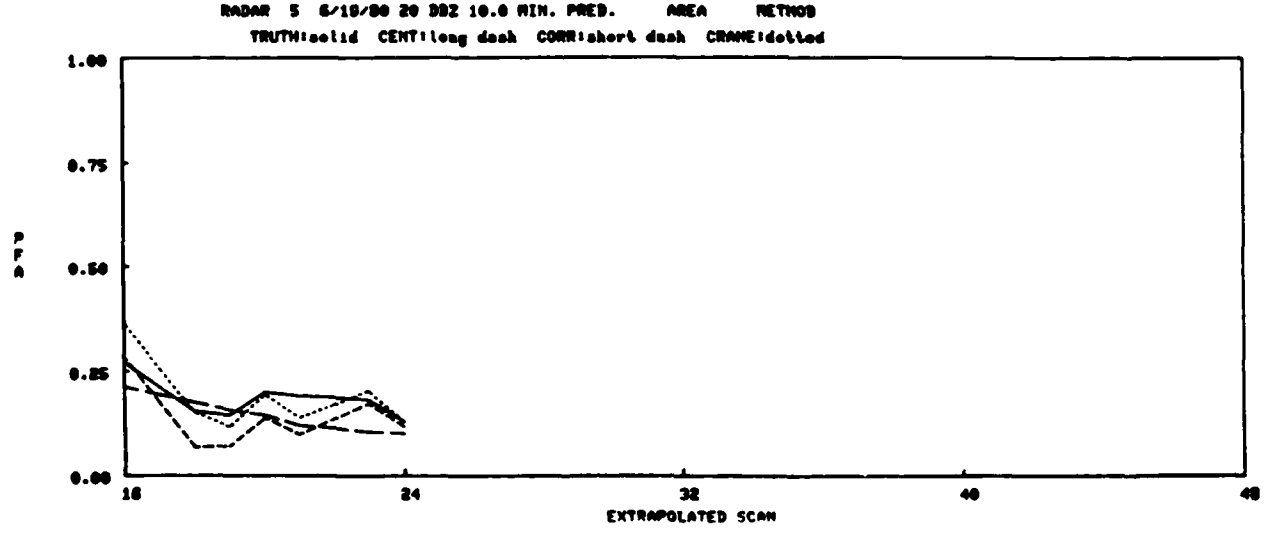

Figure IV-59. 6/19/80 10 min. pred., Area method.

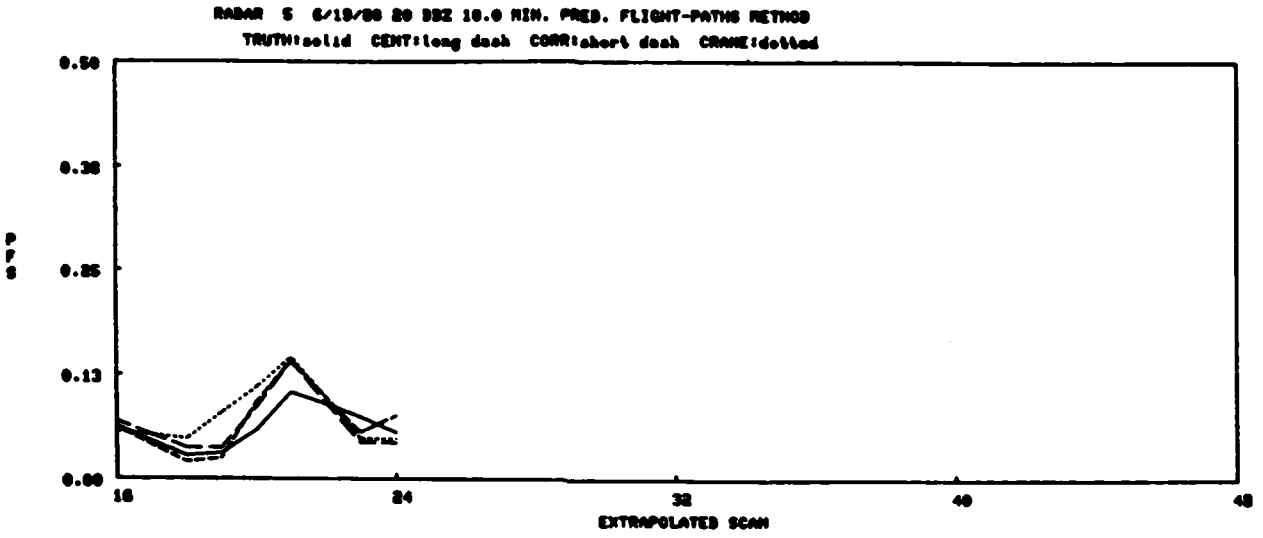

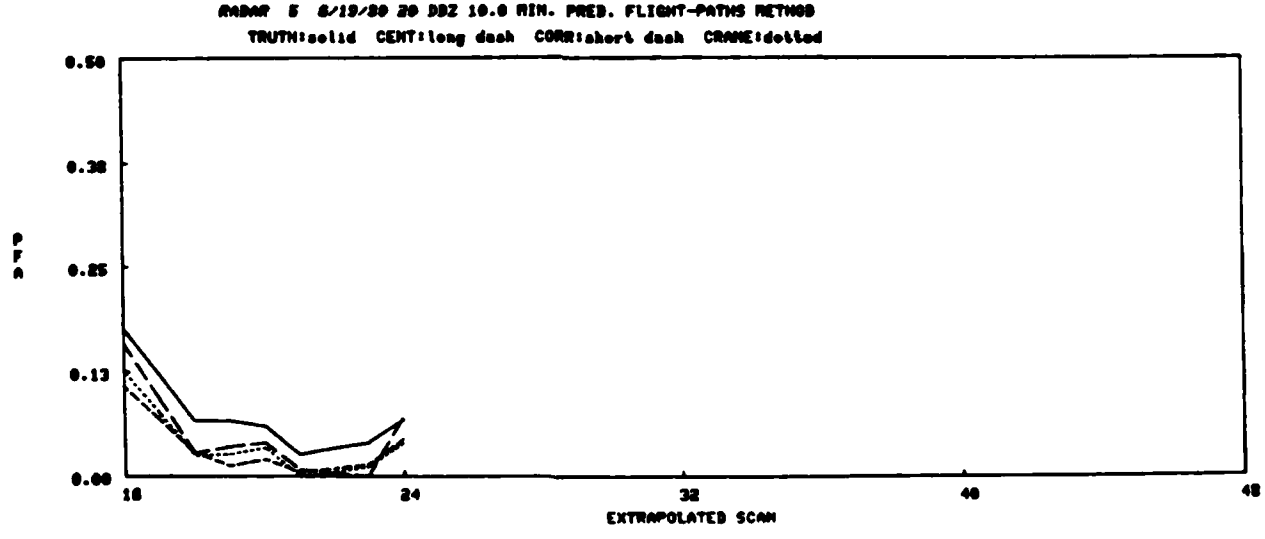

Figure IV-60. 6/19/80 10 min. pred., Flight-paths method.

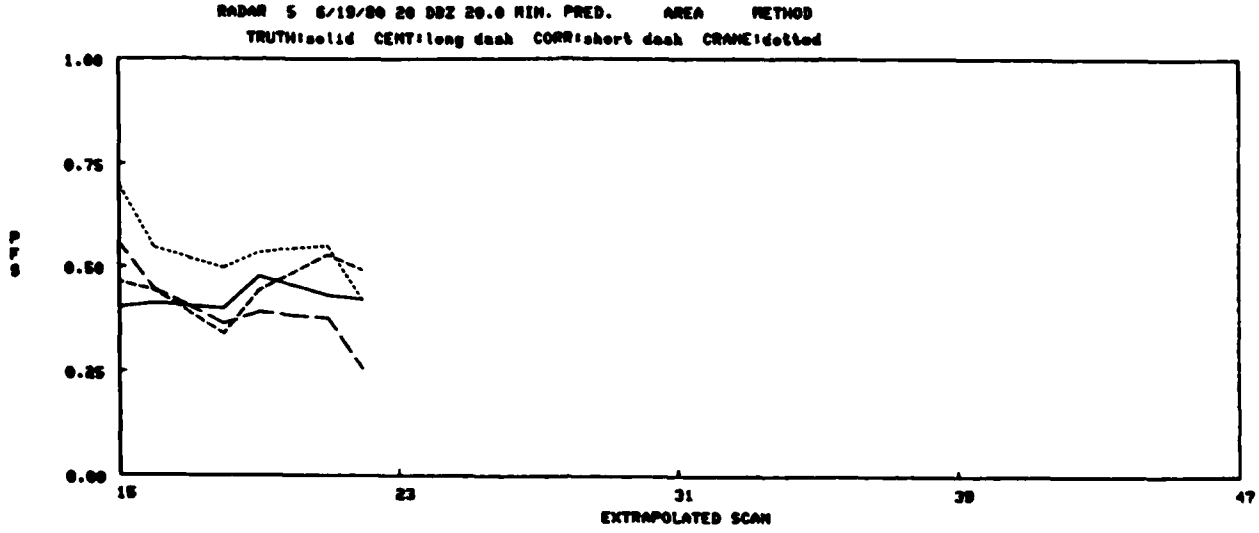

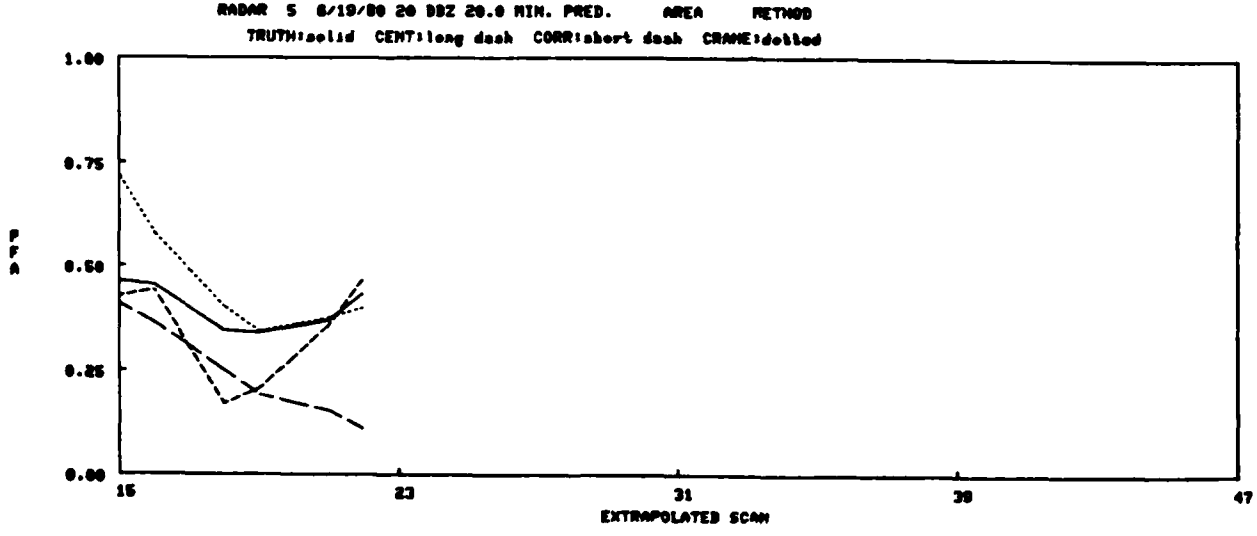

Figure IV-61. 6/19/80 20 min. pred., Area method.

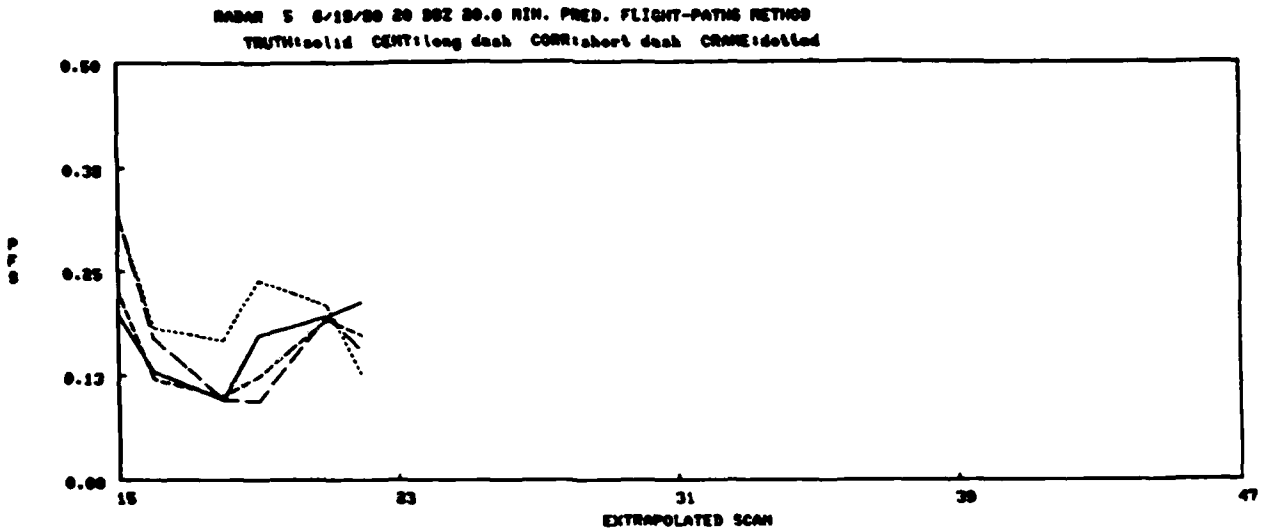

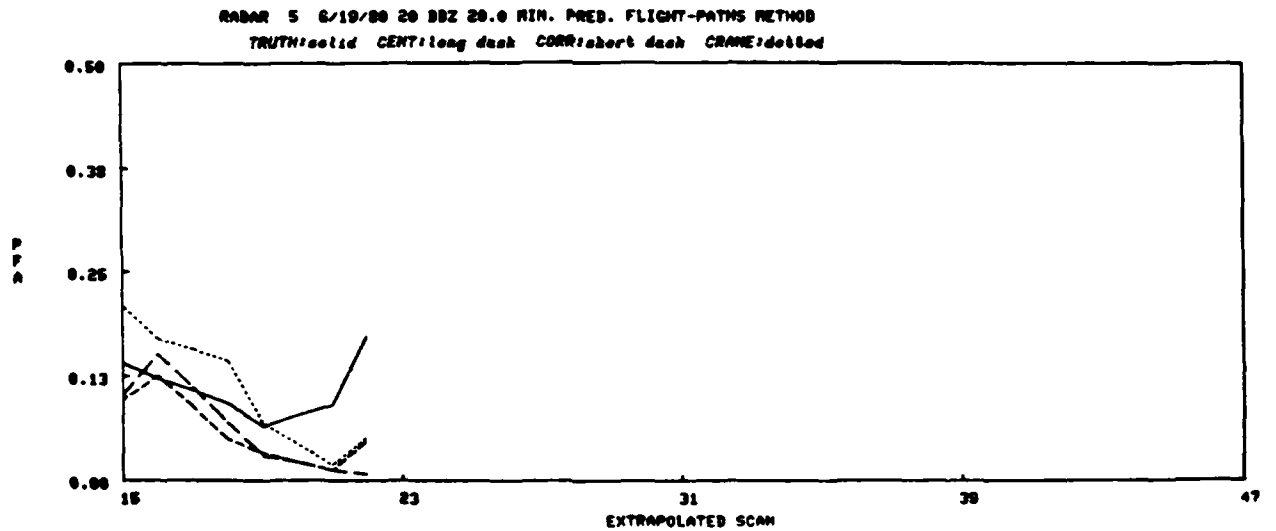

Figure IV-62. 6/19/80 20 min. pred., Flight-paths method.

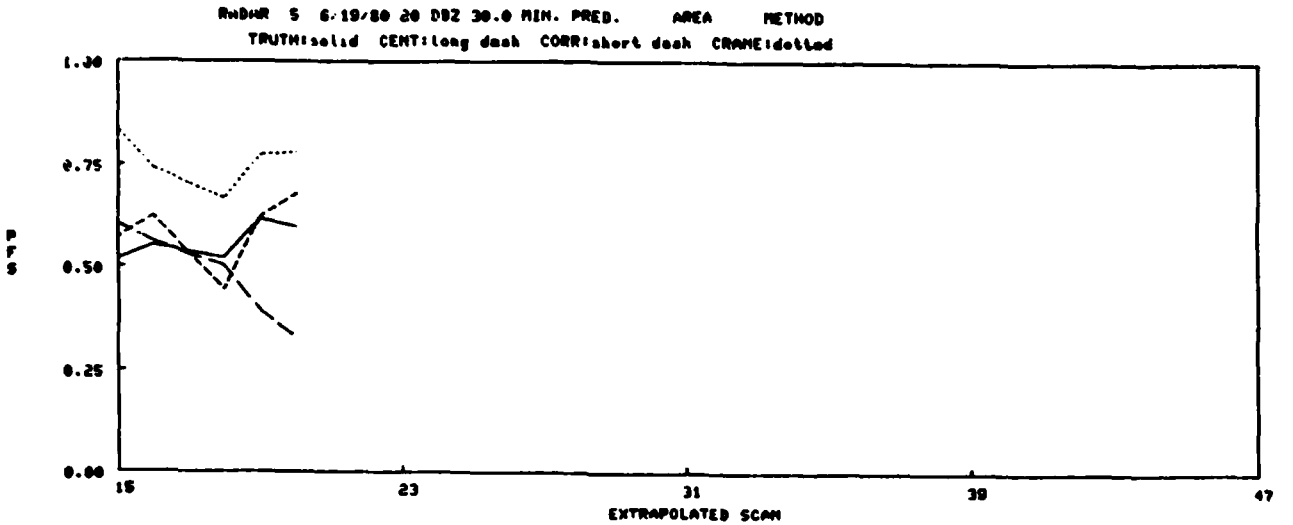

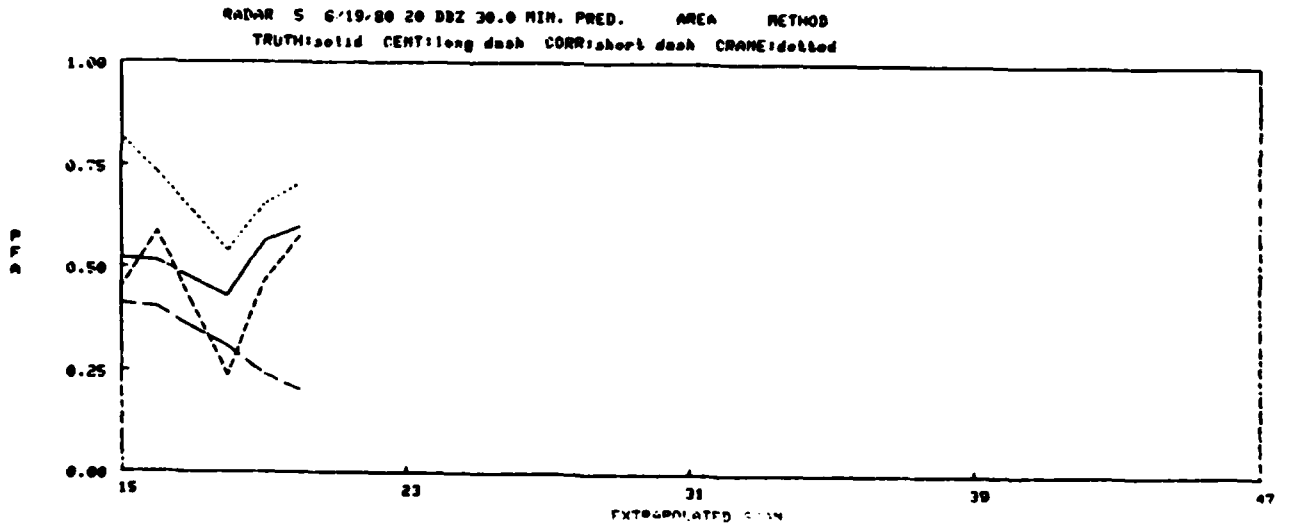

Figure IV-63. 6/19/80 30 min. pred., Area method.

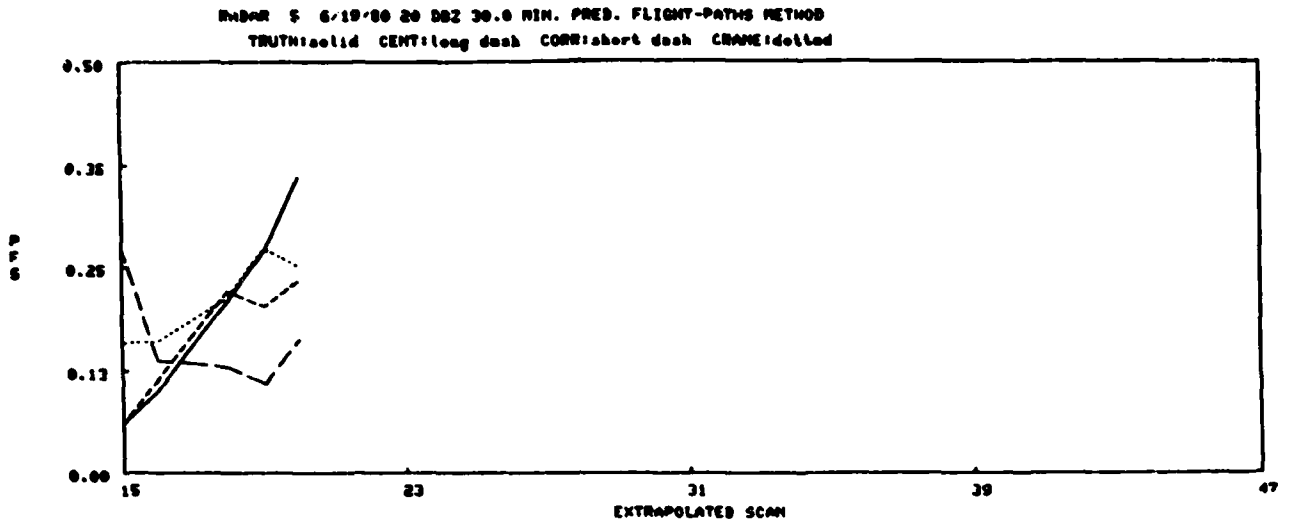

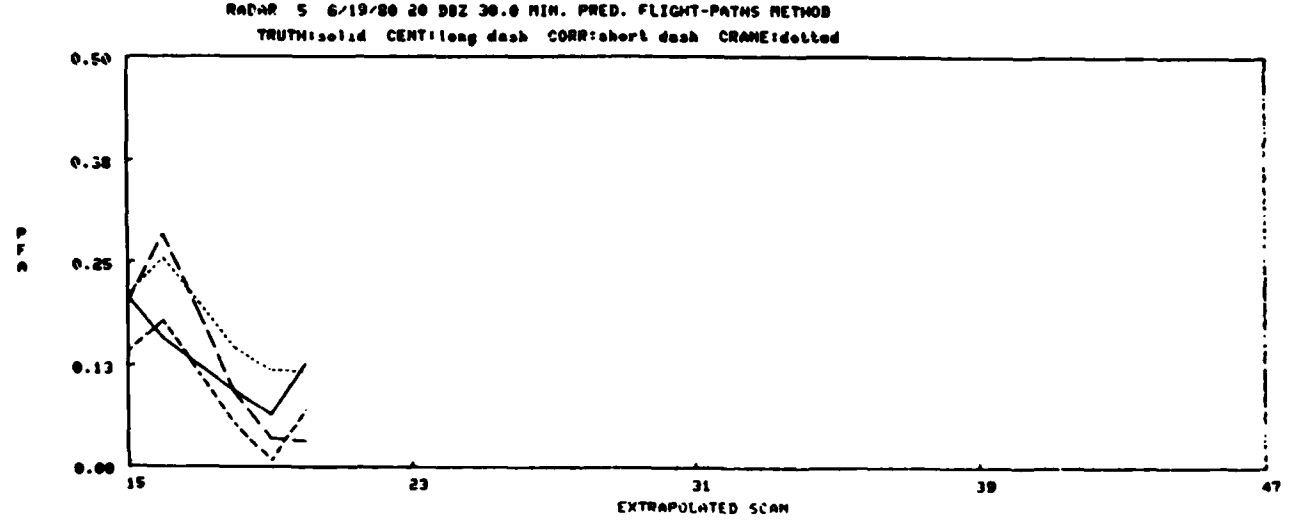

Figure IV-64. 6/19/80 30 min. pred., Flight-paths method.

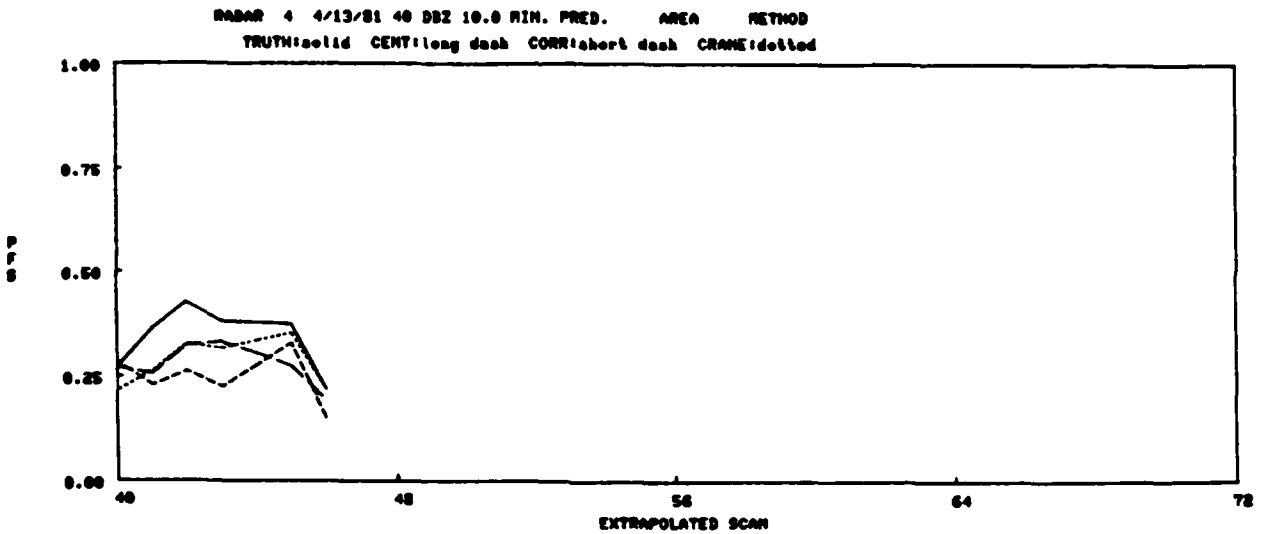

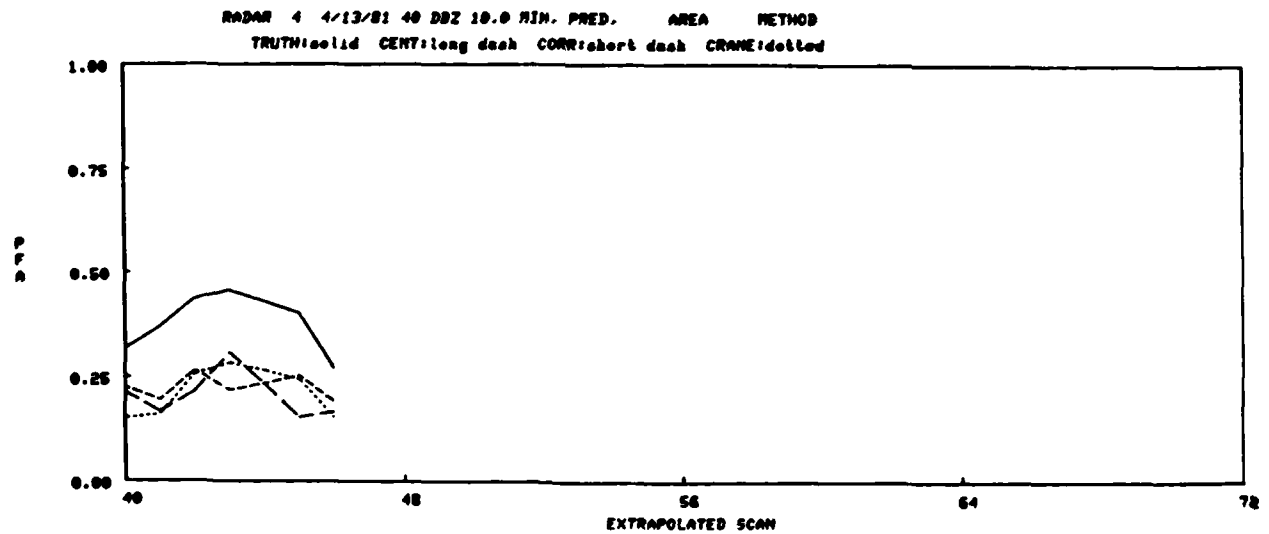

Figure IV-65. 4/13/81 10 min. pred., Area method.

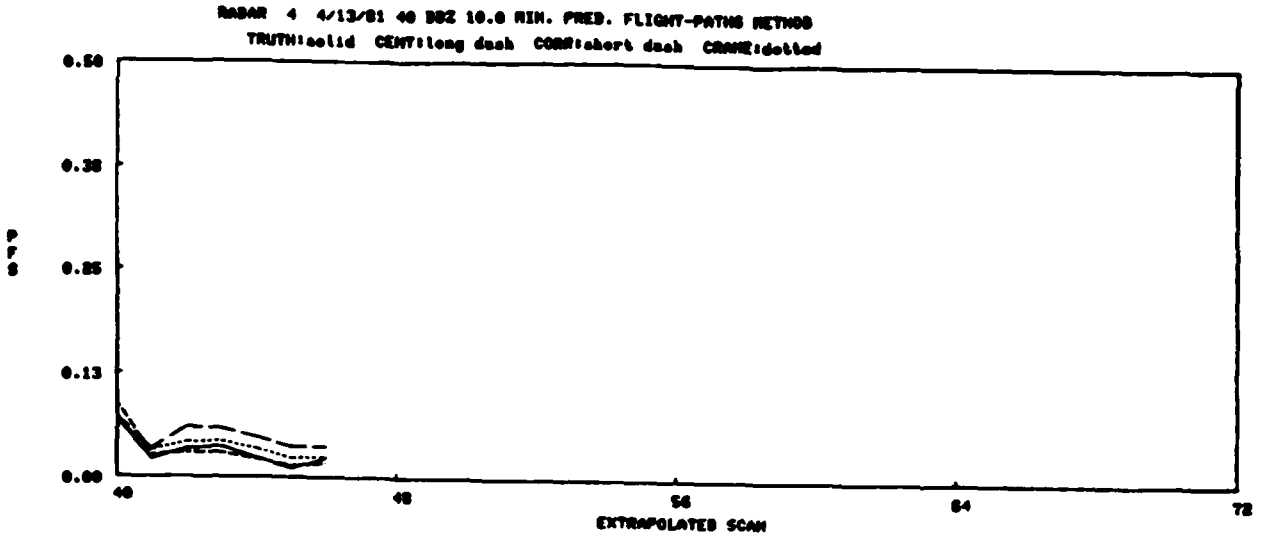

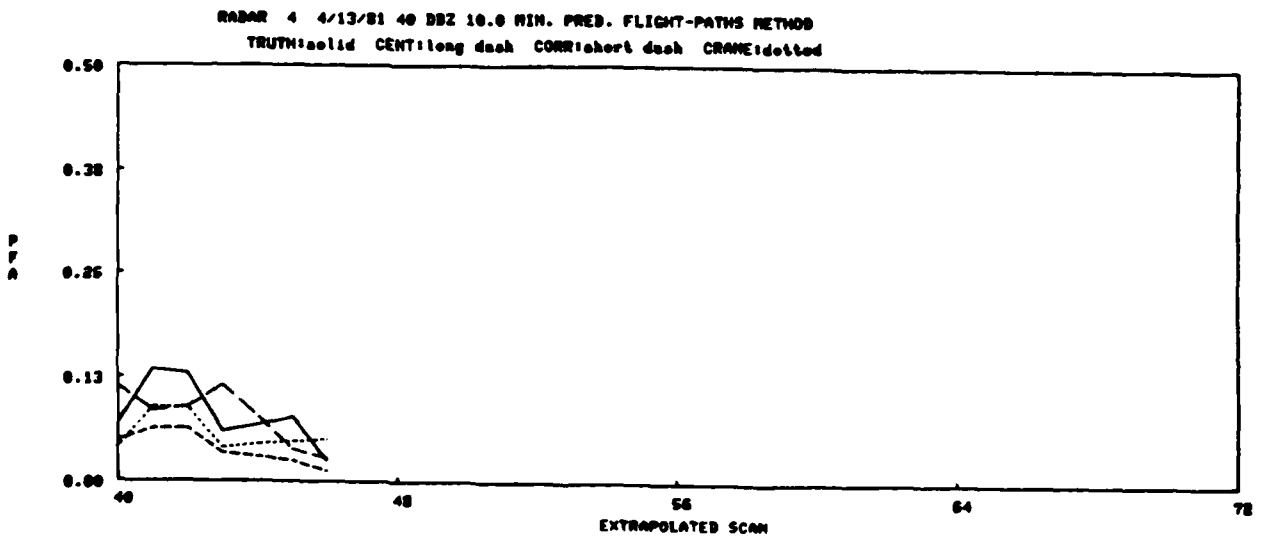

Figure IV-66. 4/13/81 10 min. pred., Flight-paths method.

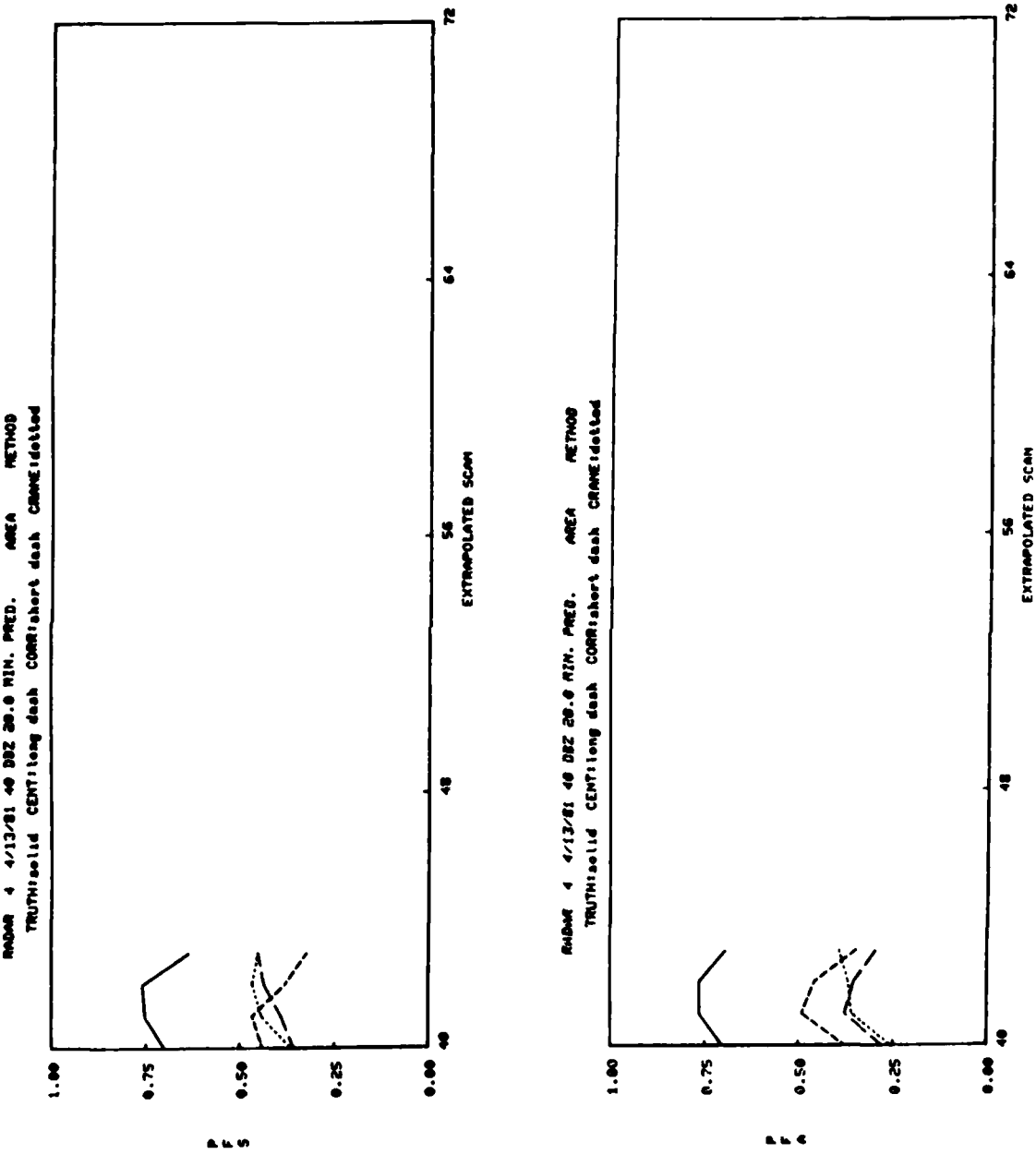

Figure IV-67. 4/13/81 20 min. pred., Area method.

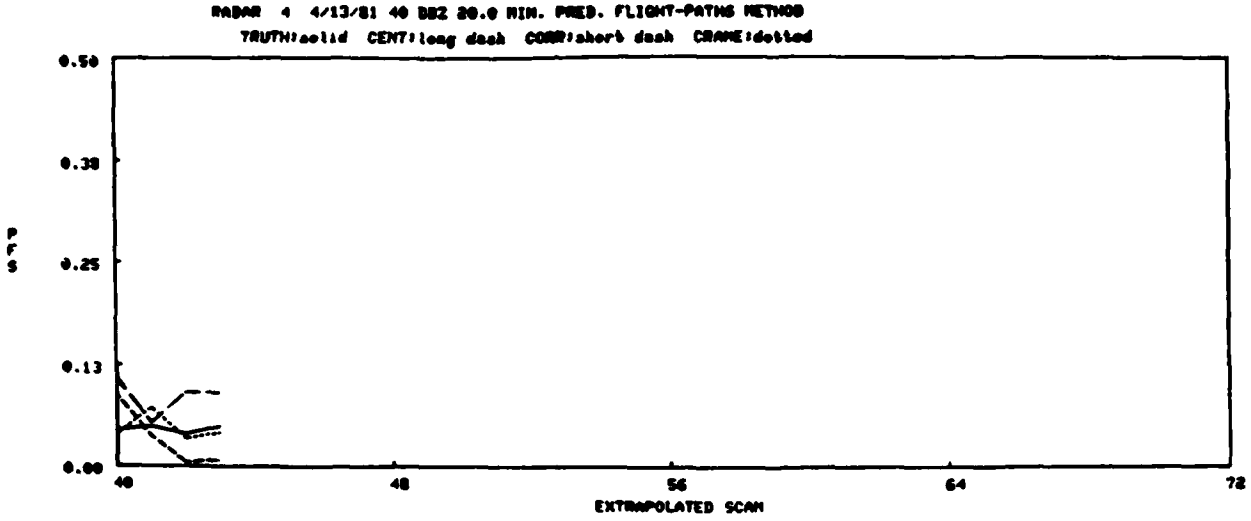

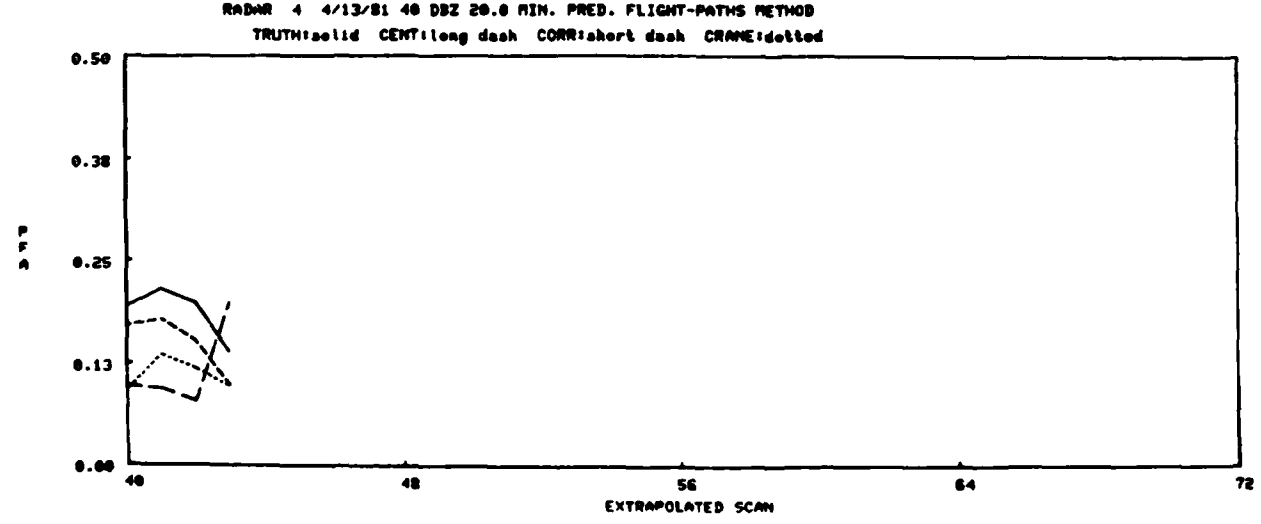

Figure IV-68. 4/13/81 20 min. pred., Flight-paths method.

The June 19 case at NSSL presents quite a different picture. Here the Crane tracker is clearly the worst, and this is believed due to the substantial propagation present. The centroid tracker works quite well on this compact storm, being skillful relative to persistence under the area criterion for 20- and 30-minute forecasts. Correlation appears to be intermediate in skill between the centroid and Crane trackers. There is no consistent skill under the flight-paths criterion for any of the trackers.

On the April 13 NSSL storm, the centroid tracker was hindered by the extended nature of the storm, and there was less vertical shear of the horizontal wind. Thus it is not surprising that under the area criterion, the three trackers are more closely matched in performance for 30-minute predictions. All three show skill at 30-minute predictions; apparently skill is easier to achieve for extended storms. There is not much skill under the flight-paths criterion, except for the correlation tracker.

V. INTERPRETATION

A. General Characteristics

The three MIT cases generally had low vertical shear of the horizontal wind, and the storm motions agreed with the correlation and Crane tracker to within 15° in direction. Agreement was somewhat poorer between the storm motion and the 10-20 kft winds. In one case, storm fragments appeared to travel 30° to the left of the winds. The centroid tracker was generally quite erratic.

The two NSSL cases were characterized by higher vertical shear of the horizontal wind. The storms moved 20-25° to the right of the upper-level winds, and these winds roughly agreed with the correlation and Crane trackers. The centroid tracker performed well when the storm was not extended.

Thus we see that there are several failure modes for the trackers. The centroid tracker performs poorly when storms are extended; then contour merging and splitting leads to erratic centroid motion. The correlation and Crane trackers perform poorly when there is substantial propagation, since they tend to follow the translation alone rather than the vector sum of translation and propagation. Propagation can be ascribed to "steady-state" growth/decay, and propagation to the right of the mean environmental winds occurs when the horizontal wind turns clockwise with height (veering, as opposed to backing). Finally, all the trackers are sensitive to non-steady-state growth/decay.

Translation represents the motion of particular convective cells, which typically move with the steering-level wind. Propagation represents the impulsive growth of new cells. When the environment has an organizing shear, the propagation can occur in a uniform fashion such that the storm envelope steadily moves in a direction different from the individual cells, which have lifetimes around 15 minutes. Atkinson (1981) summarized the research done on propagation, and presented a table demonstrating the tendency of storms to move to the right of the mean wind (see Fig. V-1); the data in this figure are from storms where the wind veered. Table V-1 further demonstrates the rightward tendency of storms.

Propagation can cause storms to move to the right when the winds are veering because new cell growth tends to form on the right flank (see Fig. V-2). Case (a) is the generally accepted case, where individual cells follow the mean wind and new cells form on the right flank. The other cases allude to the possibility that the cells themselves may move to the left or the right of the winds. New cell formation on the right flank can be qualitatively understood in terms of the conservation of horizontal momentum. As upper-level air descends, lower-level air approaches it on the right flank and is forced upward, leading to new cell growth. The right flank will also be the site of greatest shear, turbulence, and general hazardous weather.

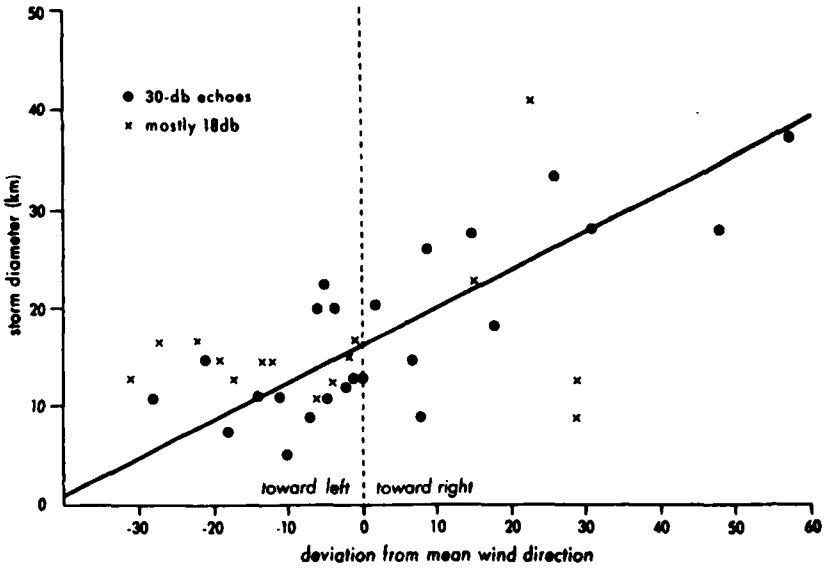

Deviation of storm motion from direction of mean wind as a function of echo diameter. Regression line based on radar echo observations as shown. (After Newton and Fankhauser 1964*a,b*.)

Figure V-1. Storm deviation. (Atkinson)

TABLE V-1

THERMODYNAMIC STABILITY, WINDSHEAR AND MOVEMENT OF CERTAIN WELL-DOCUMENTED MULTI-CELL STORMS

Case study	(°C)	Veering in subcloud (deg)	Mean wind in subcloud (deg/m s^{-1})	Mean wind from surface to 10 km (deg/m s^{-1})	Storm motion (deg/m s^{-1})	Shear in cloud layer (s^{-1})	Propagation	
							Individual cells	Discrete
Browning and Ludlam (1960)	+1	160	150/08	210/21	225/18	2.5×10^{-2}	No propagation	Right
Chisholm (1966), 18 July 1964	+4	40	240/07	235/26	250/12	—	No propagation	Right
Chisholm (1966), 21 July 1964	+4	−90	250/06	230/17	250/10	—	No propagation	Right
Alhambra storm, 12 July 1969	+2	30	020/30	245/11	300/09	2.0	Right	Right
Rimbey storm, 16 July 1969	+4	30	150/04	240/11	240/11	2.0	Left	Right
Benalto storm, 17 July 1968	+3	45	150/04	265/07	305/09	1.5	Right	Right
Sylvan lake storm, 25 July 1968	+6	80	010/04	275/13	315/16	2.0	Right	Right
Carstairs storm, 17 July 1969	+4	120	250/03	265/15	295/12	4.0	Right	Right
Butte storm, 11 July 1970	+7	10	140/06	235/16	310/07	4.5	Right	Right

Source: Marwitz (1972*b*).

(Atkinson)

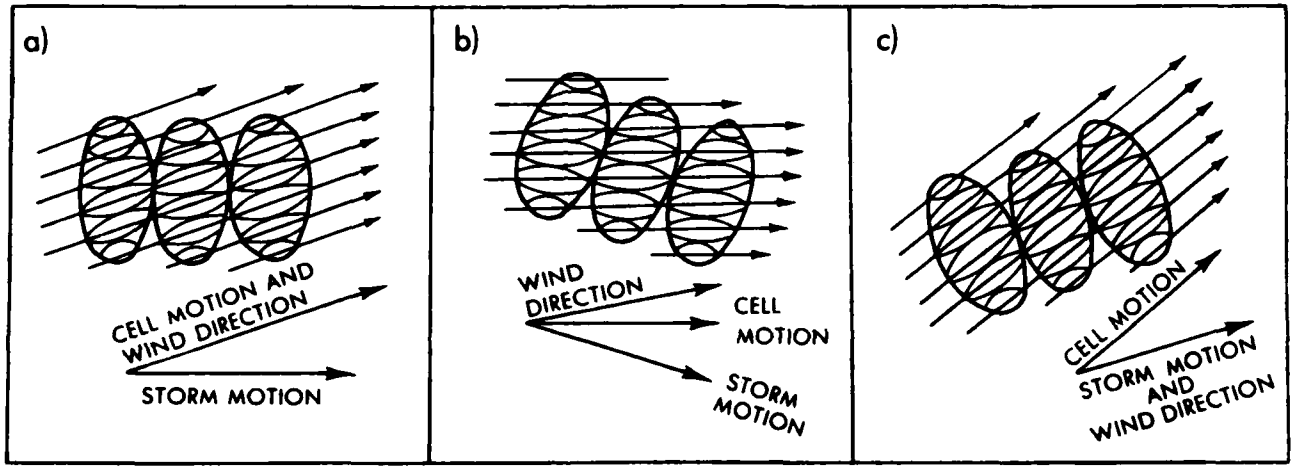

Schematic diagrams of storm movement by propagation (see text). (After Marwitz, 1972*b*.)

Figure V-2. Theory of propagation.

(Atkinson)

Ludlam (1980) suggests that -(Ri), the negative of the bulk Richardson number, should not be much greater than 1 for an organized cumulonimbus updraft to develop (and hence severe storms). The bulk Richardson number is defined as

$$-(\overline{Ri}) = (\Delta w)^2/(\Delta u)^2 \quad ,$$

where Δw is the updraft speed determined from parcel theory and Δu is the vertical shear of the horizontal wind. Strong shear tends to organize the thunderstorm flow and allow the storm to become severe, while buoyancy disrupts the flow. The stronger storms tend to propagate. We saw this in our June 19 data, and Ludlam notes it, too (see Fig. V-3). In Ludlam's figure, storms initially moving with the wind turned to the right when they became more severe. Thus strong shear indicates that propagation can occur, not necessarily that it will occur. Ludlam notes that storms sometimes split into diverging pairs, with the storm moving more to the right more likely to be accompanied by a tornado.

Propagation is relevant to this study because we are trying to predict the motion of storm envelopes; this motion is the vector sum of translation and propagation. The Crane algorithm appears to follow translation alone. This result also seems to appear in Wieler et al. (1982), a comparison of the Crane and centroid trackers applied to two Oklahoma storms. They show six instances where the centroid tracker goes 20-50° to the right of the Crane tracker; one case where the centroid tracker goes 30° to the left; and one case where the trackers are about the same.

The correlation tracker also tends to follow translation alone. Austin and Bellon (1974) note the tendency of some Montreal-area storms to move to the right of correlation-based predictions. More extensive follow-up work by Bellon and Austin (1978) sees no such tendency, but propagation is not generally expected in a low-shear environment such as Montreal. Smythe and Zrnic' (1983) express the belief that correlation would follow the total motion, but we see that it generally tends to follow the translation alone. As described earlier in this report, correlating scans 15 minutes apart can make the correlation tracker follow the total motion. Improved correlation performance in terms of following total motion might also be achieved with the binary-match algorithm in which displacements are determined by maximizing the overlap of a previous contour with the current field of contours.

The amount of shear present is related to the type of thunderstorms which can be expected. When the shear is high, supercell storms are possible. Storms will be long-lasting, perhaps accompanied by hail and tornadoes, and may have erratic motions. When the shear is moderate multicell storms are likely, such as squall lines. Propagation is a possibility. When the shear is low, expect poorly-organized air-mass storms.

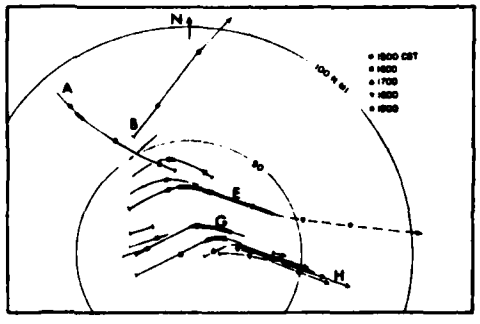

The paths of several cumulonimbus near Oklahoma City on the afternoon of 26 May 1963, as determined by radar situated at the center of the range rings. The thickened lines indicate where the storms were severe and had hook echoes (191).

Figure V-3. Veering storms.

(Ludlam)

Theorists have attempted to model propagation. Marroquin and Raymond (1982) were able to model propagation in multicell storms, but not in supercell storms. Wilhelmson and Chen (1982) were able to achieve rough agreement with new cell development.

B. Area and Flight-Path Results

The objective comparisons show that the centroid tracker performed poorly on extended storms, and on one of the compact storms. Correlation and Crane performed well on the low-shear MIT cases, but less well on the highly-sheared NSSL cases. Generally, the algorithms showed less skill (relative to persistence) at 10-minutes forecasts than at 20 minutes or 30 minutes. Generally, the trackers showed more relative skill under the area criterion than the flight-paths criterion. Overall, compact storms appeared the hardest to forecast well.

The relatively lower skill at 10 minutes is easy to understand. The goodness of a reflectivity forecast is largely dependent on three factors: the goodness of the extrapolated cell slices; the goodness of the translation vectors; and the extent to which non-steady-state growth/decay can be ignored. For short forecasts, the first factor is dominant. For a zero-minute forecast, a truth prediction is perfect. However, any of the trackers use cell slices, and these typically cover only 85-90 percent of the area covered by truth. Hence a very-short tracker forecast will have more false safes than persistence. Zero-minute tracker forecasts for August 5, 1981, have no false alarms, and typically 10 percent "area" false safes and 6 percent "flight-paths" false safes.

When cell slices are translated for a non-zero forecast interval, the total area covered by the slices can either increase or decrease. This depends on whether the translated contours have more or less overlap, and on whether more contours enter or leave the verification space.

The goodness of the trackers is more evident in the area statistics than in the flight-path statistics. The question arises of whether any of our trackers is close to optimal. Since the August 11, 1981 storm had little differential motion, we tried as an "optimal" tracker the observed, overall velocity (determined by a binary matching procedure) and applied this velocity to all of the cells. The resulting statistics were nearly identical to the Crane results indicating the Crane tracker performed about as well as possible. On the other hand, this result indicates one can equal the performance of any of the trackers by guessing a single vector (for storms with little differential motion). On a low shear day, an obvious candidate would be the 700 mb (millibar) or 500 mb wind; however the correlation velocities seem generally to be superior. Hence a correlation or Crane tracker derived velocity makes about as good a forecast as the observed storm velocity on low-shear days; this is also stated in Bellon and Austin (1978). Best-fit track velocities provide little improvement over correlation or Crane, because forecast errors are due largely to echo growth and decay.

Since the trackers show very little relative skill under the flight-paths criterion, this indicates that growth and decay cannot be ignored in the division of flight-paths into "safe" and "hazardous". On the other hand, storm areas can be forecast with relative skill, even while ignoring growth/decay.

VI. CONCLUSIONS AND RECOMMENDATIONS

A. Which Trackers to Use

The data requirements and processing times of the various trackers (coded in Fortran and run on a Perkin-Elmer 3240 computer) are shown in Table VI-1. It is felt that the current version of the Crane algorithm should be dropped from serious consideration for a NEXRAD algorithm because a performance benefit has not been found that merits the substantial computations required. It is possible that the high-spatial-resolution velocities provided by a refined Crane algorithm may prove useful in turbulence or cell growth/decay studies. However, Crane (1982) has reported that the cluster divergence and rotation numbers produced by the current algorithm are not reliable.

The challenges to any tracker are contour merging and splitting, translation/propagation, and growth/decay (including genuine storm merging/splitting, as opposed to contour merging/splitting). None of the trackers investigated attempts to address growth/decay. The Crane algorithm is immune to merging/splitting, but does not follow propagation. The centroid tracker is bothered by merging/splitting, but otherwise can follow translation and propagation. The correlation tracker is immune to merging/splitting, but usually does not follow propagation. It can follow propagation, also, if scans a sufficient time apart are correlated. A binary-match correlation algorithm may follow propagation.

The choice of tracker is influenced by the kind of storm expected. This expectation will be partly determined by site, and partly determined by the particular conditions on a particular day. Correlation would be preferred for storms similar to the Massachusetts cases considered, and centroid tracking might sometimes be preferred for storms similar to the Oklahoma cases. These results are applicable to other areas; for instance, Montreal has Massachusetts-like storms. A morning sounding will indicate whether enough shear is present to make propagation possible. Table VI-2 indicates how the tracker choice might be made on the basis of such a sounding.

B. Implications for Air Traffic Decision Making

It was determined that the trackers do show skill relative to persistence under the area criterion, but not under the flight-paths criterion. The interpretation is that the trackers can forecast storm areas with relative skill, but do not separate safe from hazardous flight-paths with skill. It must be borne in mind that the flight-paths in this study were straight-line segments in a circle of radius 135 km; hence their mean length is 4/3 the radius, or 180 km. En route airways often have straight-line segments even longer than this. The area criterion is mathematically

TABLE VI-1

TRACKING ALGORITHMS

Algorithm	Input Spatial Resolution (x,y,z)	Required Reflectivity Resolution	Computing Time on PE 3240	Required Update
persistence	-	-	-	-
centroid tracker (*)	raw data	~3 dB	~3 seconds	?
correlation tracker	2x2x4 km	~3 dB	~50 seconds	<15 min.
peak-cell	raw data (**)	1 dB	~500 seconds	<15 min.

(*) not including time to generate cell slices
(**) performance degradation when beamwidth exceeds 2 km

TABLE VI-2

TRACKER CHOICE

PREFERRED TRACKER

	MOSTLY TRANSLATION	MOSTLY PROPAGATION (STEADY GROWTH/DECAY)
COMPACT STORM	CENTROID	CENTROID
EXTENDED STORM	CORRELATION	CORRELATION*

*WITH LARGER TIME DIFFERENCE; 10-15 MINUTES INSTEAD OF 6 MINUTES

THE CHOICE OF TRACKER IS PARTLY SITE DEPENDENT

STORMS IN OKLAHOMA TEND TO BE MORE COMPACT THAN IN MASSACHUSETTS

THE CHOICE OF TRACKER IS PARTLY DEPENDENT ON SYNOPTIC CONDITIONS

SOUNDING WILL INDICATE WHETHER ENVIRONMENTAL WINDS SUPPORT PROPAGATION

UPPER-LEVEL JET MAY PLAY A ROLE

equivalent to employing very short flight-paths. Hence this study indicates that forecasts not employing growth/decay are skillful in flight-path selection only for paths shorter than 180 km. If an attempt were made to plan a 180 km or greater storm penetration path 30 minutes in advance, persistence would be as good as a tracker-based forecast, even if the forecast correctly predicted the actual storm motion.

Hence, the trackers do not help in planning in advance a long, storm penetration path; one can do just as well using persistence. However, the trackers do show skill in forecasting storm areas (and therefore short flight-paths). Hence the trackers can be used to predict the time interval when storms will impact on approach/departure gates, descent corridors, and runways. It does not appear justified to predict precisely a long penetration path once the impacting has begun, but the forecasts could prove useful in anticipating when one may need to divert traffic to another gate or another corridor, or to plan a short penetration path. The role of these forecasts lies more in route planning for weather avoidance than in route planning for weather penetration. Also, since the trackers do show skill in estimating storm speed and direction, they could be used for estimating arrival times of storm complexes for times longer than thirty minutes, although for longer time intervals it must be borne in mind that the storm motion may not be steady.

C. Future Work

There are various avenues for further research. The flight-path statistics could be calculated with an avoidance buffer around the predicted storm elements. The flight-paths statistics could be run with actual air routes and/or descent corridors. Multi-dBz-level predictions could be made, as advocated in Appendix A.

A more ambitious endeavor will be to attempt to predict growth and decay. As described in the introduction to this report, a detailed mesoscale model based on fundamental physics will not be feasible in an operational environment, and in fact is only beginning to appear in the research community. Less ambitious approaches to predicting growth/decay involve: simple, linear extrapolation; statistical models based on the concept of a typical life history; and simple models based on isolated physical phenomena such as topographic forcing.

Alaka et al. (1979) and Saffle and Elvander (1981) have found the extrapolation of dBz tends useful for 12-minute forecasts, but not for 36 minutes. Tsonis, Bellon and Austin (1981) have not found any benefit to dBz extrapolation in the Montreal area. Hence it does not appear that linear extrapolation of dBz levels has much to offer.

Bellon (1981) examined orographic effects in the Montreal area. He found the inclusion of preferred areas of growth and decay would lead to

only moderate forecasting improvements. However, orographic effects would be more important in other areas such as Britain, and there the inclusion of topography may prove beneficial. Whether to include topography in reflectivity forecasts would therefore be site dependent.

There remain several promising areas for growth/decay research. Research should be pursued in relating storm growth/decay to storm convergence/divergence as derived from Doppler data. Research should also be pursued in developing a statistical model of convective cells, to decide when to forecast growth/decay. And topography could be included when the site warrants it.

ACKNOWLEDGMENTS

Mark Merritt played a major role in the initial algorithm design, implementation and data analysis. James Fullmer and John Prohaska provided programming support. Mike Keohan and Ken Callwood coaxed the programs through production mode.

Dusan Zrnic' (NSSL) and Marilyn Wolfson were instrumental in providing the NSSL data. John DiStefano provided meteorological insight. Jim Evans provided managerial guidance and made important technical suggestions. Useful comments were received from Bob Crane of Dartmouth and Bob Elvander of the NWS.

Michelle Dalpe' produced the manuscript.

REFERENCES

1. M. A. Alaka, R. C. Elvander, R. E. Saffle, "Nowcasts and Short-Range (0-2 Hour) Forecasts of Thunderstorms and Severe Convective Weather for Use in Air Traffic Control," Report No. FAA-RD-79-98, Techniques Development Laboratory, National Weather Service (1979).

2. J. R. Anderson, "Evaluating Ground Clutter Filters for Weather Radars," 20th Radar Meteor. Conf., Boston, Massachusetts, 314 (1981).

3. B. W. Atkinson, Meso-Scale Atmospheric Circulation, (Academic Press), p. 337 (1981).

4. G. L. Austin and A. Bellon, "The Use of Digital Weather Radar Records for Short-Term Precipitation Forecasting," Quart. J. R. Met. Soc., 100, 658 (1974).

5. L. J. Battan, Radar Observation of the Atmosphere, (University of Chicago Press), p. 209 (1973).

6. A. Bellon and G. L. Austin, "The Evaluation of Two years of Real-Time Operation of a Short-Term Precipitation Forecasting Procedure (SHARP)," J. Appl. Meteor. 17, 1778 (1978).

7. A. Bellon, "Geographical Distribution of Radar Echoes' Growth and Decay," 20th Radar Meteor. Conf., Boston, Massachusetts, 170 (1981).

8. C. J. Bjerkaas and D. E. Forsyth, "An Automated Real-Time Storm Analysis and Storm Tracking Program (WEATRK)," Report AFGL-TR-80-0316, Air Force Geophysics Laboratory (1980a).

9. C. L. Bjerkaas and D. E. Forsyth, "Operational Test of a Three-Dimensional Echo Tracking Program," 19th Radar Meteor. Conf., Miami Beach, Florida, 244 (1980b).

10. J. C. Brasunas and M. W. Merritt, "Evaluation and Modification of AFGL Echo Tracking Algorithm," Project Memorandum 46PM-471-0003, Lincoln Laboratory, M.I.T. (1981).

11. J. C. Brasunas and M. W. Merritt, "Short Term Prediction of High Reflectivity Contours for Aviation Safety," 9th Aerosp. and Aeron. Meteor. Conf., Omaha, Nebraska, 118 (1983).

12. K. A. Browning, C. G. Collier, P. R. Larke, P. Menmuir, G. A. Monk, and R. G. Owens, "On the Forecasting of Frontal Rain Using a Weather Radar Network," Mon. Wea. Rev., 110, p. 534 (1982a).

13. K. A. Browning, Nowcasting, (Academic Press) (1982b).

14. R. K. Crane, "Automatic Cell Detection and Tracking," IEEE Trans. Geos. Elec., GE-17, 250 (1979).

15. R. K. Crane, "Radar Analysis for Severe Weather Detection and Tracking," Final Report for Project A579, Environmental Research and Technology, Inc. (1982).

16. R. O. Duda and R. H. Blackmer, "Application of Pattern Recogniation Techniques to Digitized Weather Radar Data," Stanford Research Institute Contract 1-36072 (1972)

17. R. C. Elvander, "An Evaluation of the Relative Performance of Three Weather Radar Echo Forecasting Techniques," 17th Radar Meteor. Conf., Seattle, Washington, 526 (1976).

18. S. Hamidi, R. E. Rinehart, and J. D. Tuttle, "Test of a Transverse Wind Algorithm for NEXRAD in Real-time," 21st Radar Meteor. Conf., Edmonton, Canada, 409 (1983).

19. B. G. Laird, "On Ambiguity Resolution By Random Phase Processing," 20th Radar Meteor. Conf., Boston, Massachusetts, 327 (1981).

20. F. H. Ludlam, Clouds and Storms, (Pennsylvania State U. Press), p. 247 (1980).

21. A. Marroquin and D. J. Raymond, "A Linearized Convective Overturning Model for Prediction of Thunderstorm Movement," J. Atmos. Sci., 39, 146 (1982).

22. R. E. Reinhart and E. T. Garvey, "Three-Dimensional Storm Motion Detection by Conventional Weather Radar," Nature, 273, 287 (1978).

23. R. E. Saffle and R. C. Elvander, "Use of Digital Radar Data in Automated Short Range Estimates of Severe Weather Probability and Radar Reflectivity," 7th Conf. on Prob. and Stat. in Atmos. Sci., Monterey, California, 192 (1981).

24. G. R. Smythe and D. S. Zrnic', "Correlation Analysis of Doppler Radar Data and Retrieval of the Horizontal Wind," J. Clim. and Appl. Meteor., 22, 297 (1983).

25. A. A. Tsonis, A. Bellon, and G. L. Austin, "The Evaluation of Predictive Schemes for the Growth or Decay of Rain Areas," 20th Radar Meteor. Conf., Boston, Massachusetts, 174 (1981).

AD-A146 638 A COMPARISON OF STORM TRACKING AND EXTRAPOLATION ALGORITHMS(U) MASSACHUSETTS INST OF TECH LEXINGTON LINCOLN LAB J C BRASUNAS 31 JUL 84 ATC-124 2/2

UNCLASSIFIED DOT/FAA/PM-84-1 DTFA01-80-Y-10546 F/G 4/2 NL

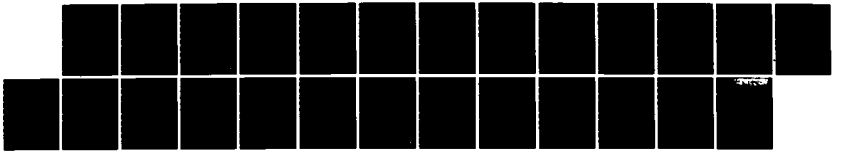

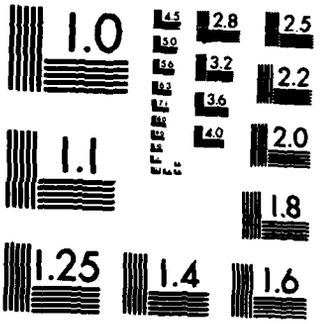

OPY RESOLUTION TEST CHART

26. J. G. Wieler, F. I. Harris, and M. R. Snapp, "An Evaluation of an Automatic Cell Detection and Tracking Algorithm," Report AFGL-TR-82-0368, Air Force Geophysics Laboratory (1982).

27. R. B. Wilhelmson and C. Chen, "A Simulation of the Development of Successive Cells Along a Cold Outflow Boundary," J. Atmos. Sci., 39, 1466 (1982).

28. W. D. Zittel, "Echo Interpretation of Severe Storms on Airport Surveillance Radars," Report No. FAA-RD-78-60, National Severe Storms Laboratory, 21 (1978).

APPENDIX A. RECOMMENDED NEXRAD ALGORITHM FOR PREDICTED PIXEL MAPS OF REFLECTIVITY

0.0 FOREWORD

This appendix describes the tracking/extrapolation procedure recommended for adoption as a NEXRAD algorithm on the basis of the work discussed in the body of this report. The algorithm wording assumes that the reader is conversant with contemporary weather tracking techniques and terms such as are discussed in the NEXRAD algorithm document (Ref. 3). The FAA needs short term (5-30 minute) predicted locations of hazardous weather regions for real time air traffic control use by controllers and/or pilots. These predictions will be used for tactical planning of air route usage, airport approach/departure corridors and runway usage. The predicted regions from various NEXRAD radars used by an ATC control facility will be automatically mosaiced in a Center Weather Processor (CWP) and then distributed to the various users in response to user requests.

The initial capability for tracking and prediction will consist of extrapolated high reflectivity regions as embodied in predicted pixel maps for time periods 10, 20 and 30 minutes in the future. Pixel maps are preferred (as opposed to contours) to facilitate the CWP mosaicing task. Certain ATC users with a very limited communications/display capability (e.g., general aviation aircraft) may not be in a position to effectively display the predicted regions as well as the current weather situation. For these users, it will be necessary to provide vectors showing the direction and speed of movement for major storm features.

1.0 PROLOGUE

1.1 Functional Description

The prediction maps represent estimates for reflectivity fields TP minutes ahead, where TP will typically be 10, 20 or 30 minutes. These reflectivity maps contain Cartesian pixels, each representing a maximum reflectivity between specified lower and upper altitude coverage limits. The predicted maps are generated by extrapolating discrete regions of a current reflectivity map at a constant vector velocity for time TP. There are two types (TYP) of velocities: TYP=1 come from the NEXRAD Storm Tracking algorithm, and TYP=2 come from a correlation tracker very similar to the Transverse Wind algorithm. The choice of TYP will be based on site specific meteorological experience and input from the principal user. A more complete description now follows.

a. Velocity Vectors and Storm Components from the Storm Processing Algorithms

The current NEXRAD Storm Segments and Storm Centroids Algorithms [Ref. 3] determine various parameters, including the centroid, of isolated storm elements known as volume cells. These volume cells are those parts of the storm whose reflectivity exceeds a threshold (ZT). Currently, one threshold (typically 30 dBz) is used.* In addition to the calculations performed in these two algorithms, the prediction map algorithm requires for each volume cell the total x-y extent (i.e. the volume cell "footprint"). From the Storm Tracking and Storm Forecast Algorithms, the speed and direction of the volume cells are computed. The volume cell footprints, centroids and velocities are inputs for the prediction map generation algorithm described below.

b. Cross-correlation Velocity Vectors

The second type of translation vector is computed by cross-correlating layered reflectivity maps. In the current NEXRAD implementation, there are three layers and the choice of level is to be a user-selectable option. The 0 - 12,000 layer is recommended as a default.

The linear size of the Cartesian pixel in the reflectivity layer (XSCALE) is an important factor in the algorithm accuracy and computation time. Preliminary investigations indicate that 1) 2.4 km is a good value for correlating maps acquired five minutes apart if a parabolic fit (see Fig. A-1) is used to determine the peak of the correlation matrix, 2) 4.8 km is too coarse to determine accurately motion in a five minute period, and 3) true 1.2 km resolution is often not available in the data due to beamwidth constraints and in any case does not improve the overall performance.

Assign the storms a maximum speed, SPDLIM, set to 2.0 km/min as a default. Then the maximum lag IDX which must be computed is

$$IDX = \frac{SPDLIM \times \Delta T}{XSCALE} \quad ,$$

where ΔT is the time interval between the two layers being correlated.

Boxes within the earlier reflectivity layer map are to be correlated with displaced boxes in the later layer. A margin IDX around the edge of the earlier layer is ignored (see Fig. A-2) to avoid storm segments which may leave the coverage area. Within the border, boxes with a length of

*It is our understanding that in the future, three or more threshold levels may be used in the storm processing algorithms.

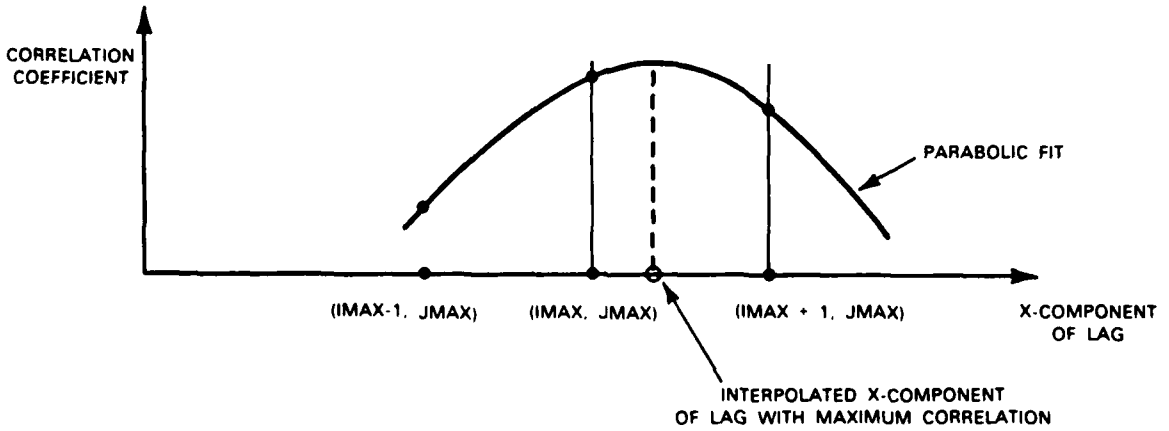

Figure A-1. Interpolation-derived correlation peak.

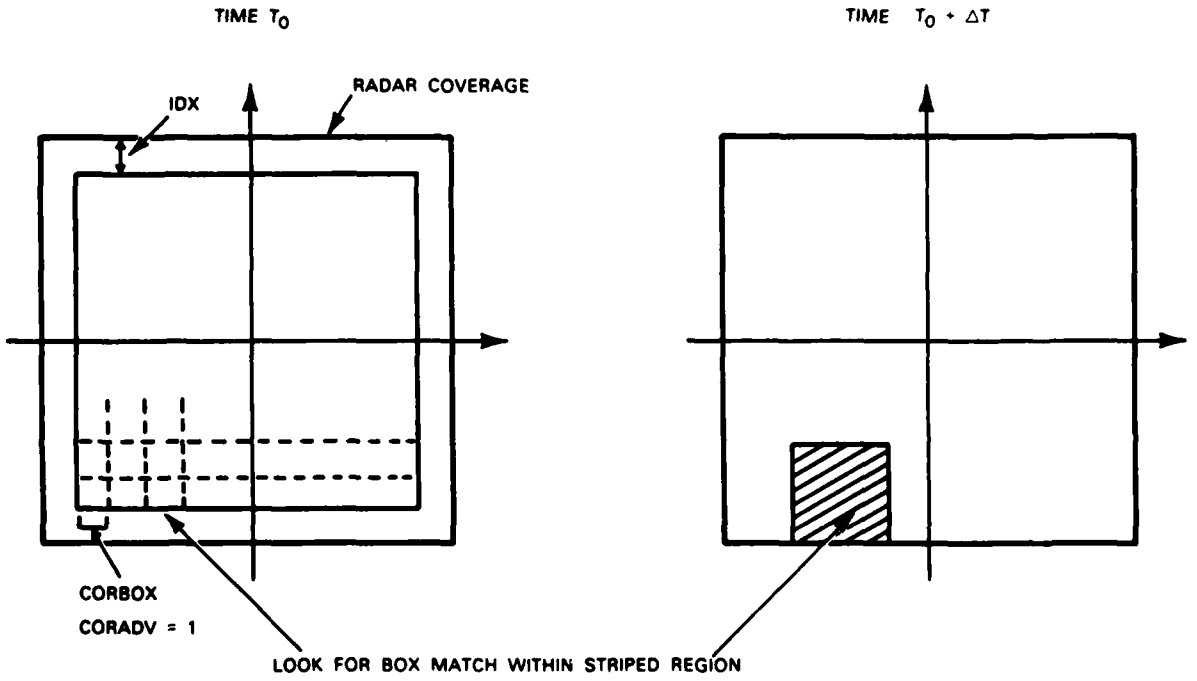

Figure A-2. Cross-correlation, box by box.

CORBOX km are to be correlated. Preliminary work indicates CORBOX = 28.0 km is a reasonable value. The box centers are to be spaced by an amount CORBOX*CORADV. CORADV = 1.0 is suggested as a default (boxes non-overlapping).

The correlation can be performed either on fields of dBz or of liquid water content (LWC), which satisfies the equation $LWC^2 = z/0.048$, where z is in units of mm^6/m^3 and LWC has units of g/m^3. Similar results have been obtained for dBz and LWC, so LWC is suggested. IF LWC is chosen, pixels with undefined reflectivities (due, for instance, to low S/N) are to be assigned 0. If dBz is chosen, pixels with undefined reflectivities are to be assigned DBZMIN (suggested default = 10 dBz), and pixels with defined reflectivities below DBZMIN are to be reset to DBZMIN. In either case, to insure meaningful correlations demand that a fraction FRAC (suggested default = 0.36) of the pixels in both the earlier and later boxes be defined -- if not, a correlation coefficient is not computed for that particular box and lag. Correlation coefficients are not to be used to compute a displacement unless the peak correlation exceeds RHOMIN (suggested default = 0.55).

The correlation-determined displacements are now defined on a (partly-filled) checkboard; when divided by ΔT, these are correlation velocities. The velocities are determined at other points by a process of extrapolation which preserves the original values. The process is an iterative one, where boxes with undefined values are assigned unweighted averages of the eight nearest neighbors. Correlation-determined velocities can now be assigned to the volume cells, by assigning to each cell the velocity closest to the cell centroid.

c. Prediction Map Generation Given Volume Cell Vector Velocities

For each volume cell there is now available a footprint, a centroid and a centroid-based or correlation-based velocity. For each x-y pixel within the radar coverage there are three reflectivities at differing altitudes; assign to each x-y pixel the maximum dBz. From the maximum-dBz product so created, select out the set of pixels falling within the x-y extent of a volume cell footprint, on a cell-by-cell basis. Move each set by an amount V x TP, where V is the velocity corresponding to that cell. In general, the footprint will not move an integral number of pixels in the x and y directions, and so the projected footprint must be resampled onto the pixel map. To do this, assign to each pixel in the prediction map the maximum dBz of the projected, overlapping pixels. If projected footprints overlap, assign maximum values to the pixels involved. In addition to the prediction maps, the fields of velocity vectors (with x-y position) are to be available as output. For either tracker, the output field is to be just those velocities assigned to volume cells.

1.2 Source

The volume cell selection and centroid tracker are existing NEXRAD algorithms[3]. The correlation tracker is very similar to the existing transverse wind algorithm. Additional research on the centroid and correlation tracker has been done at MIT/Lincoln Laboratory by Mark Merritt and John Brasunas[1,2] who developed the prediction map algorithm described here.

Differences between the correlation tracker described above and the Transverse Wind Algorithm [3] are:

Correlation Tracker	Transverse Wind
• works on layer	works on PPI
• x-y coordinate system	r, θ coordinate system
• radius of search dependent on ΔT only	radius of search depends on centroid-tracker output
• correlation box is 28x28 km	box size variable between 5x5 and 50x50 km
• calculates vectors for all boxes	calculating vectors for up to four viewing windows, 10 boxes per window
• uses lower spatial resolution	uses original resolution

References

1. J. C. Brasunas and M. W. Merritt, Short-Term Prediction of High Reflectivity Contours for Aviation Safety, 9th Conference on Aerospace and Aeronautical Meteorology, June 1983.

2. J. C. Brasunas, this report.

3. NEXRAD Algorithm document, May 1983.

1.3 Processing Environment

This algorithm requires the results already available from the Storm Segments, Storm Centroids, Storm Tracking and Storm Position Forecast algorithms. Results are also required from the layered reflectivity products. It is assumed that the reflectivity data and storm components used meet the NEXRAD accuracy requirements. In particular, it is assumed that

clutter from ground and moving objects has been suppressed in generation of the layered reflectivity maps and the storm components, as have other reflectivity error sources such as:

(1) obscuration by out of trip weather,

(2) asynchronous pulse interference,

(3) transmitter leak through, and

(4) sidelobe leak through by strong weather echoes in the same range rings.

2.0 INPUTS

2.1 Identification

PREDTIM	=	extrapolation time, in minutes, of prediction map
VECTYP	=	1 for centroid tracking, 2 for correlation tracking
NOMVEL	=	nomimal tracking velocity when no output is available from the trackers
THRESHOLD	=	which of the thresholds in the storm processing algorithms to use (if more than 1 exists)
VCEN(I)	=	centroid velocity for Ith volume cell
CENT(I)	=	centroid of Ith volume cell
STORM(I)	=	storm components and identifiers of the Ith volume cell
ZLAYER(J)	=	Jth reflectivity layer
LEVEL	=	reflectivity layer to correlate
PIXMIN	=	desired pixel size (km) of reflectivity layer before correlation (corresponds to XSCALE)
SPDLIM	=	storm speed limit (km/min)
TDELTA	=	desired time difference in minutes between correlated layers (corresponds to ΔT)
CORBOX	=	length of correlation box (km)
CORADV	=	spacing of correlation boxes
DBZMIN	=	lower threshold for dBz fields
FRAC	=	fraction of pixels within correlation box which must have valid reflectivities in order to compute correlation-based displacement
ICORTYP	=	type of correlation to perform - 1 for LWC and 2 for DBz
RHOMIN	=	minimum correlation for which a correlation-based displacement is condsidered valid

2.2 Acquisition

PREDTIM, VECTYP and THRESHOLD and NOMVEL are stored in a table; the values in this table can be changed by the user. THRESHOLD is limited to the set of thresholds present in the storm processing algorithms.

VCEN(I), CENT(I) and STORM(I) are acquired from the storm processing algorithms.

ZLAYER(J) is acquired from the reflectivity layering algorithm LEVEL, PIXMIN, SPDLIM, TDELTA, CORBOX, CORADV, DBZMIN, FRAC, ICORTYP and RHOMIN have default values which are stored in a table; the values in this table can be changed by the user.

3.0 PROCEDURE

3.1 Algorithm

BEGIN ALGORITHM (prediction and velocity maps)

1.0 GET PREDTIM, VECTYP, THRESHOLD and NOMVEL from the table.

2.0 DO FOR ALL (current volume cells of chosen theshold)

2.1 Get centroids and velocities

2.2 WRITE (centroids into CENT)

2.3 WRITE (centroid velocities into VCEN)

2.4 Get storm components and identifiers

2.5 Determine X-Y extent of volume cell

2.6 WRITE (X-Y extent into FPRINT)

END DO

3.0 Get the latest reflectivity layers

4.0 IF (VECTYP is 2) THEN

4.1 Get correlation parameters from the table. Set flag if an unreasonable computing load will result.

4.2 Get specified LEVEL of reflectivity layer closest to TDELTA minutes in the past. Store actual time difference in ΔT.

4.3 DO WHILE (layer pixel size is less than 0.8*PIXMIN) Degrade resolution of past and current reflectivity layers by a factor of two, by averaging four pixels into one. Each layer now has 1/4 as many pixels as before.

END DO

4.4 Store actual pixel size, after averaging, in XSCALE.

4.5 COMPUTE (NPTS)

4.6 COMPUTE (NSPAC)

4.7 COMPUTE (IDX)

4.8 COMPUTE (IMINPT)

4.9 IF (ICORTYP IS 1) THEN

COMPUTE (LWC)

ELSE

Replace undefined reflectivities with DBZMIN.
If any reflectivities are below DBZMIN, reset
them to DBZMIN.

END IF

4.10 Excluding a margin of IDX pixels in the older layer, partition the observation space into boxes NPTS pixels on a side. Box centers are to be spaced NSPAC points.

4.11 DO FOR ALL (Boxes in older layer)

4.11.1 IF (MORE THAN IMINPT POINTS IN BOX ARE VALID THEN)

DO FOR ALL (LAGS OUT TO +-IDX)

COMPUTE (CORRELATION)

END DO

ELSE Set flag for not enough valid points.

END IF

4.11.2 IF (peak of correlation array has X or Y component equal to ± IDX) THEN
Flag this box as exceeding speed limit.

ELSE IF (Any of the four nearest neighbors of peak have an undefined correlation) THEN

Flag this box as having a poorly determined peak.

ELSE

COMPUTE (Interpolated peak of correlation array)

END IF

4.11.3 WRITE (Peak correlation into CORVAL)

4.11.4 WRITE (Interpolated displacement of peak correlation)

4.11.5 WRITE (Center of correlation box into CORPOS)

END DO

4.12 DO FOR ALL (BOXES)

IF (CORVAL exceeds RHOMIN AND interpolated peak is defined) THEN
COMPUTE (Correlation-based velocities)

ELSE Set flag for low correlation.

END IF

END DO

4.13 WRITE (CORRELATION VELOCITIES INTO VCOR)

4.14 IF (There is at least one defined velocity) THEN
DO WHILE (There are undefined velocities)
Assign temporary velocities to undetermined boxes — the average of the defined subset of the eight nearest neighbors. When finished with field, consider the temporary velocities to be defined. Keep track of which velocities were originally undefined.

END DO

END IF

4.15 Assign to each volume cell the nearest correlation velocity.

END IF

5.0 Assign to each X-Y pixel in the radar coverage the maximum of the reflectivities in the three altitude layers. This creates a composite reflectivity map.

6.0 IF (VECTYP is 1) THEN
VPRED is centroid velocity.

ELSE IF (VECTYP is 2) THEN
VPRED is the extrapolated set of correlation velocities.

END IF

7.0 IF (VPRED is undefined) THEN
VPRED is NOMVEL

END IF

8.0 DO FOR ALL (Current volume cells of chosen threshold, and PREDTIM)

8.1 Select out the pixels in the composite reflectivity map which fall within the volume cell footprint.

8.2 Move the subset of pixels by the amount (VPRED*PREDTIM)

8.3 Resample projected pixels onto Cartesian array.

8.4 IF (A projected pixel lands on a pixel previously defined by moving another volume cell) THEN
Assign greater dBZ value to that pixel.

END IF

9.0 Establish a quality control table, which contains the flags for high processing load, no defined velocities, NPTS, NSPAC, IDX, and which volume cells have been assigned correlation velocities which were not in the originally defined set. Also establish a map of flags for the correlation boxes: speed limit exceeded, peak poorly determined, low correlation, and not enough valid points.

END ALGORITHM (PREDICTION AND VELOCITY MAPS)

3.2 Computation

3.2.1 Notation

IMINPT = minimum number of pixels within box required to be valid

LWC = liquid water content corresponding to a pixel (g/m^3)

Z = reflectivity of a pixel (mm^6/m^3)

C = correlation coefficient

N = NPTS*NPTS

X = Z or LWC in earlier layer

Y = Z or LWC in later layer

IMAX = X-coordinate of peak correlation lag

JMAX = Y-coordinate of peak correlation lag

IINT = X-coordinate of interpolated peak correlation lag

JINT = Y-coordinate of interpolated peak correlation lag

EPSX, EPSY = offsets of interpolated peaks

S(1),S(2),S(3) = correlation coefficients at (IMAX-1, JMAX),
(IMAX, JMAX), (IMAX+1, JMAX)

T(1),T(2),T(3) = correlation coefficients at (IMAX, JMAX-1),
(IMAX, JMAX), (IMAX, JMAX+1)

VCOR = correlation-based velocity (km/min)

DISP = interpolated displacement (km)

ΔT = time difference between current and past reflectivity layers (min)

XSCALE = pixel size (km) after averaging (if any)

3.2.2 Symbolic Formulas

COMPUTE (NPTS)

NPTS = IFIX(CORBOX/XSCALE + 0.5). Flag if less than 2.

COMPUTE (NSPAC)

NSPAC = IFIX(NPTS*CORADV + 0.5). Flag if zero.

COMPUTE (IDX)

IDX = IFIX (ΔT*SPDLIM/XSCALE + 0.5). Flag if less than 4.

COMPUTE (IMINPT)

IMINPT = NPTS*NPTS*FRAC

COMPUTE (LWC)

LWC = $(Z/4.8E\text{-}2)^{1/2}$, where dBZ = 10log10(Z). LWC=0 if Z not defined.

COMPUTE (CORRELATION)

$$C = \frac{\sum XY-(\sum X)(\sum Y)/N}{(\sum X^2-(\sum X)^2/N)^{1/2}\ (\sum Y^2-(\sum Y)^2/N)^{1/2}}$$

Summation is over all pixels in a box.

If these are not IMINPT valid pairs, leave correlation undefined.

COMPUTE (INTERPOLATED PEAK OF CORRELATION ARRAY)

EPSX = 0.5* (S(3)-S(1))/S(1)+S(3)-2.*S(2))

EPSY = 0.5* (T(3)-T(1))/(T(1)+T(3)-2.*T(2))

IINT = IMAX-EPSX

JINT = JMAX-EPSY

COMPUTE (CORRELATION-BASED VELOCITIES)

VCOR = DISP/ΔT

4.0 OUTPUTS

4.1 Identification

A set of vectors VCOR which are the correlation-determined velocities. (The centroid-based velocities are available from the storm processing algorithm.)

The various parameters which are under the user's control.

Pixel-based maps of predicted reflectivity.

Quality control outputs: processing load; no defined velocities; bad NPTS, NSPAC or IDX; speed limit, poor peak, low correlation, not enough valid points, which volume cells use an extrapolated correlation velocity.

5.0 INFERENCES

5.1 Constraints and Validity Range of Parameters

Unrestricted setting of parameters can lead to unreasonably long computation times. Most parameters should not be changed. The dependence of the correlation algorithm on many of the parameters has been investigated. CORBOX, which controls the size of the correlation area and thus the scale on which correlation is preformed, did not greatly impact the algorithm when changed from 28 to 56 km. If FRAC is reduced from 0.36 to 0.18, erratic correlation displacements are considerably more common.

VECTYP, PIXMIN, and TDELTA are the parameters most subject to change, and their choice depends on the type of weather expected. A reasonable choice of these parameters can be based on atmospheric soundings. VECTYP=1 (centroid tracking) is more suited to small storms, since large storms give problems due to contour merging and splitting. Centroid tracking works well in the presence of strong storm propagation, as may be present in supercell storms. Correlation works well with either small or extended storms (e.g., multicell) if there is no significant propagation (using the default values PIXMIN=2.4, TDELTA=6 min.). If the storm is extended and has substantial propagation, a partial solution has been to increase ΔT (by increasing TDELTA) in the correlation tracker.

Choice of ΔT does have a marked effect on the performance of the correlation tracker. For ΔT = five minutes, correlation tracking tends to agree with the steering level wind. For ΔT = 15 minutes, correlation tracking begins to reflect the vector sum of cell translation and storm propagation (if present). ΔT = 20 minutes tends to give erratic results. If substantial propogation is suspected, ΔT = 10 or 15 minutes would be preferable to 5 minutes (which is suitable in the absence of propagation) or 20 minutes.

Finding the maximum correlation can be a lengthy exercise, if a first guess is not available. Each box (producing one velocity vector) requires the computation of $(2IDX + 1)^2$ lags, each of which involves $\sim NPTS^2$ multiplies. Thus the number of multiplies goes as

$$\text{Multiplies} \approx \frac{CORBOX^2\ SPDLIM^2\ \Delta T^2}{XSCALE^2\ XSCALE^2}$$

Note the strong dependence on XSCALE. If we let XSCALE vary linearly with ΔT, the computation time goes as $1/XSCALE^2$. For ΔT = six minutes, the above default values, and a radius of coverage of 135 km, the correlation algorithm coded in Fortran typically requires 50 seconds on a Perkin-Elmer 3240, using fixed-point multiply. Going to the full NEXRAD layer coverage of $\approx$ 230 km radius, and roughly doubling XSCALE and ΔT, would give 1/4 the computation time per box, and four times as many boxes, leading again to about 50 seconds per correlation of two reflectivity layers. Thus ΔT = 12 minutes and XSCALE = 4 km are suggested as a second set of reasonable default values, consistent with the NEXRAD update rate and reflectivity layer pixel size. In the absence of propagation, either set is suitable.

APPENDIX B. SOFTWARE DESCRIPTION

The tracking and prediction software is written in Fortran and runs on a Perkin-Elmer 3240. There are over 16,000 lines of code, of which about 7,000 are in the Crane algorithm.

Table B-1 shows some of the programs, together with output files. Figure B-1 shows the procedure for making and evaluating centroid-tracker-based prediction maps. "CFT" refers to the common format tape - all radar data tapes are re-formatted. Figures B-2 and B-3 show the corresponding procedures for correlation and Crane tracking.

TABLE B-1

EXTENSION FOR FILES GENERATED

ext	Generating Program	Description
MPT	VERITAS	Truth maps
CEN	FLCONT	Centroids
CNT	FLCONT	Contours
TRK	TRKN	Centroid tracks
TOT	TRKN	Centroid totals
MP0	FLPTG2	Centroid prediction maps
CAP	COMCAP2	CAPPI's
VEC	ONEVEC	Correlation vectors
MP1	FLPTG2	Correlation prediction maps
CRN	CRANE	Crane output
VEL	GRID	Crane velocities
MP2	FLPTG2	Crane prediction maps

File Description

NBD: _____.EXT

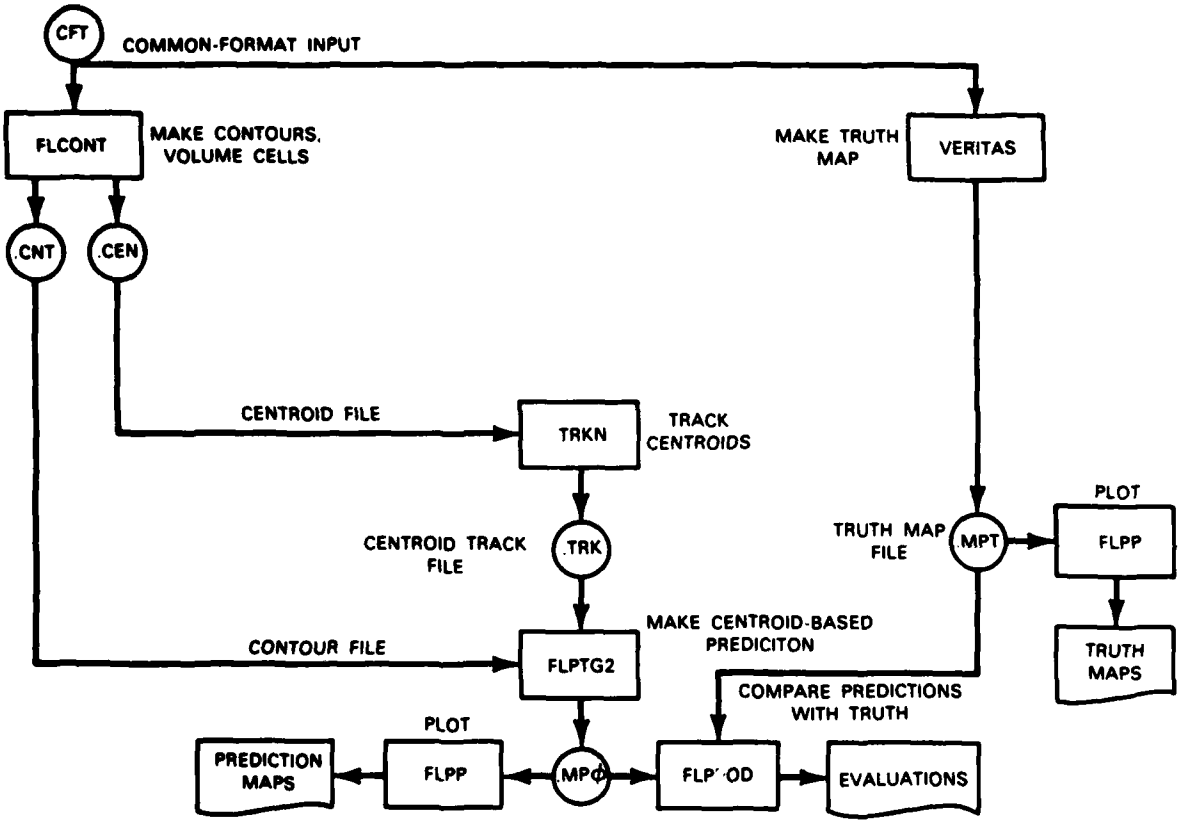

Figure B-1. Centroid tracker flowchart.

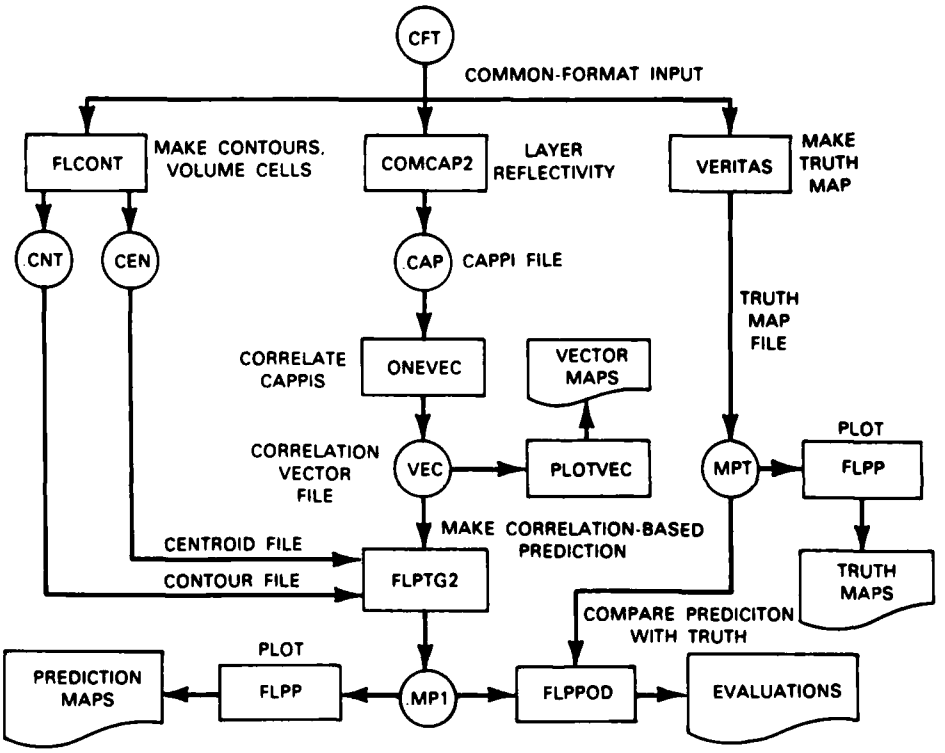

Figure B-2. Correlation tracker flowchart.

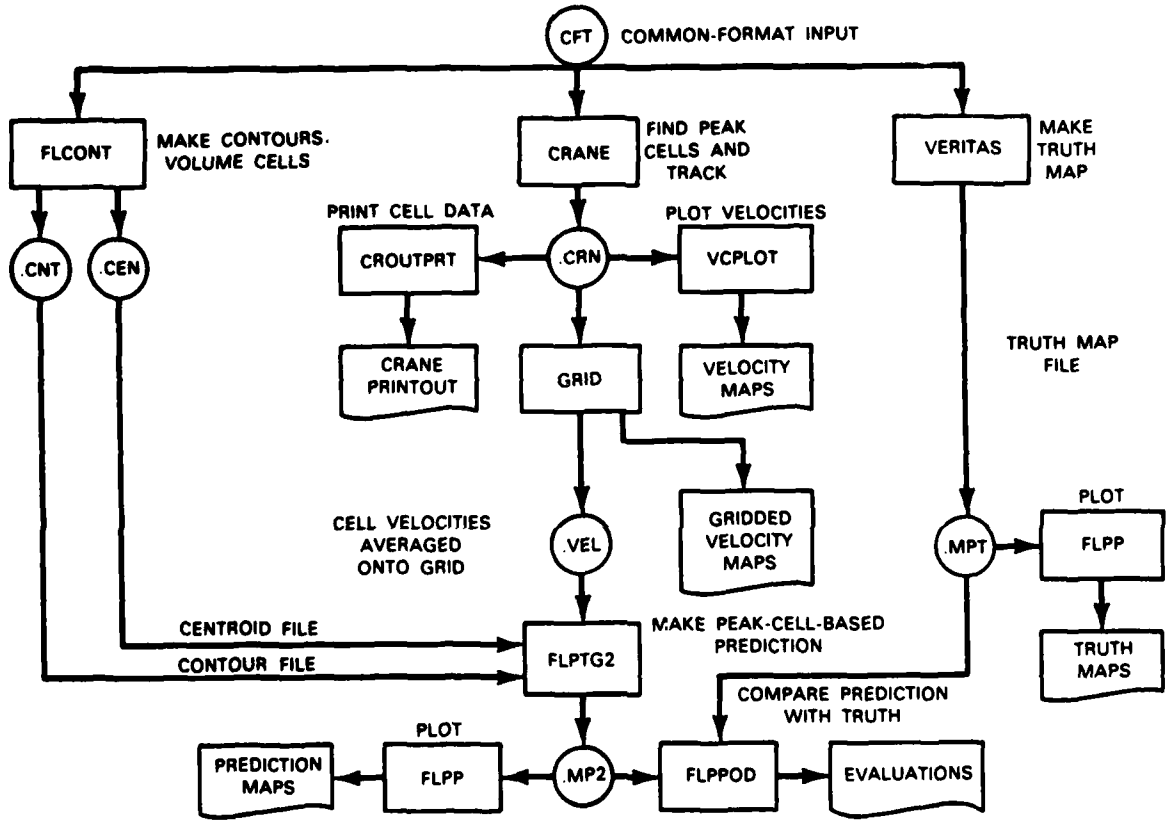

Figure B-3. Crane-tracker flowchart.

APPENDIX C: ALGORITHM FOR REMOVAL OF NSSL RANGE RINGS

Pulse-pair data taken in the expanded integrator mode at NSSL usually appear to have high-dBz thin rings. These rings are usually 1, 2 or 3 range gates wide, and are roughly at range gates 192,384 and 576 (out of 762). There is a slight shift in range gate number if the PRF is changed. Sometimes the ring will be centered on a gate, and sometimes it will be centered between gates.

The goal in tracking and prediction software has been to design software that can be run by a data editor under the supervision of a programmer or staff scientist. Therefore, a completely automatic ring-removal program has been written, which has as input a common format tape (old style) and has as output a corrected common format tape.

The first step is to find the rings. The program takes the highest elevation angle PPI in a volume scan, and hopes to find at least 100 radials. Reflectivity in dBz is computed for each range bin; the dBz is set to zero if the S/N is less than 0 dB. For each range, the dBz's are averaged over azimuth angle. Then, the radial gradient in angle-averaged dBz is computed for each range gate. Going out in range, a ring is said to begin when a gradient over 7 dBz/range gate is encountered. The ring is said to terminate when the gradient goes below 7. Since the ring may have a flat center, the ring is allowed to coast across ICOASTMX low-gradient points. ICOASTMX is currently 1.

The next step in RINGOUT is to replace ringed range-gates with a local average.

The algorithm has been tested on two NSSL data sets: the first one was used to determine the various adjustable parameters, and the second is an independent data set. Excellent results have been obtained in both cases.

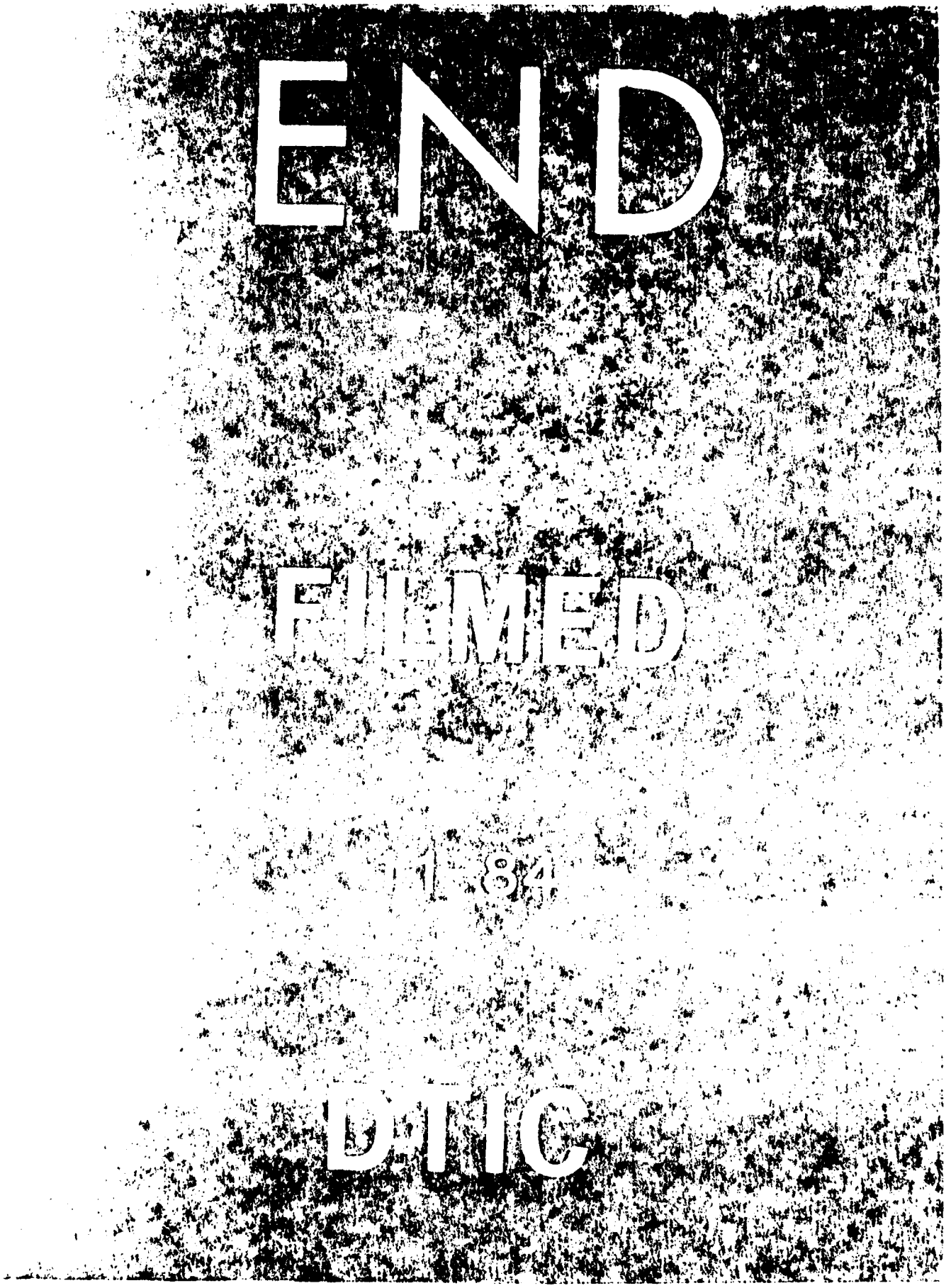
END
FILMED
1-84
DTIC